Self-supervised Video Representation Learning

WANG, Jiangliu

A Thesis Submitted in Partial Fulfilment
of the Requirements for the Degree of
Doctor of Philosophy
in
Mechanical and Automation Engineering

The Chinese University of Hong Kong
September 2020

Thesis Assessment Committee

Professor HENG Pheng Ann (Chair)

Professor LIU Yunhui (Thesis Supervisor)

Professor DOU Qi (Committee Member)

Professor WANG Jun (External Examiner)

Abstract of thesis entitled:

Self-supervised Video Representation Learning

Submitted by WANG, Jiangliu

for the degree of Doctor of Philosophy

at The Chinese University of Hong Kong in September 2020

Powerful video representations serve as the foundation for many video understanding tasks, such as action recognition, action proposal and localization, video retrieval, *etc.* Applications of these tasks vary from elderly caring robots at home to large scale video surveillance in public places. Recently, remarkable progresses have been achieved by data-driven approaches for video representation learning. Ingenious network architectures, millions of human-annotated video data, and substantial computation resources are three vital elements to such a success. However, further development of supervised video representation learning is impeded by its heavy dependence on human-annotated labels, which restricts it from relishing massive video resources freely on the Internet.

To solve the aforementioned problem, this thesis aims to learn video representations in a self-supervised manner. The essential solution to *self-supervised video representation learning* is to propose appropriate *pretext tasks* that can generate training labels automatically. While previous works mainly focused on the usage of video order predictions as their pretext tasks, this thesis proposes a completely new perspective for designing pretext tasks – by spatio-temporal statistics regression. It encourages a neural network to regress both motion and appearance statistics along the spatio-temporal axes. Unlike prior works that learn video representation on a frame-by-frame basis, this pretext task allows spatio-temporal features learning, which is applicable to many video analytic tasks. By using a classic C3D, we already achieve competitive performances.

Based on the proposed statistics pretext task, we further conduct in-depth investigation with extensive experiments and uncover three crucial insights to significantly improve the performance of self-supervised video representation leaning. First, architectures of backbone networks play an important role in self-supervised learning while no best model is guaranteed for different pretext tasks. Second, downstream task performances are log-linearly correlated with the pre-training dataset scale. Attentive selection should be given on the training samples. To this end, a curriculum learning strategy is further adopted to improve video representation learning. Third, besides the main advantages of self-supervised video representation learning to leverage a large number of unlabeled videos, features learned in a self-supervised manner are more generalizable and transferable than features learned in a supervised manner.

Considering that the computation of optical flow is both time and space consuming in the statistics pretext task, we further propose a new pretext task – video pace prediction, which asks a model to predict video play paces. Without using the pre-computed optical flow, this pretext task is more preferable when the pre-training dataset scales to millions/trillions of data in real world application. Experimental evaluations show that it achieves state-of-the-art performance. In addition, we also introduce contrastive learning to push the model towards discriminating difference paces by maximizing the agreement on similar video content.

With all the works described above, this thesis provides novel insights in self-supervised video representation learning, a newly developed yet promising filed. The experimental results strongly validate the feasibility of leveraging unlabeled data for video representation learning. We believe that the journey of self-supervised learning just begins and its great potential is far from explored.

摘要

自監督的視頻表示學習

有效的視頻表示是許多視頻理解任務（如動作識別，動作定位，視頻檢索等）的根本。這些任務的應用範圍很廣，從家用的老人護理機器人到公共場所的大規模視頻監控，不一而足。近來，受益於數據驅動方法的發展，視頻表示學習已取得了顯著進展。巧妙的網絡結構，數百萬的由人類標註的視頻數據以及大量的計算資源是取得成功的三個關鍵要素。但是，目前的有監督視頻表示學習嚴重依賴於標註的數據，這使得它無法充分利用互聯網上大量免費的視頻資源，因此其進一步發展受到了阻礙。

為了解決上述問題，本論文旨在以一種自監督的方式來學習視頻表示。自監督視頻表示學習的基本解決方案是提出可以自動生成訓練標籤的適當代理任務。先前的工作主要集中於將視頻順序預測用作代理任務，而本文提出了一種的全新視角-通過時空統計回歸-來設計代理任務。它鼓勵神經網絡沿時空坐標系回歸運動統計和外觀統計。與以前逐幀學習的視頻表示不同，該任務任務可以學習時空特徵，因此適用於許多視頻分析任務。通過使用經典的 C3D 網絡，我們已經可以取得出色的性能。

在提出的統計代理任務的基礎上，我們通過廣泛的實驗進一步進行深入調查並發現三個關鍵的見解，以顯著提高自監督視頻表示學習的性能。首先，骨幹網絡的結構在自監督學習中起著重要作用，但對於不同的代理任務無法保證最佳模型。其次，下游任務效果與預訓練數據集規模呈對數線性相關，因此應在

訓練樣本上仔細選擇訓練數據。為此，我們進一步採用漸進式學習策略來改善視頻表示學習。第三，除了自監督視頻表示學習可以利用大量未標記視頻的主要優勢外，以自監督方式學習的特徵比通過監督方式學習的特徵更具通用性和可移植性。

考慮到在統計代理任務中光流的計算既佔用時間又耗費空間，因此我們進一步提出了一種新的代理任務-視頻速度預測，該任務要求一個模型來預測視頻播放速度。在不使用預先計算的光流的情況下，當在實際應用中將預訓練數據集擴展到數百萬/萬億數據時，此代理任務將更適用。實驗評估表明它達到了最先進的性能。此外，我們還引入了對比學習，以通過最大化相似視頻內容的一致性來推動模型區分差異視頻速度。

基於上述所有工作，本論文為自監督的視頻表示學習提供了新的見解。這是一個新興的但很有希望的領域。實驗結果驗證了利用未標記數據進行視頻表示學習的可行性。我們認為，自監督學習的旅程才剛剛開始，其巨大潛力還沒有得到探索。

Acknowledgement

First of all, I would like to express my sincere gratitude to my supervisor Prof. Yunhui LIU for his generous advice and consistent support. He always encouraged me to investigate on some new directions and novel approaches rather than just follow others. He is very open to new ideas/fields and sets a high standard for good research. It really inspires me during my PhD study. Without his support, there would be no possibility for this thesis to come into being.

Special thanks to Prof. Pheng Ann HENG, Prof. Qi DOU, and Prof. Jun WANG in the assessment committee, for their time and suggestions on the improvement of this thesis, especially during this hard time of COVID-19.

Thank Dr. Jianbo JIAO from Oxford University, as we work closely and have a wonderful time to explore the beautiful computer vision world together. Thank Dr. Linchao BAO and Dr. Wei LIU from Tencent AI Lab, for their helpful advice in my research work during my internship at Tencent AI Lab. Thank Prof. Wei LI from Nanjing University, for his leading me to the door of research in my undergraduate study.

Thank my colleagues from CUHK for their help, including Dr. Yang LIU, Mr. Qiang NIE, Mr. Xin WANG, Ms. Manlin WANG *etc.*. Thank the colleagues from Tencent AI Lab for their help during my internship, including Dr. Yibin Song, Dr. Xuefei ZHE, Mr. Pengpeng LIU, Ms. Yajing CHEN, *etc.*.

Finally, loving thanks to my parents and my boyfriend Dr. Fan ZHENG for

their unconditional love and support. It is them who allow me to be unrestricted in both research and life.

Contents

List of Figures

List of Tables

Chapter 1

Introduction

1.1 Background

Video understanding, from the computer vision perspective, aims to develop techniques that allow a computer to analyze and understand the visual world from videos, as human visual system does. Compared with images, video data contains diverse information from both spatial and temporal dimensions, which is beneficial for mitigating the ambiguities in visual understanding with spatial information only. For example, it is much easier for human to recognize a car moving forwards or backwards from a video than from a single image.

While enjoying the advantages of diverse signals, on the other hand, video understanding confronts the essential challenge of processing high-dimensional data. For example, a ten-seconds HD video contains around *155 million* dimensional elements. With 100 billion neurons [13] and elusive neural system [14], human beings can easily analyze and understand the video content. However, this is not a trivial task for a computer to solve, especially considering the limited computational resources. It is natural to ask, can these high-dimensional videos be compressed into compact and abstract representations without affecting the video

content understanding so that they can be processed by a computer? The key to this question is termed as *video representation*.

Powerful video representations serve as the most essential foundation for many video understanding tasks, such as action recognition [11, 15], video retrieval [16, 17], action proposal and localization [18, 19, 20], video captioning [21, 22], *etc*. Relative applications are in a wide rage, including elderly caring robots, human-computer interaction, large scale video surveillance in public places, sports video analysis, robot manipulation, to name a few cases.

Specifically, good video representations should preserve the vital and distinct information of videos while neglect those redundant and obscure signals. Previously, extensive efforts have been made to develop handcrafted descriptors/features as video representations. Some exemplary works include space-time interest points (STIP) [23], HOG3D [24], improved dense trajectories (iDT) [25], *etc*. While promising results have been achieved, these representations are usually elaborately designed by researchers to address the video understanding problem in a controlled and relatively simple setting. Therefore, video representations designed by handcrafted approaches are usually vulnerable to diverse variations in real-world applications.

To overcome the drawbacks of handcrafted video features, extensive studies have been conducted these years on data-driven approaches for video representation learning. Typically, convolutional neural networks (CNN) have witnessed its absolute success [11, 26, 27] with human-annotated labels, *i.e.*, *supervised video representation learning*. Researchers have developed a wide range of neural networks [28, 10, 26] ingeniously, which aim to learn powerful spatio-temporal representations for video understanding. Meanwhile, millions of labeled training data [29, 30] and powerful computational resources are also the fundamental recipes for such a great success.

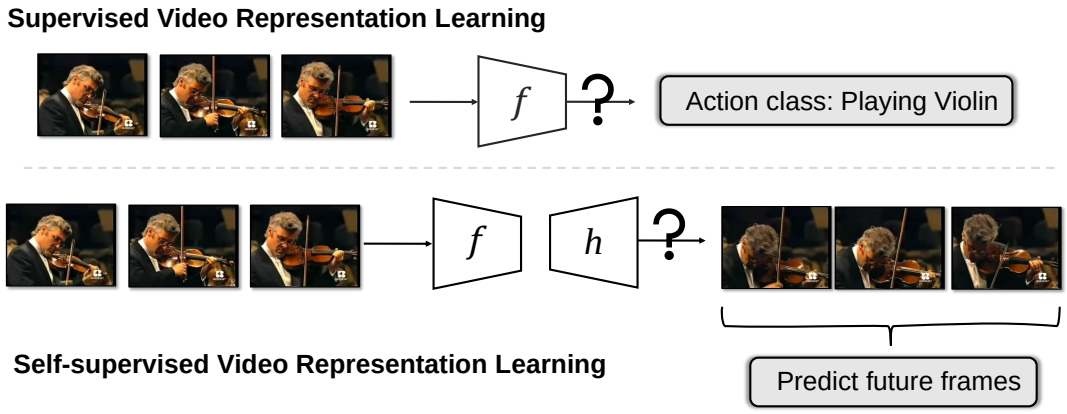

Figure 1.1: **Illustration of supervised and self-supervised video representation learning**. *Supervised video representation learning*: training labels are annotated by human beings. For example, regarding the typical action recognition problem, a neural network is trained with action classes annotated by human for video representation learning. *Self-supervised video representation learning*: training labels are usually self-contained and will be generated without human annotation. For example, a natural method for self-supervised video representation learning is to predict the future frames.

However, supervised video representation learning is running into its bottleneck due to the heavy dependence on human-annotated video labels. Indeed, obtaining a large number of labeled video samples requires massive human annotations, which is expensive and time-consuming. Whereas at the same time, billions of unlabeled videos are available freely on the Internet. For example, users in YouTube upload more than 500 hours videos every single minute [31]. Intuitively, one may wonder that *can we learn video representations from unlabeled data, i.e., unsupervised learning?* And if so, *how can we leverage the large amount of unlabeled data for video representation learning?*

To leverage the large amount of unlabeled video data, *self-supervised video representation learning* is proved to be one promising methodology [32, 33]. Fig. 1.1 shows an illustration of supervised video representation learning and self-supervised video representation learning. Regarding supervised video represen-

tation learning, one typical training target is to recognize action classes of videos and the training labels are annotated by human. While concerning self-supervised video representation learning, the neural networks are not trained with human annotated action class labels. Instead, the essential solution is to propose other appropriate training targets, usually termed as *pretext tasks*, that can generate free training labels automatically and encourage neural networks to learn powerful video representations. For example, as shown in Fig. 1.1, to predict future frames [6] can be a pretext task for self-supervised video representation learning. The assumption here is that the neural network can only succeed in these pretext tasks, including the future frame prediction task, when it understands the video content and learns powerful video representations.

Self-supervised learning can be considered as a subset of unsupervised learning since it does not require human annotated labels. While in order to evaluate the video representations learned by self-supervised pretext tasks from unlabeled video data, *downstream tasks* are usually adopted on some relatively small human-annotated datasets, *e.g.*, HMDB51 [35]. Typically, two types of application modes are used in evaluation: transfer learning (as an initialization model) and feature learning (as a feature extractor). Regarding transfer learning, backbone networks pre-trained with pretext tasks will be used as weight initialization and finetuned on human action recognition datasets [34, 35]. The other kind of evaluation mode is to use the pre-trained models as feature extractors for the downstream video analytic tasks, such as video retrieval [7, 36, 4], dynamic scene recognition [5, 37], *etc.* Without finetuning, such a mode can directly evaluate the generality and robustness of the learned features.

1.2 Related Work

In this section, we first introduce the most related works to ours, including supervised video representation learning, self-supervised image representation learning, and self-supervised video representation learning. Based on these works, we then discuss the limitations of current self-supervised video representation learning methods, which motivate our approaches presented in this thesis.

1.2.1 Supervised Video Representation Learning

Video understanding, especially action recognition, has been extensively studied for decades, where video representation serves as the fundamental problem of other video-related tasks, such as complex action recognition [38], action temporal localization [18, 19, 20], video captioning [21, 22], *etc.*

Initially, various handcrafted local spatio-temporal descriptors are proposed as video representations, such as STIP [23], HOG3D [24], *etc.* Wang *et al.* [25] proposed improved dense trajectories (iDT) descriptors, which combined the effective HOG, HOF [39] and MBH descriptors [40], and achieved the best results among all handcrafted features. Inspired by the impressive success of CNN in image understanding problem [49, 48] and with the availability of large-scale video datasets such as sports1M [29], ActivityNet [41], Kinetics-400 [11], Something-something [42], and Charades [43], studies on developing convolutional neural networks for video representation learning have attracted extensive interests.

According to the input modality, these network architectures for video representation learning can be roughly divided into two categories: one is to directly take RGB videos as inputs, while the other is to take both RGB videos and optical flows as inputs. Tran *et al.* [10] extended the 2D convolution kernels to 3D and proposed C3D network to learn spatio-temporal representations. Simonyan

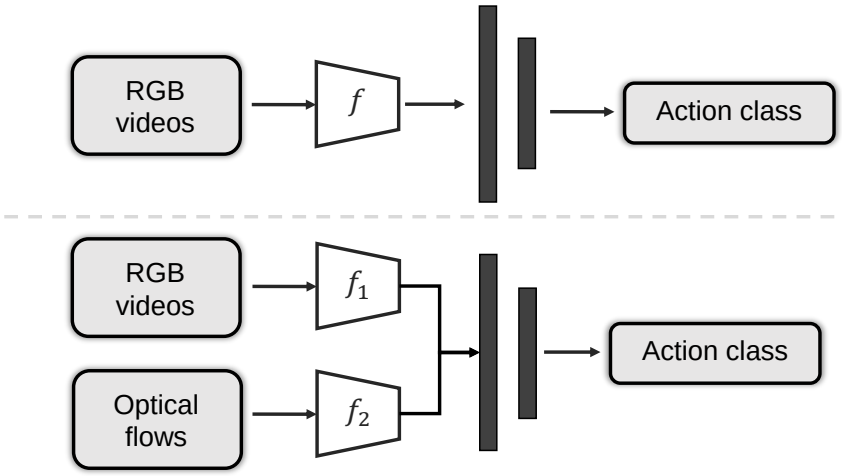

Figure 1.2: **Two classic neural network architectures for supervised video representation learning**. Top: a neural network directly takes the original RGB videos as inputs and learns spatio-temporal features. Bottom: two stream neural networks are used for video representation learning. One is appearance branch, which takes the original RGB videos as inputs. The other is motion branch, which takes pre-computed optical flows as inputs. And the output scores are fused to generate the final predicted probabilities.

and Zisserman [28] proposed a two-stream network that extracts spatial features from RGB inputs and temporal features from optical flows, followed by a fusion scheme. Fig. 1.2 shows the illustration of these two classic network architectures.

Based on these two classic methods, a series of neural network architectures are proposed to learn video representations, such as P3D [44], I3D [11], 3D-ResNet [45], R(2+1)D [26], S3D-G [46], slowfast networks [27], *etc.* In this thesis, instead of developing neural network architectures for video representation, our contributions lie in the development of novel and effective pretext tasks for self-supervised video representation learning. Therefore, following prior works [7, 114], we only use several popular networks, such as C3D [10] 3D-ResNet [45], *etc.*, to validate the proposed pretext tasks. More details of the network architectures are described in Sec.2.2.4.

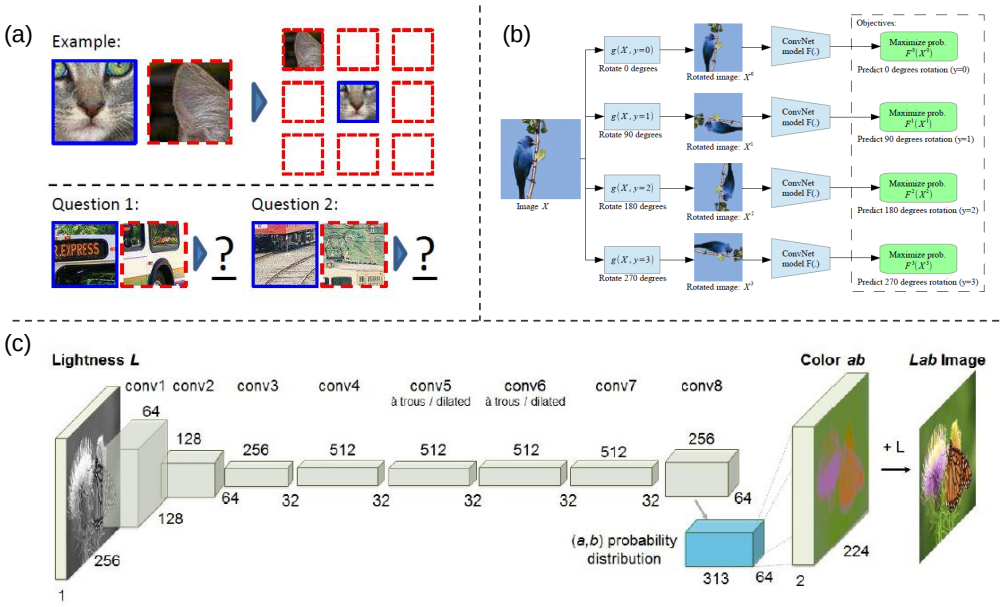

Figure 1.3: **Three exemplary pretext tasks for self-supervised image representation learning**. (a) Context prediction [1]. (b) Image rotation prediction [2]. (c) Gray image colorization [3].

1.2.2 Self-supervised Image Representation Learning

Self-supervised learning is first proposed and explored in image domain [1]. Despite the remarkable success achieved by image representation learning (image classification) with human annotated labels [47, 48, 49, 50, 51], the further development is reaching its bottleneck due to the lack of large amount of human-annotated images. Consequently, self-supervised learning is becoming increasingly attractive because of its great potential to leverage the large amount of unlabeled data.

Doersch *et al.* [1] proposed to use context-based prediction as a pretext task. Inspired by this work, various pretext tasks have been proposed for self-supervised image representation learning. Noroozi *et al.* [52] extended the context prediction task to a jigsaw puzzles task. Image colorization [3] proposed to cast the RGB

image into LAB color space and then use the network to colorize the gray images. Image rotation prediction [2] proposed to randomly rotate an image and then ask a neural network to predict the corresponding rotation angles. Despite its simplicity, the performance is quite remarkable. Some other pretext tasks include inpainting [53], clustering [54], super resolution [55], virtual primitives counting [56], *etc.* Fig. 1.3 illustrates the frameworks of these exemplary pretext tasks for self-supervised image representation learning. Very recently, contrastive learning in a self-supervised manner has shown great potential and achieved comparable results with supervised visual representation learning [32, 66, 67, 68, 69, 70].

1.2.3 Self-supervised Video Representation Learning

Taking inspiration from the success of self-supervised image representation learning, researchers explore to extend the self-supervised learning concept from image domain to video domain. In fact, self-supervised video representation learning is of more urgent necessity, as the annotation of videos is much more time-consuming compared with the annotation of images.

Various pretext tasks have been proposed for self-supervised video representation learning. Intuitively, a large number of studies [71, 72, 4] leveraged the distinctive temporal information of videos and proposed to use frame sequence ordering as their pretext tasks. Büchler *et al.* [73] further used deep reinforcement learning to design the sampling permutations policy for order prediction tasks. Gan *et al.* [5] proposed to learn video representations by predicting the optical flow or disparity maps between consecutive frames.

Although these methods demonstrate promising results, the learned representations are only based on one or two frames as they used 2D CNN for self-supervised learning. Consequently, some recent works [69, 36, 7, 74] proposed to use 3D CNNs as backbone networks for spatio-temporal representations learning,

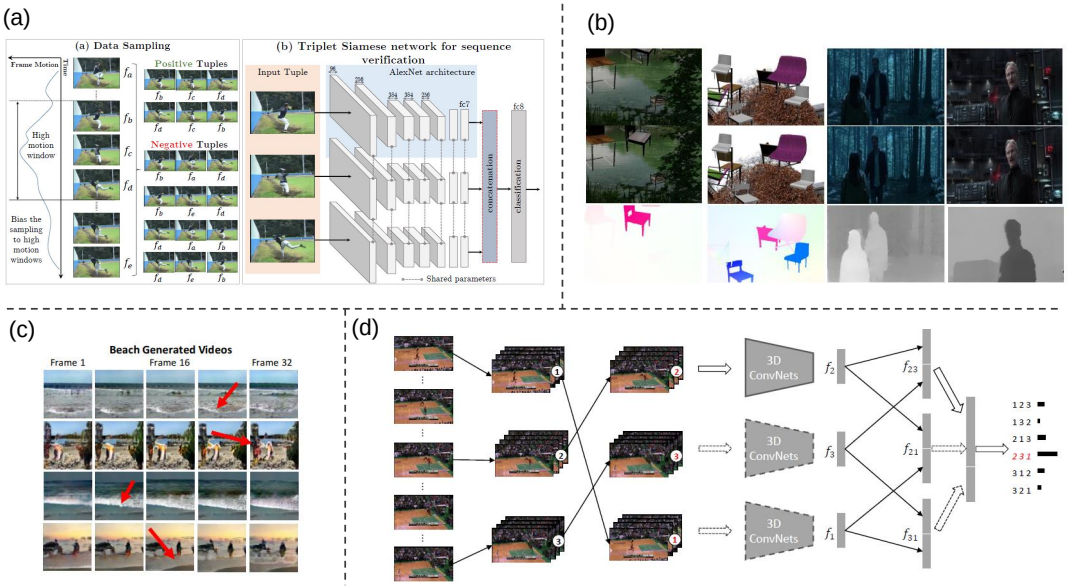

Figure 1.4: **Four exemplary pretext tasks for self-supervised video representation learning**. (a) Video order verification [4]. (b) Optical flows and disparity maps prediction [5]. (c) Future frames prediction [6]. (d) Video clips order prediction [7].

among which [74, 7, 36] extended the 2D frame ordering pretext tasks to 3D video clip ordering, and [69] proposed a pretext task to predict future frames embedding. Fig. 1.4 illustrates the frameworks of several exemplary pretext tasks for self-supervised video representation learning.

Self-supervised learning from cross-modality sources [75, 76, 33], *e.g.*, video and audio, also attracts considerable interests recently, as video sources inherently contain the audio data. A typical pretext is to recognize the synchronization between video and audio [75]. Alwassel *et al.* proposed to use cross-modal audio-video clustering [33] and by pre-training on a extreme large dataset IG65M [77] with millions of videos, this method for the first time achieved better performances than supervised learning with kinetics-400 [30] on the action recognition task [34, 35]. In this thesis, we focus on the video modality only and leave the potential

extension to multi-modality as our future research.

To summarize, prior pretext tasks proposed for self-supervised video representation learning can be roughly divided into two categories: (1) *generative approaches*, such as flow fields prediction [5], future frame prediction [78, 6], *etc.* (2) *discriminative approaches*, such as video order prediction [4, 71, 72, 7, 74], rotation transformation prediction [79], *etc.* Usually the performances of generative methods are not competitive with discriminative methods [7, 74]. We hypothesis that this is because the generative methods are more inclined to waste the model capacity towards learning the pretext task itself rather than learning the desired transferable video representations. To this end, in this thesis, pretext tasks proposed by us also fall into the discriminative category. Regarding the discriminative approaches, prior pretext tasks are mainly focused on video order prediction [4, 71, 72, 7, 74], which to some extent restricts the further development of self-supervised video representation learning. To solve this problem, in this thesis, we explore completely new perspectives and propose novel pretext tasks for self-supervised video representation learning.

1.3 Contributions

In this thesis, we focus on the self-supervised video representation learning problem and aim to propose novel pretext tasks that can encourage neural networks to learn expressive video representations without human annotated labels.

The contributions of this thesis are summarized as follows:

- We propose a novel pretext task, spaito-temporal statistics regression, for self-supervised video representation learning. It aims to encourage a neural network to regress both motion and appearance statistics along the spatio-temporal axes. Unlike prior works that are concentrated on or to some

extent confined to the video order conception, this pretext task presents a completely new perspective for self-supervised video representation learning. It is also the first work that uses 3D convolutional neural network to learn spatio-temporal features in a self-supervised manner. By using a classic and simple neural network C3D, the proposed spaito-temporal statistics regression task can already achieve competitive results. Related Work has been published in *Proceedings of IEEE Conference on Computer Vision and Pattern Recognition 2019 [80]*.

- We further propose a novel pretext task, video pace prediction, which, unlike prior works including the proposed statistics pretext task, does not require the usage of pre-computed optical flow and thus, is more preferable in real world applications with millions/trillions of unlabeled videos. In addition, we are also the first to introduce contrastive learning for self-supervised video representation learning based on two strategies: same pace and same context. It must be remarked that due to the simplicity and effectiveness of the pace prediction task, it will motivate a wide rage of applications in the future. For example, the pace prediction task can be used an auxiliary loss to further improve video representation learning, or an exemplary task to investigate the essence or principles of self-supervised video representation learning. Related Work has been published in *Proceedings of the European conference on computer vision 2020 [81]*.

- Last but not least, by systematically investigating the architecture of backbone networks, the scale of pre-training dataset, and the learning strategies, we drastically improve the performance of self-supervised video representation learning, for the first time *outperforming fully supervised pre-training on ImageNet*. We extend the research scope from simply designing pretext

tasks to in-depth investigation of network architectures, feature transferability, curriculum learning strategies, *etc.* We conduct extensive experiments and uncover three fundamental insights to further boost performance of self-supervised video representation learning: (1) Architectures of backbone networks play an important role in self-supervised learning. However, no best model is guaranteed for different pretext tasks. In most cases, the combination of 2D spatial convolution and 1D temporal convolution achieves better results. (2) Downstream task performances are log-linearly correlated with the pre-training dataset scale. Attentive selection should be given on the training samples. (3) We demonstrate that features learned in a self-supervised manner are more generalizable and transferable than features learned in a supervised manner. Related work is submitted to *IEEE Transactions on Pattern Analysis and Machine Intelligence* as an extension of the proposed spatio-temporal statistics pretext task work [80].

With the works presented in this thesis, we provide novel insights and take a lead in self-supervised video representation learning, a newly-developed yet promising field. The code and pre-trained models of these works are all provided online to facilitate future research.

1.4 Organization

In the remainder of this thesis, we first elaborate on the spatio-temporal statistics regression pretext task, with a preliminary validation of its effectiveness on several downstream tasks in Chapter 2. Then in Chapter 3, we take an in-depth investigation on the proposed sptio-temporal statistics. Extensive experiments are conducted to understand the proposed approach and to uncover crucial insights on self-supervised video representation learning in a general perspective.

In Chapter 4, we further propose a simple-yet-effective pretext task – pace prediction, to dispense with the usage of optical flow in the spatio-temporal statistics pretext task. Finally, in Chapter 5, we summarize this thesis and discuss on some future directions based on the findings illustrated in the thesis.

□ End of chapter.

Chapter 2

Spatio-temporal Statistics Regression for Self-supervised Video Representation Learning

2.1 Motivation

Powerful video representations serve as the foundations for solving many video content analysis and understanding tasks, such as action recognition [11, 15], video retrieval [16, 17], video captioning [21, 22], *etc*. Various network architectures [28, 11, 26] are designed and trained with massive human-annotated video data to learn video representations for individual tasks specifically. While great progresses have been made, supervised video representation learning is impeded by a major obstacle that the annotation of video data is labour-intensive and expensive, thus restricting supervised learning to relish a large quantity of free video resources on the Internet.

To tackle the aforementioned challenge, multiple approaches [4, 72, 74, 7] have emerged to learn more generic and robust video representations in a self-

supervised manner. Neural network are first pre-trained with unlabeled videos using some *pretext tasks*, where supervision signals are derived from input data without human annotations. Then the learned representations can be employed as weight initialization for training models or be directly used as features in succeeding *downstream tasks*.

Among the existing self-supervised video representation learning methods, video order verification/prediction [4, 71, 72, 74, 7] is one of the most popular pretext tasks. It randomly shuffles video frames and asks a neural network to predict whether the video is perturbed or to rearrange the frames in a correct chronological order. By utilizing the intrinsic temporal characteristics of videos, these pretext tasks have been shown useful for learning high-level semantic features. However, the performances of these approaches are limited since the contents of individual frames are mostly unexploited during learning. Other approaches include flow fields prediction [5], future frame prediction [6, 82, 83], dense predictive coding [69], *etc*. Although promising results have been achieved, the above mentioned pretext tasks may lead to redundant feature learning towards solving the pretext task itself, instead of learning generic representative features for downstream video analytic tasks. For example, predicting the future frame requires the network to precisely estimate each pixel in each frame in a video clip. This increases the learning difficulties and causes the network to waste a large portion of the capacity on learning features that may be not transferable to high-level video analytic tasks.

In this work, we argue that a pretext task should be intuitive and relatively simple to learn, enlightened by the human visual system, and mimicking the video understanding process of humans. To this end, we propose a novel pretext task to learn video representations by regressing spatio-temporal statistical summaries from unlabeled videos. For instance, given a video clip, the network is encouraged

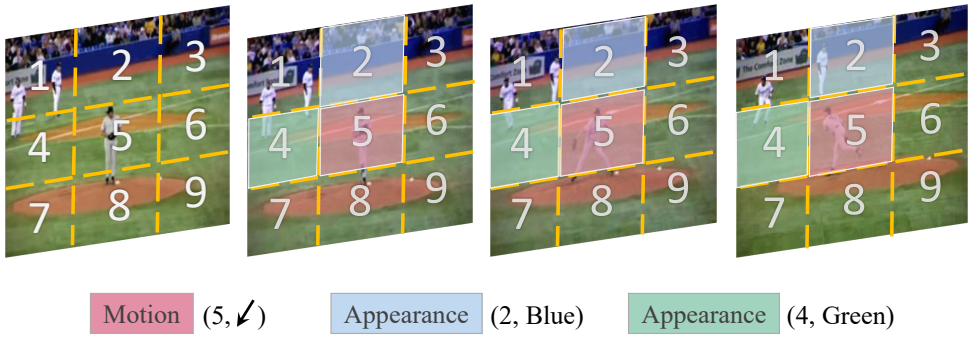

Figure 2.1: **The main idea of the proposed spatio-temporal statistics.** Given a video sequence, we design a pretext task to regress the summaries derived from spatio-temporal statistics for video representation learning without human-annotated labels. Each video frame is first divided into several spatial regions using different partitioning patterns like the grid shown in the figure. Then the derived statistical labels, such as *the region with the largest motion and its direction* (the red patch), *the most diverged region in appearance and its dominant color* (the blue patch), and *the most stable region in appearance and its dominant color* (the green patch), are employed as supervision signals to guide the representation learning.

to identify the largest moving area with its corresponding motion direction, as well as the most rapidly changing region with its dominant color. Fig. 2.1 shows the main idea of the proposed spatio-temporal statistics. The idea is inspired by the cognitive study on human visual system [84], in which the representation of motion is found to be based on a set of learned patterns. These patterns are encoded as sequences of 'snapshots' of body shapes by neurons in the *form pathway*, and by sequences of complex optic flow patterns in the *motion pathway*. In our work, these two pathways are defined as the appearance branch and motion branch, respectively. In addition, we define and extract several abstract statistical summaries accordingly, which is also inspired by the biological hierarchical perception mechanism [84].

We design several spatial partitioning patterns to encode each spatial location and its spatio-temporal statistics over multiple frames, and use the encoded

vectors as supervision signals to train the neural network for spatio-temporal representation learning. The novel objectives are simple to learn and informative for the motion and appearance distributions in videos, *e.g.*, the spatial locations of the most dominant motions and their directions, the most consistent and the most diverse colors over a certain temporal cube, *etc.* We conduct extensive experiments with 3D convolutional neural networks to validate the effectiveness of the proposed approach. The experimental results show that, compared with training from scratch, pre-training using our approach demonstrates a large performance gain for video action recognition problem. By transferring the learned representations to dynamic scene recognition task, we further demonstrate the generality and robustness of the video representations learned by the proposed approach.

2.2 Proposed Approach

In the following, we introduce the implementation details of the proposed regressing spatio-temporal statistics pretext task, including a preliminary illustration of the statistical concepts (Sec. 2.2.1), formal definition of the motion statistics and appearance statistics (Sec. 2.2.2 and 2.2.3), and the learning framework of the pretext task (Sec. 2.2.4).

2.2.1 Statistical Concepts

Inspired by human visual system, we break the process of video contents understanding into several questions and encourage a CNN to answer them accordingly: (1) Where is the largest motion in a video? (2) What is the dominant direction of the largest motion? (3) Where is the largest color diversity and what is its dominant color? (4) Where is the smallest color diversity, *e.g.*, the potential back-

ground of a scene, and what is its dominant color? The motivation behind these questions is that the human visual system [84] is sensitive to large motions and rapidly changing contents in the visual field, and only needs impressions about rough spatial locations to understand the visual contents. We argue that a good pretext task should be able to capture necessary representations of video contents for downstream tasks, while at the same time does not waste model capacity on learning too detailed information that is not transferable to other downstream tasks. To this end, we design our pretext task as learning to answer the above questions with only rough spatio-temporal statistical summaries, *e.g.*, for spatial coordinates we employ several spatial partitioning patterns to encode rough spatial locations instead of exact spatial Cartesian coordinates. In the following, we use a simple illustration to explain the basic idea.

Fig. 2.2 shows an example of a three-frame video clip with two moving objects (blue triangle and green circle). A typical video clip usually contains much more frames while here we use the three-frame clip example for a better understanding of the key ideas. To roughly represent the location and quantify "where", each frame is divided into 4-by-4 blocks and each block is assigned to a number in an ascending order starting from 1 to 16. The blue triangle moves from block 4 to block 7, and the green circle moves from block 11 to block 12. Comparing the moving distances, we can easily find that the motion of the blue triangle is larger than the motion of the green circle. The largest motion lies in block 7 since it contains moving-in motion between frames t and $t+1$, and moving-out motion between frames $t+1$ and $t+2$. Regarding the question "*what is the dominant direction of the largest motion?*", it can be easily observed that in block 7, the blue triangle moves towards lower-left. To quantify the directions, the full angle 360° is divided into eight angle pieces, with each piece covering a 45° motion direction range, as shown on the right side in Fig.2.2. Similar to location quantification,

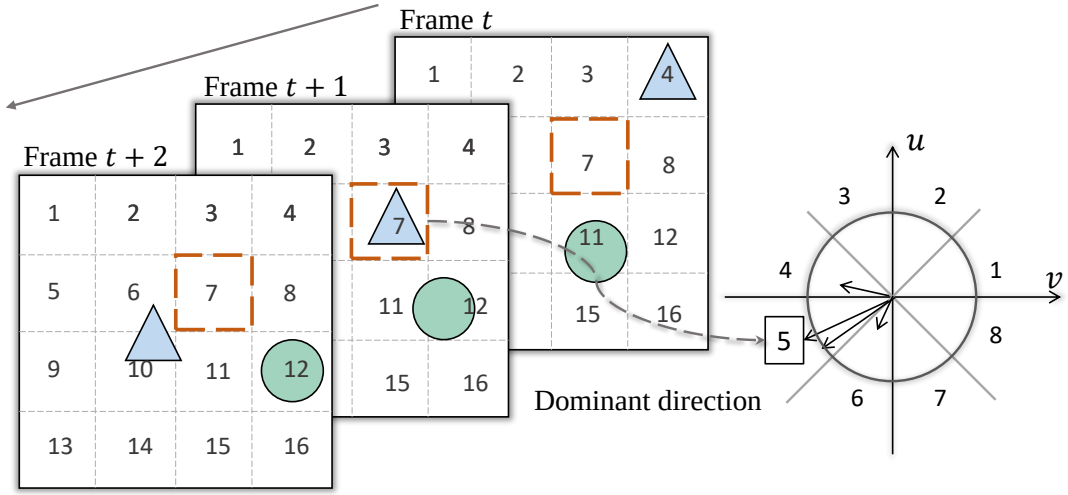

Figure 2.2: **The illustration of extracting statistical labels in a three-frame video clip.** Detailed explanation is presented in Sec. 2.2.1.

each angle piece is assigned to a number in an ascending order counterclockwise. The corresponding angle piece number of "lower-left" is 5.

The above illustration explains the basic idea of extracting statistical labels for motion characteristics. To further consider appearance characteristics "*where is the largest color diversity and its dominant color?*", both block 7 and block 12 change from the background color to the moving object color. When considering that the area of the green circle is larger than the area of the blue triangle, we can tell that the largest color diversity location lies in block 12 and the dominant color is green.

Keeping the above ideas in mind, we next formally describe the approach to extract spatio-temporal statistical labels for the proposed pretext task. We assume that by training a spatio-temporal CNN to disclose the motion and appearance statistics mentioned above, better spatio-temporal representations can be learned, which will benefit the downstream video analytic tasks consequently.

2.2.2 Motion Statistics

Optical flow is a commonly used feature to represent motion information in many action recognition methods [28, 11]. In the self-supervised learning paradigm, predicting optical flow between every two consecutive frames is leveraged as a pretext task to pre-train the deep model, *e.g.*, [5]. Here we also leverage optical flow estimated from a conventional non-parametric coarse-to-fine algorithm [85] to derive the motion statistical labels that are regressed in our approach.

However, we argue that there are two main drawbacks when directly using dense optical flow to compute the largest motion in our pretext task: (1) optical flow based methods are prone to being affected by camera motion, since they represent the absolute motion [40, 86]. (2) Dense optical flow contains sophisticated and redundant information for statistical labels computation, thus increasing the learning difficulty and leading to network capacity waste for self-supervised representation learning. To mitigate the influence from the above problems, we instead seek to use a more robust and sparse feature – motion boundary [40].

Motion Boundary

Denote the horizontal and vertical components of optical flow as u and v, respectively. Motion boundaries are derived by computing the x- and y-derivatives of u and v, respectively:

$$m_u = (u_x, u_y) = (\frac{\partial u}{\partial x}, \frac{\partial u}{\partial y}),\ m_v = (v_x, v_y) = (\frac{\partial v}{\partial x}, \frac{\partial v}{\partial y}), \tag{2.1}$$

where m_u is the motion boundary of u and m_v is the motion boundary of v. As motion boundaries capture changes in the flow field, constant or smoothly varying motion, such as motion caused by camera view change, will be cancelled out. Specifically, given an N-frame video clip, $(N-1)*2$ motion boundaries are

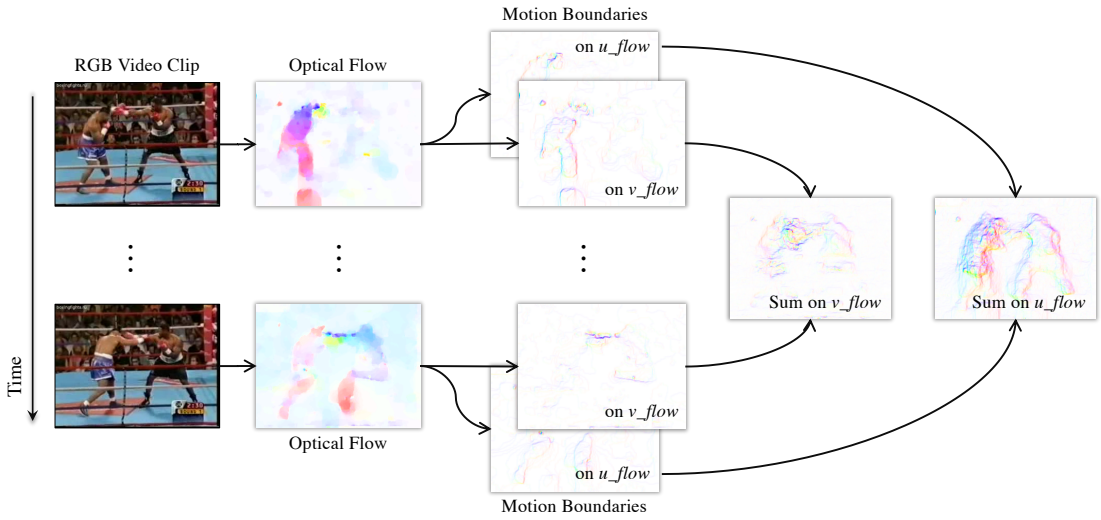

Figure 2.3: **Motion boundaries computation.** For a given input video clip, we first extract optical flow across each frame. For each optical flow, two motion boundaries are obtained by computing gradients separately on the horizontal and vertical components of the optical flow. The final sum-up motion boundaries are obtained by aggregating the motion boundaries on *u_flow* and *v_flow* of each frame separately.

computed based on $N-1$ optical flows. Only motion boundaries information is kept, as shown in Figure 2.3. Diverse video motion information can be encoded into two summarized motion boundaries by summing up all these $(N-1)$ sparse motion boundaries m_u and m_v:

$$M_u = (\sum_{i=1}^{N-1} u_x^i, \sum_{i=1}^{N-1} u_y^i), \;\; M_v = (\sum_{i=1}^{N-1} v_x^i, \sum_{i=1}^{N-1} v_y^i), \tag{2.2}$$

where M_u denotes the summarized motion boundaries on horizontal optical flow u, and M_v denotes the summarized motion boundaries on vertical optical flow v.

Spatial-aware Motion Statistical Labels

Based on motion boundaries, we next describe how to compute the spatial-aware motion statistical labels that describe the largest motion location and the dom-

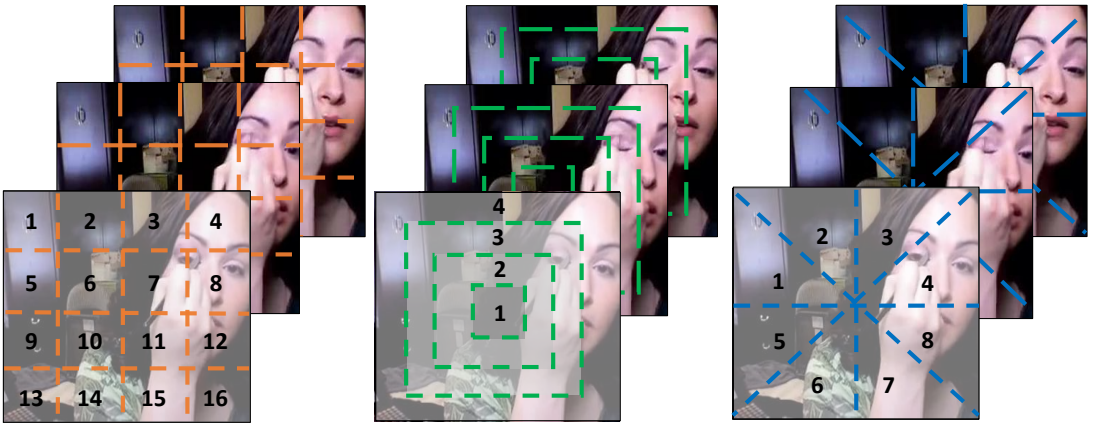

(a) Pattern 1 (b) Pattern 2 (c) Pattern 3

Figure 2.4: **Three different partitioning patterns.** They are used to divide video frames into different spatial regions. Each spatial block is assigned with a number to represent its location.

inant direction of the largest motion. Given a video clip, we first divide it into spatial blocks using partitioning patterns as shown in Fig 2.4. Here, we introduce three simple yet effective patterns: pattern 1 divides each frame into 4×4 grids; pattern 2 divides each frame into 4 different non-overlapped areas with the same gap between each block; pattern 3 divides each frame by two center lines and two diagonal lines. Then we compute summarized motion boundaries M_u and M_v as described in Eq. 2.2. Motion magnitude and orientation of each pixel can be obtained by casting M_u and M_v from the Cartesian coordinates to the Polar coordinates.

We take pattern 1 as an example to illustrate how to generate the motion statistical labels, while other patterns follow the same procedure. For the *largest motion location labels*, we first compute the average magnitude of each block, ranging from block 1 to block 16 in Pattern 1. Then we compare and find out block B with the largest average magnitude from the 16 blocks. The index number of B is taken as the largest motion location label. Note that the largest

motion locations computed from M_u and M_v can be different. Therefore, two corresponding labels are extracted from M_u and M_v, respectively.

Based on the largest motion block, we compute the *dominant orientation label*, which is similar to the computation of motion boundary histogram (MBH) [40]. We divide 360° into 8 bins evenly, and assign each bin to a number to represent its orientation. For each pixel in the largest motion block, we use its orientation angle to determine which angle bin it belongs to and add the corresponding magnitude value into the angle bin. The dominant orientation label is the index number of the angle bin with the largest magnitude sum. Similarly, two orientation labels are extracted from M_u and M_v, respectively.

Global Motion Statistical Labels

We further propose global motion statistical labels that provide complementary information to the local motion statistics described above. Specifically, given a video clip, the model is asked to predict the frame index (instead of the block index) with the largest motion. To succeed in such a pretext task, the model is encouraged to understand the video contents from a global perspective. Motion boundaries m_u and m_v between every two consecutive frames are used to calculate the largest motion frame index accordingly.

The implementation details of how to generate the motion statistical labels are shown in Algorithm 1 in the following. By using this algorithm, with inputs horizontal and vertical optical flow set $(\boldsymbol{U}, \boldsymbol{V})$, partitioning patterns P_1, P_2, and P_3, we will get motion statistical labels $\boldsymbol{y}_{mot}$ as output.

Algorithm 1 Generating motion statistical labels.

Input: Horizontal and vertical optical flow set $(\boldsymbol{U}, \boldsymbol{V})$, partitioning patterns P_1, P_2, and P_3.
Output: Motion statistical labels $\boldsymbol{y}_{mot}$.

Sample mini-batch optical flow clips with each clip containing $N-1$ frames
for mini-batch optical flow clips $\{(\boldsymbol{u}_1, \boldsymbol{v}_1), \ldots, (\boldsymbol{u}_m, \boldsymbol{v}_m)\}$ **do**
  for $i = 1$ to m **do**
    Initialize $M_u^i = (0, 0)$, $M_v^i = (0, 0)$
    for $j = 1$ to $N-1$ **do**
      $m_u^j = (\frac{\partial u_i^j}{\partial x}, \frac{\partial u_i^j}{\partial y})$
      $m_v^j = (\frac{\partial v_i^j}{\partial x}, \frac{\partial v_i^j}{\partial y})$
      $M_u^i = M_u^i + m_u^j$
      $M_v^i = M_v^i + m_v^j$
    end for
    $M_u^i \rightarrow (mag_u^i, ang_u^i)$, $M_v^i \rightarrow (mag_v^i, ang_u^i)$.
    for $j = 1$ to 3 **do**
      Divide M_u^i and M_v^i by pattern P_j
      Compute local motion statistical labels (p_u, o_u, p_v, o_v)
    end for
    Compute global motion statistical labels (I_u, I_v)
    Obtain motion label y_{mot}^i
  end for
end for

2.2.3 Appearance Statistics

Spatio-temporal Color Diversity Labels

Given an N-frame video clip, we divide it into spatial video blocks by patterns described above, same as the motion statistics. For an N-frame video block, we compute the 3D distribution V_i in 3D color space of each frame i. We then use the Intersection over Union (IoU) along the temporal axis to quantify the spatio-temporal color diversity as follows:

$$\text{IoU}_{score} = \frac{V_1 \cap V_2 \cap ... \cap V_i ... \cap V_N}{V_1 \cup V_2 \cup ... \cup V_i ... \cup V_N}. \tag{2.3}$$

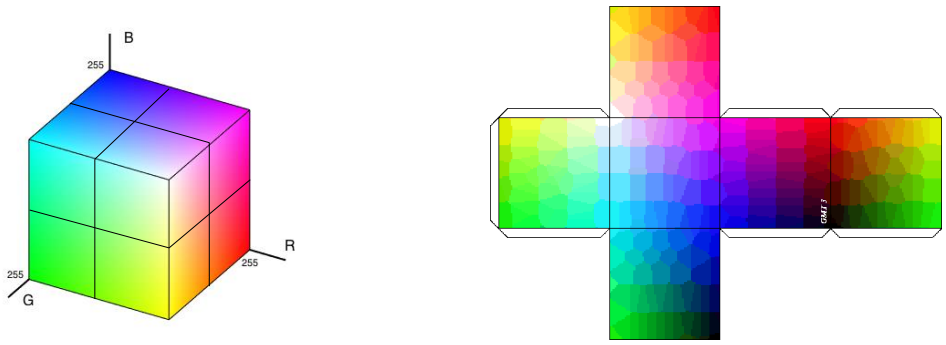

(a) 3D RGB color space

(b) Unpacked RGB color space

Figure 2.5: **Illustration of RGB color space.** (a) Illustration of the divided 3D color space with 8 bins. (b) An unpacked 2D RGB color space [8].

The largest color diversity location is the block with the smallest IoU_{score}, while the smallest color diversity location is the block with the largest IoU_{score}. In practice, we calculate the IoU_{score} on R, G, B channels separately and compute the final IoU_{score} by averaging them.

Dominant Color Labels

Based on the two video blocks with the largest/smallest color diversity, we compute the corresponding dominant color labels. We divide the 3D RGB color space into 8 bins evenly and assign each bin with an index number. Then for each pixel in the video block, based on its RGB value, we assign a corresponding color bin number to it. Finally, color bin with the largest number of pixels is the label for the dominant color. Fig. 2.5 shows the illustration of the color space.

Global Appearance Statistical Labels

We also propose global appearance statistical labels to provide supplementary information. Particularly, we use the dominant color of the whole video (instead

of a video block) as the global appearance statistical label. The computation method is the same as the one described above.

The implementation details of how to generate the appearance statistical labels are shown in Algorithm 2 in the following. By using this algorithm, with inputs video set $\boldsymbol{X}$, partitioning patterns P_1, P_2, and P_3., we will get motion statistical labels $\boldsymbol{y}_{app}$ as output.

Algorithm 2 Generating appearance statistical labels.

Input: Video set $\boldsymbol{X}$, partitioning patterns P_1, P_2, and P_3.
Output: Appearance statistical labels $\boldsymbol{y}_{app}$.

Sample mini-batch video clips with each clip containing N frames
for mini-batch video clips $\{\boldsymbol{x}_1, \ldots, \boldsymbol{x}_m\}$ **do**
  for $i = 1$ to m **do**
    for $j = 1$ to 3 **do**
      Divide $\boldsymbol{x}_i$ by pattern P_j, obtain blocks $\boldsymbol{B}_i$
      ALL_IoU$_{score}$ = []
      for block in $\boldsymbol{B}_i$ **do**
        Compute IoU$_{score}$ = $\frac{V_1 \cap V_2 \cap ... \cap V_i ... \cap V_N}{V_1 \cup V_2 \cup ... \cup V_i ... \cup V_N}$
        Add IoU$_{score}$ to ALL_IoU$_{score}$
      end for
      p_l = min(ALL_IoU$_{score}$)
      p_s = min(ALL_IoU$_{score}$)
      Compute dominant color c_l, c_s by $B_i^{p_l}, B_i^{p_s}$
    end for
    Compute global dominant color$C$
    Obtain appearance label y_{app}^i
  end for
end for

2.2.4 Learning with Spatio-temporal CNNs

In the following, we first elaborate on the spatio-temporal CNN in details and then present how to use the state-of-the-art backbone network for self-supervised video representation learning with the proposed statistics pretext task.

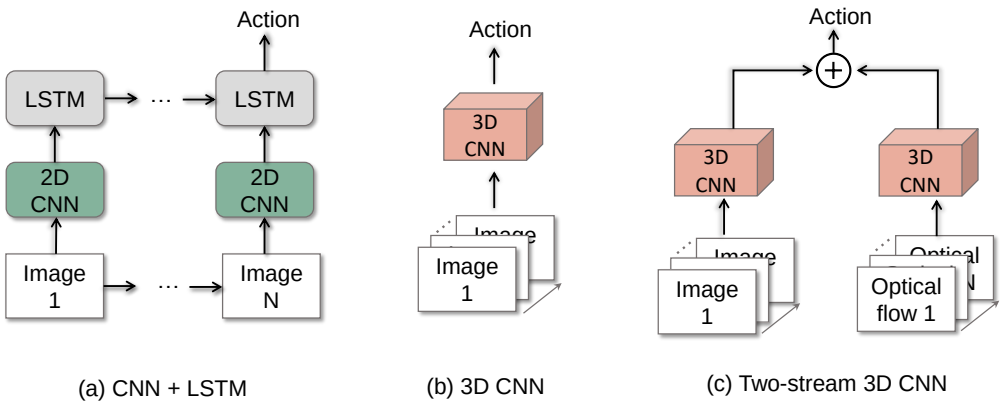

Figure 2.6: Three network architectures for video representation learning: (a) CNN+LSTM [1, 9] (b) 3D CNN [10] (c) Two-stream 3D CNN [11].

Spatio-temporal CNN

Convolutional neural networks (CNN) usually consists of three kinds of building blocks: convolutional layers, pooling layers, and fully connected layers. Given an input image, convolutional layers, the core building block, slide across the input volume and computes dot products between the entries of the filter and the input volume. A pooling layer is usually adopted after each convolutional layer to reduce the spatial size of the representation and the number of parameters in the network, by sliding across the input volume and computing the average/maximum value in the small window. The fully connected layer connects to all activations in the previous layer and finally predicts the desired output. Finally, the CNN is trained to minimize the training errors between the training targets and the predicted outputs iteratively. A comprehensive introduction of convolutional neural networks can be found in [87].

Inspired by the great success of CNN in image domain [49, 48], researchers seek to extend the convolutional neural networks to video domain, where the fundamental problem is to model the temporal information and extract powerful spatio-temporal features by designing different backbone network architec-

tures. Fig. 2.6 shows three basic network architectures for video representation learning:(1) CNN+LSTM [88, 9], which extracts frame-level features by using a 2D CNN and then progressively uses recurrent layer, Long Short-Term Memory (LSTM) [89], for temporal modeling. (2)3D CNN [10], which extends the 2D convolutional kernels to 3D convolutional kernels for spatio-temporal representations learning. (3) Two stream 3D CNN [11], which extracts spatial features from RGB inputs in spatial stream and temporal features from optical flows in temporal stream, and finally fuses the performances from these two streams.

In this thesis, we mainly focus on the development of novel pretext tasks for self-supervised video representation learning; therefore, we will not investigate and improve the network architectures. Instead, we use these state-of-the-art networks as off-the-shelf tools to learn video representations by our proposed pretext tasks. Actually, the proposed approaches in this thesis is model-agnostic and can be applied to any of the three basic network architectures. While in this work, to align the experimental setup with prior works [5, 72], we first use the classic 3D CNN, C3D [10], as the backbone network for self-supervised video representation learning. In order to have a fair comparison with previous methods which use CaffeNet [90] as their backbone networks, in this work, we adopt a light C3D architecture with only five convolutional layers, five pooling layers and three fully connected layers as described in [10]. The details of the network architecture are shown in Table 2.1.

Learning Spatio-temporal Statistics

The proposed Spatio-temporal Statistics prediction task is formulated as a regression problem. The whole framework of the proposed method is shown in Figure 2.7. For each local motion pattern, 4 ground-truth labels are to be regressed. p_u, o_u represent the spatial location of the largest magnitude based

Table 2.1: The detailed network architectures of the proposed approach. We use a light C3D [10] as the backbone network and follow the same network parameters setting as in [10], where the authors empirically investigated the best kernel size, depth, *etc.*

stage	Motion	Appearance	Output sizes
Raw input	-	-	3 x 16 x 112 x 112
Conv 1	*channel* 64, *kernel* 3, *stride* 1		64 x 16 x 112 x 112
Pool 1	*kernel* 1,2,2, *stride* 1,2,2, *pad* 0		64 x 16 x 56 x 56
Conv 2	*channel* 128, *kernel* 3, *stride* 1		128 x 16 x 56 x 56
Pool 2	*kernel* 2 *stride* 2, *pad* 0		128 x 8 x 28 x 28
Conv 3	*channel* 256, *kernel* 3, *stride* 1		256 x 8 x 28 x 28
Pool 3	*kernel* 2 *stride* 2, *pad* 0		256 x 4 x 14 x 14
Conv 4	*channel* 256, *kernel* 3, *stride* 1		256 x 4 x 14 x 14
Pool4	*kernel* 2 *stride* 2, *pad* 0		256 x 2 x 7 x 7
Conv 5	*channel* 256, *kernel* 3, *stride* 1		256 x 2 x 7 x 7
Pool 5	*kernel* 2 *stride* 2, *pad* 1		256 x 1 x 4 x 4
Fc 6	2048	2048	2048
Fc 7	2048	2048	2048
Output	*Motion labels*, 14	*Appearance labels*, 13	14/13

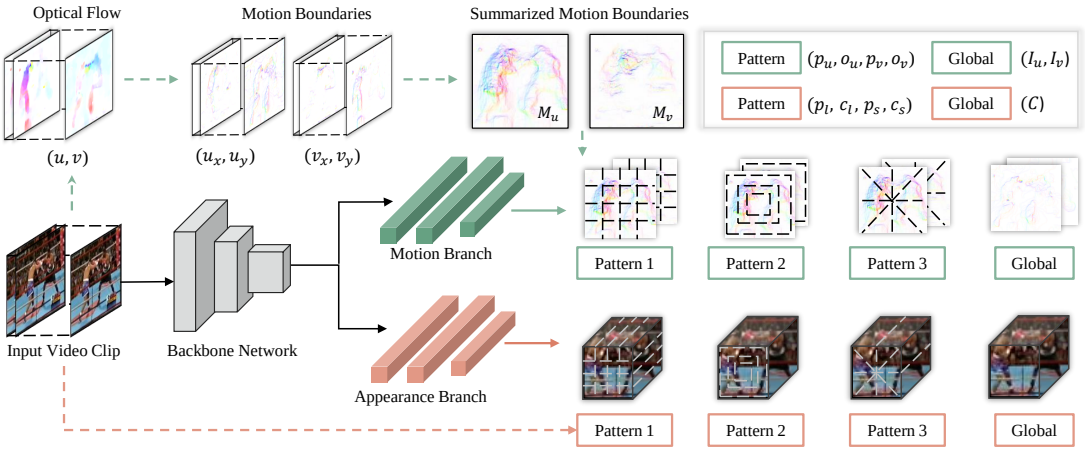

Figure 2.7: **The network architecture of the proposed method.** Given a video clip, 14 motion statistical labels and 13 appearance statistical labels are to be regressed. The motion statistical labels are computed from summarized motion boundaries. The appearance statistical labels are computed from input video clip.

on M_u and its corresponding orientation; p_v, o_v represent the spatial location of the largest magnitude based on M_v and its corresponding orientation. Two global motion statistical labels to be regressed are I_u, I_v– the frame indices of the largest magnitude sum w.r.t. m_u and m_v. For each local appearance pattern, 4 ground-truth labels are to be regressed. p_l, c_l are the spatial location of the largest color diversity and its corresponding dominant color; p_s, c_s are the spatial location of the smallest color diversity and its corresponding dominant color. The dominant color of the whole video, *i.e.*, the global appearance statistics label, to be regressed is denoted as C. We use two branches to regress motion statistical labels and appearance statistical labels separately. For each branch, two fully connected layers are used similarly to the original C3D model design. And we replace the final soft-max loss layer with a fully connected layer, with 14 outputs for the motion branch and 13 outputs for the appearance branch.

L_2-norm is leveraged as the loss function to measure the difference between

target statistical labels and the predicted labels. Formally, the loss function is defined as follow:

$$\mathcal{L} = \lambda_{mot}\|\hat{\boldsymbol{y}}_{mot} - \boldsymbol{y}_{mot}\|_2 + \lambda_{app}\|\hat{\boldsymbol{y}}_{app} - \boldsymbol{y}_{app}\|_2, \tag{2.4}$$

where $\hat{\boldsymbol{y}}_{mot}$, $\boldsymbol{y}_{mot}$ denote the predicted and target motion statistical labels, and $\hat{\boldsymbol{y}}_{app}$, $\boldsymbol{y}_{app}$ denote the predicted and target appearance statistical labels. λ_{mot} and λ_{app} are the weighting parameters that are used to balance the two loss terms.

2.3 Experimental Setup

We illustrate the basic experimental setup to validate the proposed method in the following, including the datasets and the implementation details.

2.3.1 Datasets

In this work, we consider three datasets: UCF101 [34], HMDB51 [35], and YU-PENN [37]. Specifically, we use UCF101 for self-supervised pre-training and the other datasets for evaluation.

UCF101 dataset [34] consists of 13,320 video samples with 101 action classes. It is collected from YouTube and actions are all naturally performed. Videos in it are quite challenging due to the large variation in human pose and appearance, object scale, light condition, camera view and *etc.* It contains three train/test splits. In our experiment, we use the first train split to pre-train C3D, following prior works [7, 4]. Regarding evaluation, we use train/test split 1.

HMDB51 dataset [35] is a relatively smaller dataset which contains 6766 videos with 51 action classes. It also consists of three train/test splits. In our experiment, to have fair comparison with others [7, 5], we use HMDB51 train split 1 to finetune

the pre-trained models and test the action recognition accuracy on HMDB51 test split 1.

YUPENN dataset [37] is a dynamic scene recognition dataset which contains 420 video samples of 14 dynamic scenes. We follow the recommended leave-one-out evaluation protocol [37] when evaluating the proposed method.

2.3.2 Implementation Details

We implement our approach and conduct experiments using PyTorch framework [91] on a single Titan RTX GPU [92] with 24GB memory, which is favorable for processing video clips with longer length. During the implementation, we find that the pre-processing of video data consumes most of the computational time. To solve this problem, we use solid-state disks to store the video data, which drastically reduces the video data reading time and consequently reduces the entire training time. Typically, it only takes 12 hours to train the proposed pretext task on the UCF101 dataset (self-supervised video representation learning) and another 12 hours to finetune on the labeled UCF101 dataset (downstream task). In the following, we elaborate on the implementation details of data augmentation methods, training schedule, and parameters settings.

Pre-training. Following prior works [10, 26], when pre-training on the UCF101 dataset, the batch size is set to 30 and SGD is used as the optimizer. Regarding data augmentation, both spatial jittering and temporal jittering are adopted. Each frame in a video clip is resized to 128×171 and then randomly cropped to 112×112. For each training video, 16 frames video clip are randomly sampled from it. Regarding the most important hyper-parameter, initial learning rate, we empirically find that the optimal one is 0.001 by grid search in a coarse-to-fine manner as common practices [93]. Besides, we also adopt a learning rate decay when the validation loss plateaus following prior works [10, 26]. Specifically, the

Table 2.2: Comparison different patterns of motion statistics for action recognition on UCF101.

Initialization	Accuracy (%)
Random	45.4
Motion pattern 1	53.8
Motion pattern 2	53.2
Moiton pattern 3	54.2

learning rate is divide it by 10 every 6 epochs and the training process is stopped at 18 epochs.

Transfer learning. After pre-training with the pretext task, we first evaluate the learned video representations on action recognition task by transfer learning. Typically, following prior works [5, 4], the conv layers weights are retained from the pre-trained network. And we re-initialize the fully-connected layers for action classification. The neural network is then trained action recognition datasets, UCF101 or HMDB51. The training schedule is the same as the pre-training procedure, except the optimal initial learning rate is re-searched and set to 0.003. When testing, center crop is applied and we report the average clip accuracy.

Feature Learning. We further evaluate the learned representations directly without fine-tuning on the action recognition task. Specifically, the learned models are used as feature extractors and the learned representations are evaluated on a dynamic scene recognition task following [5].

2.4 Ablation studies

In this section, we study the effectiveness of each component of the proposed spatio-temporal statistics on action recognition downstream task. Specifically, we use UCF101 training split 1 to pre-train the C3D backbone network. UCF101

training/testing split 1 and HMDB51 training/testing split 1 are used for evaluation.

Pattern

We study the performances of three partitioning patterns as described in Sec. 2.2.2. Specifically, we use the motion statistics and appearance statistics follow the same trend. As shown in Table 2.2, all the three patterns outperform the random initialization, *i.e.*, train from scratch setting, by around 8%, which strongly proves that our motion statistics is a very useful task. And all three patterns achieve comparable results.

Local *v.s.* Global

We study the performances of local statistics, *where is the largest motion location?*, global statistics, *which is the largest motion frame?*, and their ensemble. As can be seen in Table 2.3, when the three local patterns are combined together, we can further get around 1.5% improvement, compared to single pattern (Table 2.2). The global statistics also serves as a useful supervision signal with an improvement of 3%. All motion statistics labels (all three patterns and global statistics) achieve 57.8% accuracy on the UCF101 dataset, which outperforms the random initialization by 12.4%.

Motion, RGB, and Joint Statistics

We finally analyze the performances of motion statistics, appearance statistics, and their combination, in Table 2.4. It can be seen that both appearance and motion statistics serve as useful self-supervised signals for action recognition problem. But the motion statistics is more powerful as the temporal information appears to be more important for action recognition task. When combined motion

Table 2.3: Comparison of local and global motion statistics for action recognition on the UCF101 dataset.

Initialization	Accuracy (%)
Random	45.4
Motion global	48.3
Motion pattern all	55.4
Motion pattern all + global	57.8

Table 2.4: Comparison of different supervision signals on the UCF101 and the HMDB51 datasets.

Domain	UCF101 acc.(%)	HMDB51 acc. (%)
From scratch	45.4	19.7
Appearance	48.6	20.3
Motion	57.8	29.95
Joint	58.8	32.6

and appearance statistics, the performance can be further improved.

2.5 Transfer Learning on Action Recognition

We first evaluate the proposed approach and compare with other methods on the action recognition task. Specificallyt, we compare with those methods who use RGB video as inputs and directly quote the performance results from [5]. As shown in Table 2.5, our method achieves the state-of-the-art results both on UCF101 and HMDB51 daatset. Compared with methods that are pre-trained on UCF101 dataset, we improve 9.3% accuracy on HMDB51 than [5] and 2.5% accuracy on UCF101 than [72]. The results strongly support that our proposed predicting motion and appearance statistics task can really drive the CNN to learn powerful spatio-temporal features. And our method can generate multi-

Table 2.5: Comparison with the state-of-the-art self-supervised video representation learning methods on UCF101 and HMDB51.

Method	UCF101 acc.(%)	HMDB51 acc.(%)
DrLim [94]	38.4	13.4
TempCoh [95]	45.4	15.9
Object Patch [96]	42.7	15.6
Seq Ver.[4]	50.9	19.8
VGAN [6]	52.1	-
OPN [72]	56.3	22.1
Geometry [5]	55.1	23.3
Ours (UCF101)	**58.8**	**32.6**

frame spatio-temporal features transferable to many other video tasks.

We also provide the per-class accuracy on UCF101 and HMDB51 as shown in Table 2.6 and Table 2.7 respectively. We compare two scenarios: (1) Train from scratch. (2) Finetune on our self-supervised pre-trained model and highlight the action classes which benefit a lot from the pre-trained model in the table.

Concerning UCF101, action classes that achieve impressive improvement are *BoxingSpeedBag*, increasing 57.5% from 30% to 87.5%, *SalsaSpin*, increasing 54.2%, from 12.2% to 66.4%, *PushUps*, increasing 43.8%, from 0% to 43.8% and etc.

As for HMDB51, action classes that achieve impressive improvement are *PullUp*, increasing 46.5% from 15.7% to 62.2%, *PushUp*, increasing 39.8%, from 19.5% to 59.4%, *Laugh*, increasing 30.6%, from 12.5% to 43.2% and etc.

Notice that both dataset achieve impressive performance improvement on action *PushUp* and *Pullup*. These two actions are quite challenging as PushUp is body-motion only action, which has no appearance clue to be distinguished and the background of PullUp is quite chaotic. However, when finetuned on our pre-trained model, their performance imrpove a lot, which strongly supports that our

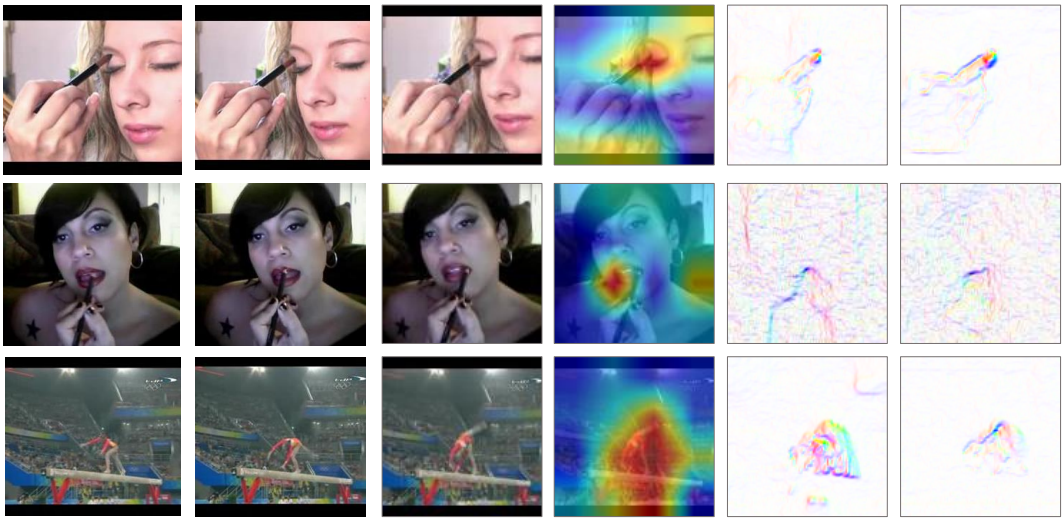

Figure 2.8: **Attention visualization.** From left to right: A frame from a video clip, activation based attention map of conv5 layer on the frame by using [12], motion boundaries M_u of the whole video clip, and motion boundaries M_v of the whole video clip.

the predicting motion-appearance statistics task really encourage CNN to learn action-spefic spatio-temporal features that are beneficial for action classification problems.

Visualization

To further validate that our proposed method really helps the C3D to learn video related features, we visualize the attention map [12] on several video frames as shown in Figure 3.7. It is interesting to note that for similar actions: *Apply eye makeup* and *Apply lipstick*, C3D is just sensitive to the location that is exactly the largest motion location as quantified by the motion boundaries as shown in the right. For different scale motion, for example, the *balance beam* action, the pre-trained C3D is also able to focus on the discriminative location.

We provide the activation-based attention maps of action classes which benefit

a lot from the pre-trained model as shown in Figure 2.9

2.6 Feature Learning on Dynamic Scene Recognition

We further evaluate the learned video representation on the feature learning mode. We transfer the learned features to the dynamic scene recognition problem based on the YUPENN dataset [37]. It contains 420 video samples of 14 dynamic scenes, as shown in Fig. 2.10.

For each video in the dataset, first split it into 16 frames clips with 8 frames overlapped. The spatio-temporal features are then extracted based on our self-supervised C3D pre-trained model from the last conv layer. The video-label representations are obtained by averaging each video-clip features, followed with L_2 normalization. A *linear* SVM is finally used to classify each video scene. We follow the same leave-one-out evaluation protocol as described in [37].

We compared our methods with both hand-crafted features and other self-supervised learning tasks as shown in Table 3.7. Our self-supervised C3D outperforms both the traditional features and self-supervised learning methods. It shows that although our self-supervised C3D is trained on a action dataset, the learned weights has impressive transferability to other video-related tasks.

2.7 Discussion

In this work, we proposed a novel pretext task for self-supervised video representation learning, by regressing spatio-temporal statistics. It was inspired by human visual system and aimed to break the video understanding process into learning motion statistics and appearance statistics, respectively. The motion statistics

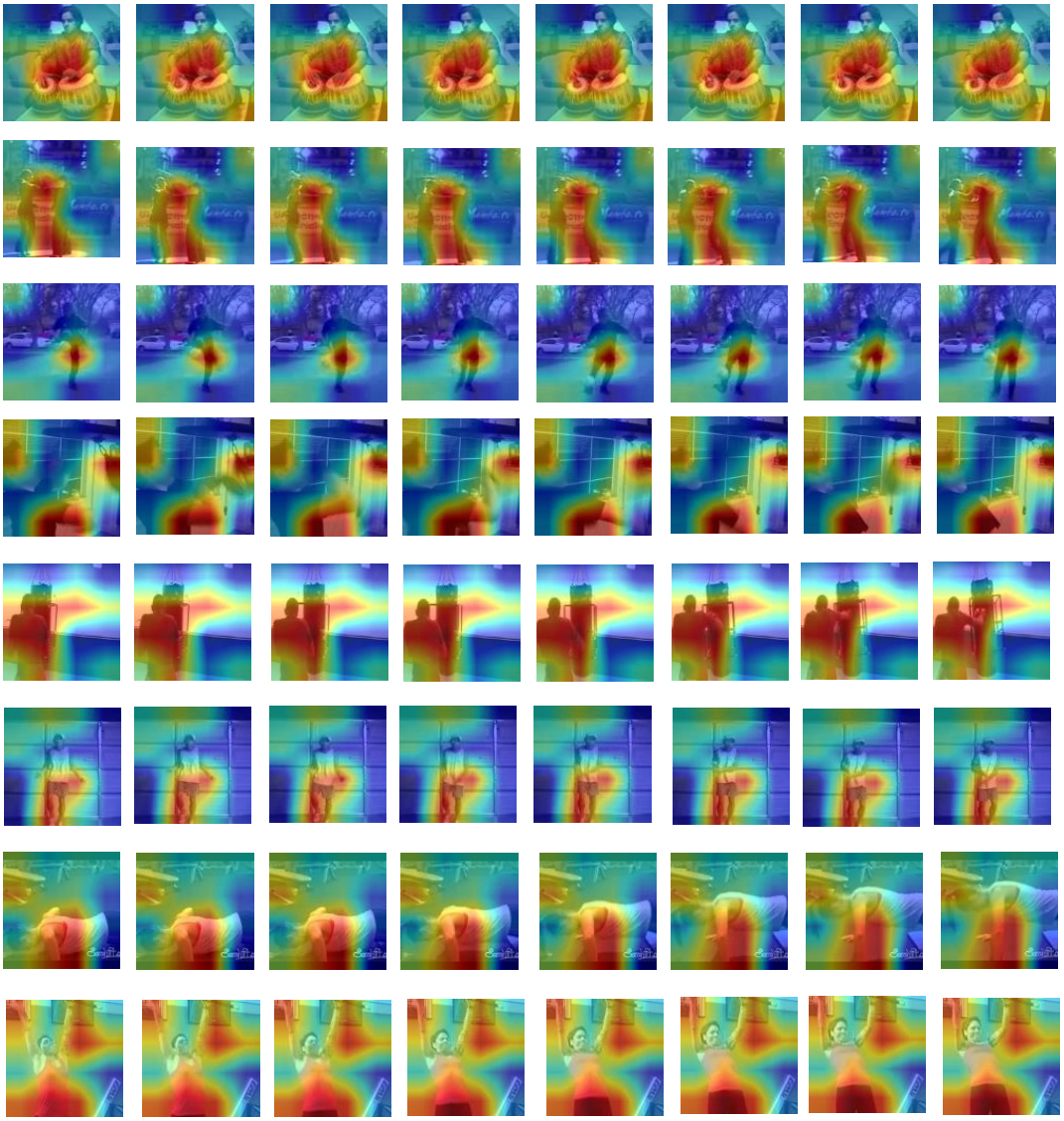

Figure 2.9: **Visualization of activation-based attention maps on UCF101 dataset.** From top to bottom: *PlayingTabla*, *SalsaSpin*, *SoccerJuggling*, *BoxingSpeedBag*, *BoxingPunchingBag*, *JumpRope*, *PushUps*, and *PullUps*.

Figure 2.10: **Several samples from the YUPENN dynamic scene dataset.** Motion in this dataset is relatively small compared with the action recognition dataset.

characterized the largest motion location and the corresponding dominant motion direction. The appearance statistics characterized the diverse/stable color space location and the corresponding dominant color. Both statistical labels were designed along the spatio-temporal axes. We validated the proposed approach on two downstream tasks: action recognition and dynamic scene recognition. The experimental results showed that the proposed approach can achieve competitive performances with other self-supervised video representation learning methods.

While promising results have been achieved, some fundamental questions are remained unsolved. For example, will the performance be further improved by using a larger pre-training dataset? In this chapter, we use UCF101 as the pre-training dataset, which is a relatively small dataset and only contains around 10k training videos. While it is necessary to evaluate the proposed approach on a

much larger dataset. As it is the promise of self-supervised video representation learning to leverage large amount of unlabeled video data. In the next chapter, we will conduct an in-depth investigation on the proposed spatio-temporal statistics regression pretext task.

□ End of chapter.

Action class	Scratch acc. (%)	Finetune acc. (%)	Action class	Scratch acc. (%)	Finetune acc. (%)	Action class	Scratch acc. (%)	Finetune acc. (%)
ApplyEyeMakeup	41.0	67.9	Hammering	8.5	10.0	PommelHorse	37.4	74.2
ApplyLipstick	44.3	66.2	HammerThrow	47.3	54.3	**PullUps**	**14.3**	**54.4**
Archery	9.3	14.6	HandstandPushups	9.7	42.5	Punch	93.5	94.1
BabyCrawling	45.7	53.2	HandstandWalking	2.7	19.8	**PushUps**	**0.0**	**43.8**
BalanceBeam	45.8	51.4	HeadMassage	35.5	31.9	Rafting	68.5	63.2
BandMarching	82.7	73.7	HighJump	14.3	19.2	RockClimbingIndoor	64.0	76.7
BaseballPitch	75.4	51.8	HorseRace	85.7	91.5	RopeClimbing	27.4	48.5
BasketballDunk	33.9	42.0	HorseRiding	85.5	92.6	Rowing	66.2	72.2
Basketball	95.9	51.4	HulaHoop	43.3	68.5	**SalsaSpin**	**12.2**	**66.4**
BenchPress	36.7	79.9	IceDancing	87.5	94.1	ShavingBeard	9.0	12.7
Biking	49.9	58.7	JavelinThrow	49.5	38.0	Shotput	13.1	26.7
Billiards	95.1	96.0	JugglingBalls	21.	77.5	SkateBoarding	68.8	70.6
BlowDryHair	31.7	41.0	JumpingJack	62.1	82.8	Skiing	45.6	40.6
BlowingCandles	44.0	51.1	**JumpRope**	**8.8**	**53.7**	Skijet	61.7	67.6
BodyWeightSquats	22.7	52.8	Kayaking	58.3	63.7	SkyDiving	56.7	76.3
Bowling	82.4	84.6	Knitting	86.5	83.3	**SoccerJuggling**	**17.5**	**73.4**
BoxingPunchingBag	**6.5**	**55.8**	LongJump	58.3	50.6	SoccerPenalty	82.3	84.1
BoxingSpeedBag	**30.0**	**87.5**	Lunges	23.0	26.6	StillRings	62.5	64.6
BreastStroke	83.2	78.0	MilitaryParade	46.5	73.9	SumoWrestling	82.1	81.8
BrushingTeeth	4.0	7.3	Mixing	29.3	30.2	Surfing	79.6	84.5
CleanAndJerk	54.7	77.2	MoppingFloor	41.1	33.4	Swing	41.3	63.2
CliffDiving	44.3	49.0	Nunchucks	26.7	18.9	TableTennisShot	16.3	47.1
CricketBowling	29.6	49.6	ParallelBars	81.6	83.2	TaiChi	33.2	35.3
CricketShot	9.2	17.7	PizzaTossing	4.6	17.4	TennisSwing	70.5	58.8
CuttingInKitchen	22.1	44.5	PlayingCello	44.4	65.6	ThrowDiscus	35.5	63.1
Diving	84.9	93.2	PlayingDaf	13.8	41.3	TrampolineJumping	70.2	73.4
Drumming	49.9	53.8	PlayingDhol	47.6	60.0	Typing	15.6	55.6
Fencing	50.4	72.7	PlayingFlute	18.2	33.7	UnevenBars	87.4	77.9
FieldHockeyPenalty	69.4	56.6	PlayingGuitar	59.4	79.0	VolleyballSpiking	80.2	81.8
FloorGymnastics	55.7	60.6	PlayingPiano	90.3	82.7	WalkingWithDog	35.4	48.2
FrisbeeCatch	59.9	70.9	PlayingSitar	40.9	51.0	WallPushups	0.0	33.6
FrontCrawl	47.2	34.8	**PlayingTabla**	**38.6**	**92.5**	WritingOnBoard	41.1	70.3
GolfSwing	62.1	59.8	PlayingViolin	41.8	59.4	YoYo	4.9	25.4
Haircut	17.8	23.7	PoleVault	51.9	43.0			

Table 2.6: Comparison of per class accuracy of UCF101 first test split on two models: (1) Random initialization, train from scratch on UCF101 first train split. (2) Pre-train on UCF101 first train split with self-supervised motion-appearance statistics labels and then finetune on UCF101 first train split.

Action class	Scratch acc. (%)	Finetune acc. (%)	Action class	Scratch acc. (%)	Finetune acc. (%)	Action class	Scratch acc. (%)	Finetune acc. (%)
BrushHair	**16.0**	**46.4**	Hit	8.6	3.4	ShootBall	3.5	24.8
Cartwheel	7.6	16.8	Hug	44.0	35.0	ShootBow	34.2	43.7
Catch	28.3	48.3	Jump	0.0	8.5	ShootGun	0.0	4.5
Chew	39.5	34.6	Kick	0.0	14.3	Sit	13.1	27.7
Clap	**0.0**	**35.4**	KickBall	8.8	20.6	Situp	38.2	37.6
Climb	25.3	24.6	Kiss	61.4	60.3	Smile	13.3	19.2
ClimbStairs	14.3	11.3	**Laugh**	**12.5**	**43.2**	Smoke	9.7	27.9
Dive	17.1	33.3	Pick	3.2	9.5	Somersault	9.2	28.3
DrawSword	17.6	20.8	Pour	30.8	42.9	**Stand**	**7.0**	**30.7**
Dribble	**28.6**	**59.3**	**Pullup**	**15.7**	**62.2**	SwingBaseball	2.9	5.8
Drink	19.9	28.6	Punch	1.6	22.7	Sword	19.4	13.9
Eat	25.7	27.1	Push	22.3	34.5	SwordExercise	0.5	12.1
FallFloor	11.3	26.3	**Pushup**	**19.5**	**59.4**	Talk	45.0	40.4
Fencing	18.4	35.7	RideBike	53.1	42.2	Throw	1.1	1.1
FlicFlac	**20.4**	**49.5**	RideHorse	21.9	31.3	Turn	12.1	26.2
Golf	86.2	90.0	Run	10.0	29.1	Walk	8.0	16.7
Handstand	5.2	12.9	ShakeHands	10.7	32.0	Wave	6.7	5.9

Table 2.7: Comparison of per class accuracy of HMDB51 first test split on two models: (1) Random initialization, train from scratch on HMDB51 first train split. (2) Pre-train on UCF101 first train split with self-supervised motion-appearance statistics labels and then finetune on HMDB51 first train split.

Table 2.8: Comparison with hand-crafted features and other self-supervised representation learning methods for dynamic scene recognition problem on the YUPENN dataset.

Method	[97]	[37]	[96]	[4]	[5]	**Ours**
Accuracy (%)	86.0	80.7	70.47	76.67	86.9	**90.2**

Chapter 3

In-depth Investigation of Spatio-temporal Statistics

3.1 Motivation

In chapter 2, we presented the basic idea of utilizing spatio-temporal statistical information for self-supervised video representation learning, where preliminary experiments were conducted to validate the proposed approach by using UCF101 [34] as the pre-training dataset. While satisfactory results have been achieved, several important and fundamental questions remain unexplored. For example, will the performance be further improved by using a much larger pre-training dataset? It is a vital question to be investigated as leveraging large amount of unlabeled video data in the real-world is the promise of self-supervised video representation learning.

In this chapter, we conduct in-depth investigation on the proposed spatio-temporal statistics and explore the following questions for a better understanding of self-supervised video representation learning, aiming to bridge the performance gap between supervised learning and self-supervised learning:

- *Will the performance be further improved by using a large scale pre-training dataset?*

  In Chapter 2, we have shown that the proposed spatio-temporal regression pretext task achieved competitive results with other self-supervised learning methods [5, 72] when using UCF101 [34] for pre-training, which is a relatively small dataset containing around 9k videos. It is then natural to ask that will the proposed statistics approach still be effective when using a much larger pre-training dataset? To answer this question, we evaluate the proposed spatio-temporal regression pretext task on a large dataset kinetics-400 [30], which contains around 24k videos. In this case, we intend to move towards the ultimate goal of self-supervised video representation learning – to leverage the large amount of data available freely. We show that by using kinetics-400, the performance can be further improved in Sec. 3.5

- *Does the backbone network architecture play an important role in self-supervised video representation learning?*

  In Chapter 2, C3D [10] with only five convolutional layers was used as backbone network to evaluate the proposed approach. In this chapter, we extend the proposed method to several modern backbone networks, *i.e.*, C3D with BN [98], 3D-ResNet [45] and R(2+1)D [26]. Extensive ablation studies are conducted to investigate whether the performance enhancement comes from the external network architectures or the internal self-supervised learning methods. We show that the proposed spatio-temporal statistics regression task outperforms other pretext tasks across all these backbone networks.

- *Does each video sample contribute equally to self-supervised video representation learning?*

In this chapter, we further investigate the effectiveness of pre-training dataset scale based on different proportions of the kinetics-400 dataset. We show that using only 1/8 of the pre-training data can already achieve 1/2 of the improvement, which suggests that attentive selection should be given on the training samples. A curriculum learning strategy is introduced based on the proposed spatio-temporal statistics to encourage the neural network to learn from simple to difficult samples. We introduce scoring function to sort the training samples and pacing functions to control the training strategy.

- *Is there any other advantages of self-supervised video representation learning apart from the promise to leverage large amount of unlabeled data?*

  We further evaluate the learned video representations on a new downstream task, video retrieval. Typically, the learned features are used directly for video retrieval task without any transformation to evaluate the generality of the video features. The experimental results show that compared with compared with supervised learning, video representations learned by the proposed pretext task achieve significant improvement, which indicates that video representations learned in a self-supervised manner are more generalizable and transferable.

To summarize, the main contributions of this chapter are three-fold: (1) We introduce a curriculum learning strategy based on the proposed spatio-temporal statistics, which is also inspired by the human learning process: from simple samples to difficult samples. (2) Extensive ablation studies are conducted and analyzed to reveal several insightful findings for self-supervised learning, including the effectiveness of training data scale, network architectures, and feature generalization, to name a few. (3) The proposed approach significantly outperforms

previous approaches across all the studied network architectures in various video analytic tasks. Code and models are made publicly available online to facilitate future research.

The rest of this chapter is organized as follows: First, we elaborate on the proposed curriculum learning strategy in Sec. 3.2 and three modern backbone network architectures in Sec. 3.3. We then introduce the implementation details in Sec. 3.4,. In Sec. 3.5, we seek to understand the effectiveness of the proposed method through comprehensive ablative analysis. We compare the proposed method with other state-of-the-art methods on several downstream tasks, including action recognition, video retrieval, dynamic scene recognition, and action similarity labeling in Sec. 3.6. Finally, we discuss the limitation of current work in Sec. 3.7 and explore to solve it in the next chapter.

3.2 Curriculum Learning

We further propose to leverage the curriculum learning strategy to improve the learning performance. Curriculum learning is first proposed by Bengio *et al.* [99] in 2009 and the key concept is to present the network with more difficult samples gradually. It is inspired by the human learning process and proven to be effective on many learning tasks [69, 76, 100]. Recently, Hacohen and Weinshall [101] further investigated the curriculum learning in training deep neural networks and proposed two fundamental problems to be resolved: (1) scoring function problem, *i.e.*, how to quantify the difficulty of each training sample; 2) pacing function problem, *i.e.*, how to feed the networks with the sorted training samples. In this work, for self-supervised video representation learning, we describe our solutions to these two problems as follows.

Scoring Function

Scoring function f defines how to measure the difficulty of each training sample. In our case, each video clip is considered to be easy or hard, based on the difficulty to figure out the block with the largest motion, *i.e.*, difficulty to regress the motion statistical labels. To characterize the difficulty, we use the ratio between magnitude sum of the largest motion block and magnitude sum of the entire videos, as the scoring function f. When the ratio is large, it indicates that the largest motion block contains the dominant action in the video and is thus easy to find out the largest motion location, *e.g.*, a man skiing in the center of a video with smooth background change. While on the other hand, when the ratio is small, it indicates that the action in the video is relatively diverse or the action is less noticeable, *e.g.*, two persons boxing with another judge walking around. See Sec. 3.5.3 for more visualized examples.

Formally, given an N-frame video clip, two summarized motion boundaries M_u and M_v are computed based on Eq. 2.2 and the corresponding magnitude maps are denoted as M_u^{mag} and M_v^{mag}. Denote the largest motion blocks as B_u, B_v and the corresponding magnitude maps as B_u^{mag}, B_v^{mag}. The scoring function f is defined as the maximum ratio between the magnitude sum of B_u, M_u and B_v, M_v:

$$f = \max\left(\frac{\sum B_u^{mag}}{\sum M_u^{mag}}, \frac{\sum B_v^{mag}}{\sum M_v^{mag}} \right). \tag{3.1}$$

Here we use the maximum ratio between the horizontal component u and the vertical component v. This is because large magnitude in *one* direction can already define large motion, *e.g.*, a person running from left to right contains large motion in horizontal direction u but small motion in vertical direction v. With the scores computed from function f, training samples are sorted in a descending

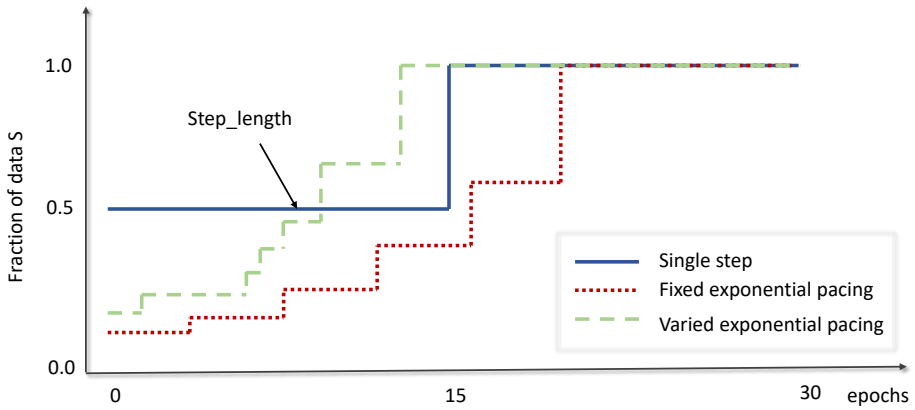

Figure 3.1: **Illustration of three different pace functions**. Single step (blue line), fixed exponential pacing (red square dots), and varied exponential pacing (green dashes) are presented.

order accordingly, representing the difficulty from easy to hard.

Pacing Function

After sorting the samples, the remaining question is how to split these samples into different training steps. Prior works [69, 76, 100] usually adopt a two-stage training scheme, *i.e.*, training examples are divided into two categories: easy and hard. In [101], the authors formally define such a problem as a pacing function g, and introduce three stair-case functions: *single step*, *fixed exponential pacing*, and *varied exponential pacing* as shown in Fig. 3.1, where they demonstrate that these functions have comparable performances [101]. In our case, we adopt the simple single step pacing function (we also tried other functions and similarly found that they show comparable performances). Specifically, we use the first half (descendingly sorted as aforementioned) examples as easy samples and the

pacing function is defined as follows:

$$g = \begin{cases} 0.5 * S, & if\ i < step\_length \\ S, & if\ i \geq step\_length \end{cases}, \tag{3.2}$$

where S is the sorted training clips, i is the training iteration, and $step\_length$ is the number of the iterations to use the entire training samples S. In practice, when the model is converged on the first half training samples, we will use the entire S for the second-stage training.

3.3 Modern Spatio-temporal CNNs

We consider C3D [10], 3D-ResNet [45], and R(2+1)D[26] as our backbone networks to learn spatio-temporal features. In the preliminary version [80] of this work, we use a light C3D network as described in [10]. It contains 5 convolutional layers, 5 max-pooling layers, 2 fully-connected layers, and a soft-max loss layer, which is similar to CaffeNet [90]. In this version, we further conduct extensive experiments on C3D with BN and adopt two additional modern network architectures for video analytic tasks: 3D-ResNet and R(2+1)D. Fig. 3.2 presents a simple illustration of these backbone networks. More details are illustrated in the following.

C3D [10] network extends 2D convolutional kernel $k \times k$ to 3D convolutional kernel $k \times k \times k$ to operate on 3D video volumes. It contains 5 convolutional blocks, 5 max-poling layers, 2 fully-connected layers, and a soft-max layer in the end to predict action class. Each convolutional block contains 2 convolutional layers except the first two blocks. Batch normalization (BN) is also added between each convolutional layer and ReLU layer.

3D-ResNet [45] is an 3D extension of the widely used 2D architecture ResNet [49],

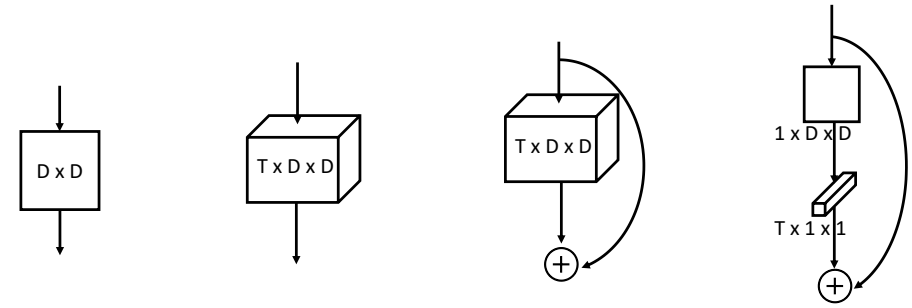

(a) 2D conv (b) C3D (c) 3D-ResNet (d) R(2+1)D

Figure 3.2: **Illustration of backbone networks.** We show a typical convolutional block of each bakcbone networks. See more details in Sec. 3.3.

which introduces shortcut connections that perform identity mapping of each building block. A basic residual block in 3D-ResNet (R3D) contains two 3D convolutional layers with BN and ReLU followed. Shortcut connection is introduced between the top of the block and the last BN layer in the block. Following previous work [45], we use 3D-ResNet18 (R3D-18) as our backbone network, which contains four basic residual blocks and one traditional convolutional block on the top.

R(2+1)D is introduced by Tran *et al.* [26] recently. It breaks the original spatio-temporal 3D convolution into a 2D spatial convolution and a 1D temporal convolution. While preserving similar network parameters to R3D, R(2+1)D outperforms R3D on the task of supervised video action recognition.

We model our self-supervised task as a regression problem. The proposed framework is illustrated in Fig. 2.7, where the *Backbone Network* can be replaced with each of the above-mentioned architectures and is thoroughly evaluated in the experiment (see Sec. 3.5.1). L_2-norm is leveraged as the loss function to measure the difference between target statistical labels and the predicted labels. Formally,

the loss function is defined as follow:

$$\mathcal{L} = \lambda_m \|\hat{y}_m - y_m\|_2 + \lambda_a \|\hat{y}_a - y_a\|_2, \tag{3.3}$$

where $\hat{y}_m$, y_m denote the predicted and target motion statistical labels, and $\hat{y}_a$, y_a denote the predicted and target appearance statistical labels. λ_m and λ_a are the weighting parameters that are used to balance the two loss terms.

3.4 Experimental Setup

3.4.1 Datasets

We conduct extensive experimental evaluations on multiple datasets in the following sections. In Sec. 4.4.1, we validate the proposed approach through extensive ablation studies on action recognition downstream task using three datasets, Kinetics-400 [30], UCF101 [34], and HMDB51 [35]. In Sec. 3.6, we demonstrate the transferability of the proposed method and compare to other state-of-the-art methods on four downstream tasks, including action recognition task and video retrieval task on UCF101 and HMDB51 datasets, dynamic scene recognition task on YUPENN dataset [37], and action similarity labeling task on ASLAN dataset [102].

Kinetics-400 (K-400) [30] is a large-scale human action recognition dataset proposed recently, which contains around 306k videos of 400 action classes. It is divided into three splits: training split, validation split and testing split. Following prior work [69], we use the training split as pre-training dataset, which contains around 240k video samples.

UCF101 [34] is a widely used dataset which contains 13,320 video samples of 101 action classes. It is divided into three splits. Following prior work [7], we use

the *training split 1* as self-supervised pre-training dataset and the *training/testing split 1* for downstream task evaluation.

HMDB51 [35] is a relatively small action dataset which contains around 7,000 videos of 51 action classes. This dataset is very challenging as it contains large variations in camera viewpoint, position, scale and *etc*. Following prior work [7], we use the *training/testing split 1* to evaluate the proposed self-supervised learning method.

YUPENN [37] is a dynamic scene recognition dataset which contains 420 video samples of 14 dynamic scenes. We follow the recommended leave-one-out evaluation protocol [37] when evaluating the proposed method.

ASLAN [102] is a video dataset focusing on the action similarity labeling problem and contains 3,631 video samples of 432 classes. In this work, we use it as a downstream evaluation task to validate the generality of the learned spatio-temporal representations. During testing, following prior work [102], we use a 10-fold cross validation with leave-one-out evaluation protocol.

3.4.2 Implementation Details

Self-supervised Pre-training Stage

When pre-training on UCF101 dataset, video samples are first split into non-overlapped 16 frame video clips and are randomly selected during pre-training. While when pre-training on K-400, following prior works [74, 69], we randomly select a consecutive 16-frame video clip and the corresponding 15-frame optical flow clip from each video sample. Each video clip is reshaped to spatial size of 128×171. As for data augmentation, we randomly crop the video clip to 112×112 and apply random horizontal flip for the entire video clip. Weights of motion statistics λ_m and appearance statistics λ_a are empirically set to be 1 and 0.1. The

batch size is set to 30 and we use SGD optimizer with learning rate 5×10^{-4}, which is divided by 10 for every 6 epochs and the training process is stopped at 20 epochs.

Supervised Fine-tuning Stage

During the supervised fine-tuning stage, weights of convolutional layers are retained from the self-supervised pre-trained models and weights of the fully-connected layers are re-initialized. The whole network is then trained again with cross-entropy loss on action recognition task with UCF101 and HMDB51 datasets. Image pre-processing procedure and training strategy are the same as the self-supervised pre-training stage, except that the initial learning rate is changed to 0.003.

Evaluation

For action recognition task, during testing, video clips are resized to 128×171 and center-cropped to 112×112. We consider two evaluation methods: clip accuracy and video accuracy. The clip accuracy is computed by averaging the accuracy of each clip from the testing set. While the video accuracy is computed by averaging the softmax probabilities of uniformly selected clips in each video [7] from the testing set. In all of the following experiments, to have a fair comparison with prior works [7, 36, 69], we use video accuracy to evaluate our approach while in previous work, chapter 2, clip accuracy is used to evaluate our method.

We further evaluate the self-supervised pre-trained models by using them as feature extractors and comparing with state-of-the-art methods on many other downstream video analytic tasks, such as video retrieval, dynamic scene recognition, *etc.* This allows us to evaluate the generality of the learned saptio-temporal representations directly without fine-tuning. More evaluation details are pre-

sented in Sec. 3.6 for individual downstream tasks.

3.5 Ablation Studies and Analyses

In this section, we conduct extensive ablation studies to validate the proposed method and investigate three important questions: (1) How does the type of backbone network affect the performance of downstream tasks? (2) How does the amount of pre-training data affect the self-supervised video representation learning? (3) Does the proposed curriculum learning strategy help to further improve the video representation learning?

3.5.1 Effectiveness of Backbone Networks

Recently, modern spatio-temporal representation learning architectures, such as R3D-18 [45] and R(2+1)D [26], have been used to validate self-supervised video representation learning methods [36, 7]. While the performances of downstream tasks are significantly improved, this practice introduces a new variable, backbone network, which could interfere with the evaluation of the pretext task itself. In the following, we first evaluate our proposed method with these modern backbone networks in Table 3.1. Following that, we compare our method with some recent works [36, 7] on these three network architectures, in Fig. 4.7.

We present the performances of different backbone networks on UCF101 and HMDB51 datasets under two settings: without per-training and with pre-training, in Table 3.1. When there is no pre-training, baseline results are obtained by training from scratch on each result. When there is pre-training, backbone networks are first pre-trained on UCF101 dataset with the proposed method and then used as weights initialization for the following fine-tuning. Best performances under each setting are shown in bold. From the results we have the following obser-

Table 3.1: Evaluation of three different backbone networks on the UCF101 dataset and HMDB51 dataset. When pre-training, we use our self-supervised pre-training model as weight initialization.

Experimental setup			Downstream task(%)	
Pre-training	Backbone	#Params.	UCF101	HMDB51
✗	C3D	33.4M	**61.7**	**24.0**
✓	C3D	33.4M	69.3	34.2
✗	R3D-18	14.4M	54.5	21.3
✓	R3D-18	14.4M	67.2	32.7
✗	R(2+1)D	14.4M	56.0	22.0
✓	R(2+1)D	14.4M	**73.6**	**34.1**

vations: (1) Drastic improvement is achieved on both action recognition datasets across three backbone networks. With C3D it improves UCF101 and HMDB51 by 9.6% and 13.8%; with R3D-18 it improves UCF101 and HMDB51 by 13.6% and 12.1%; with R(2+1)D it improves UCF101 and HMDB51 by 19.5% and 15.9% remarkably. (2) Compared to C3D, R3D-18 and R(2+1)D benefit more from the self-supervised pre-training. Despite C3D achieves the best performance in the no pre-training setting, R(2+1)D finally achieves the highest accuracy on both datasets in the self-supervised setting. (3) The proposed method using (2+1)D convolution, *i.e.*, R(2+1)D, achieves better performance than using 3D convolution, *i.e.*, R3D-18, while with similar number of network parameters. Similar observation is also demonstrated in supervised action recognition task [26], where R(2+1)D performs better than R3D-18 on K-400 dataset.

We further compare our method with two recent proposed pretext tasks VCOP [7] and VCP [36] on these three backbone networks in Fig. 4.7. Three key observations are illustrated: (1) The proposed self-supervised learning method achieves the best performance across all three backbone networks on both UCF101 and HMDB51 datasets. This demonstrates the superiority of our method and

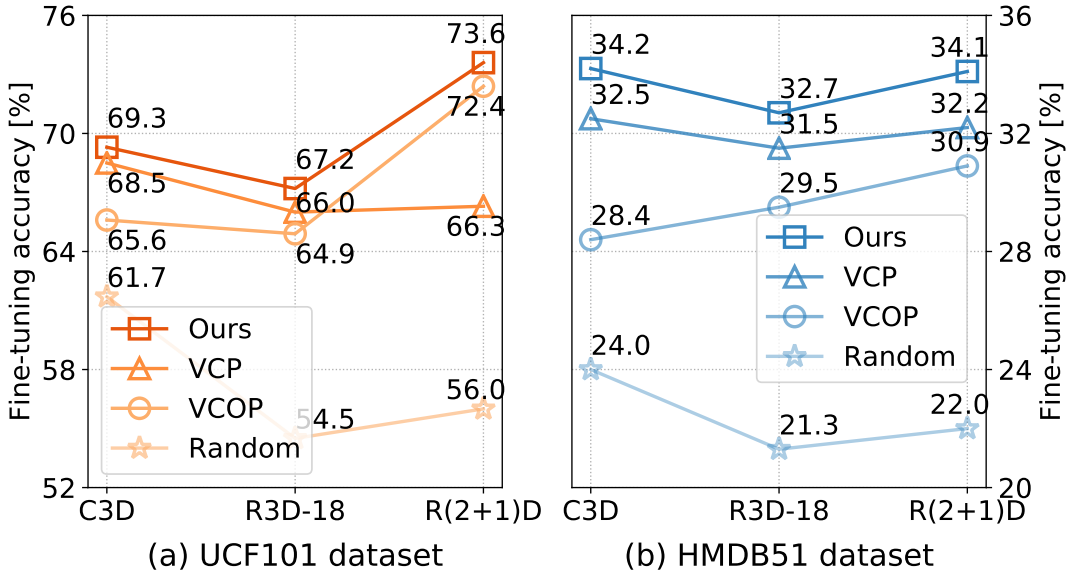

Figure 3.3: Action recognition accuracy on three backbone networks (horizontal axis) using four initialization methods.

shows that the performance improvement is not merely due to the usage of the modern networks. The proposed spatio-temporal statistical labels indeed drive neural networks to learn powerful spatio-temporal representations for action recognition. (2) For all three pretext tasks, R(2+1)D enjoys the largest improvement (compared to *Random*) for both datasets, which is similar to the observation in the above experiments. (3) No best network architecture is guaranteed for different pretext tasks. R(2+1)D achieves the best performance with our method and VCOP, while C3D achieves the best performance with VCP.

3.5.2 Effectiveness of Pre-training Data

In the following, we consider two scenarios to investigate the effectiveness of pre-training data. One is comparison on different pre-training datasets with different data scales. The other is comparison on the same pre-training dataset but with different pre-training data size.

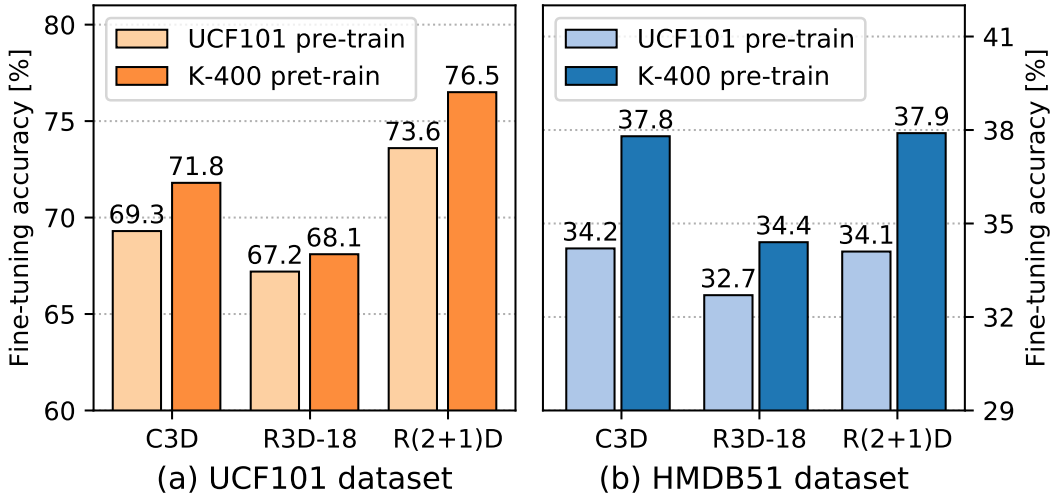

Figure 3.4: Comparison of different pre-training datasets: UCF101 and K-400, across three different backbone networks on UCF101 and HMDB51 datasets.

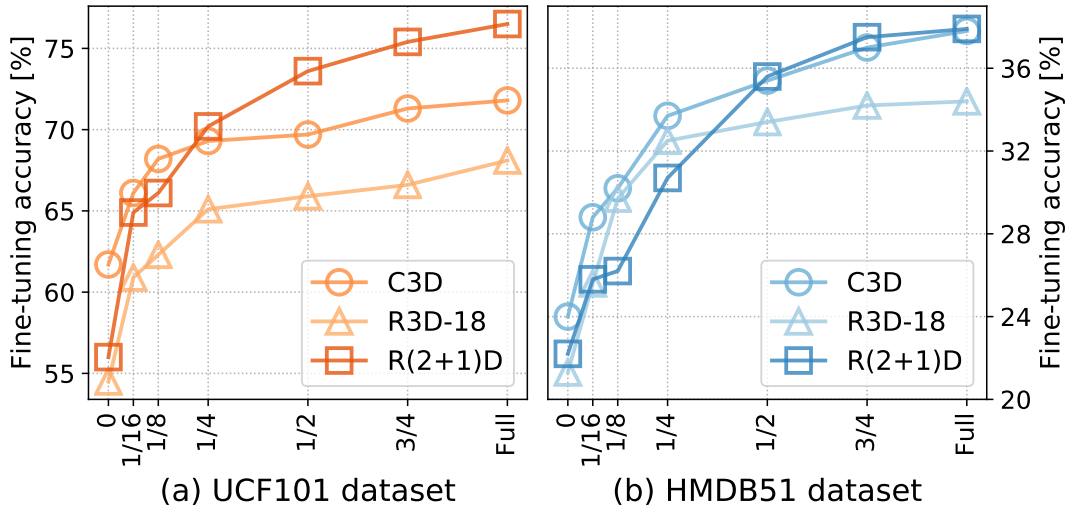

Figure 3.5: Comparison of different pre-training dataset scales of K-400 across three different backbone networks. Position "0" at the x-axis indicates random initialization.

Table 3.2: Results of different training data scale of K-400 on UCF101 and HMDB51 dataset

	Network	Random	1/16	1/8	1/4	1/2	3/4	Full
UCF101	C3D	61.7	66.1	68.2	69.3	69.7	71.3	71.8
	R3D-18	54.5	60.9	62.3	65.1	65.9	66.6	68.1
	R(2+1)D	56.0	64.9	66.1	70.2	73.6	75.4	76.5
HMDB51	C3D	24.0	28.8	30.2	33.7	35.4	37.0	37.8
	R3D-18	21.3	25.6	29.7	32.5	33.4	34.2	34.4
	R(2+1)D	22.2	25.8	26.2	30.7	35.6	37.5	37.9

Pre-training Dataset Analysis

We analyze the performances of training on a relatively small-scale dataset UCF101 [34] and on a large-scale dataset K-400 [30]. The pre-trained models are evaluated on two downstream datasets: UCF101 and HMDB51 w.r.t. three different backbone networks as shown in Fig. 3.4. It can be seen that the performance could be further improved when pre-training on a larger dataset across all the backbone networks and on both downstream datasets. The effectiveness of larger dataset is also demonstrated in prior works [69, 33].

Dataset Scale Analysis

We further consider to pre-train backbone networks on different proportions of *the same* K-400 dataset. In practice, $1/k$ of K-400 is used for pre-training, where $k = 16, 8, 4, 2, 4/3, 1$. To obtain the corresponding pre-training dataset, for $k = 16, 8, 4, 2$, we select one sample from every k samples of the original full K-400. As for $k = 4/3$, we first retain half of the K-400, and then select one sample from every 2 samples in the remaining half dataset. We conduct extensive experiments on three backbone networks and two downstream datasets as

shown in Fig. 3.5. It can be seen from the figure that increase of pre-training data scale does not lead to linear increase of the performance. The effectiveness of the data scale would saturate towards using the full K-400 dataset. Taking R(2+1)D as an example, compared with using full K-400, using half of the K-400 only leads to *inconsequential* drop from the highest performance. Besides, using 1/8 of the K-400 can already achieve half of the improvement compared to training from scratch. similar observation is also demonstrated in supervised transfer learning [103]. This suggests that when considering limited computing resources, it would be important and interesting to adopt an attentive selection of the training samples.

Table 3.3: Evaluation of the curriculum learning strategy. ↑ represents the first half of the K-400 dataset while ↓ indicates the last half of the K-400 dataset.

Experimental setup		Downstream tasks	
Curr. Learn.	Pre-training data	UCF101	HMDB51
✗	100 % K-400	76.5	37.9
✗	50 % K-400	73.6	35.6
✗	↑, 50% K-400 (simple)	72.4	35.9
✗	↓, 50% K-400 (difficult)	72.8	32.1
✓	100% K-400	**77.8**	**40.5**

3.5.3 Effectiveness of Curriculum Learning Strategy

The performances of the proposed curriculum learning strategy are shown in Table 3.3. Compared with the baseline results (100% K-400), the performances are further boosted on both UCF101 dataset(77.8% vs. 76.5%) and HMDB51 dataset (40.5% vs. 37.9%) , which validates the effectiveness of the proposed curriculum learning strategy. It is also interesting to note that when using the first half of the sorted training samples, *i.e.*, simple samples or the last half, *i.e.*,

difficult samples, the performances on UCF101 dataset are both lower than the random half of K-400. Such observations further validate that the careful selection of training samples is of necessity in self-supervised representation learning.

Three video samples ranked from easy to hard are shown in Fig. 3.6. As described in Sec. 3.2, difficulty to regress the motion statistical labels is used to define the scoring function f to rank the training samples. Note that the appearance statistics labels are not considered when computing f as they demonstrate relatively limited improvement in action recognition task as shown in Table 2.4 in Chapter 2.

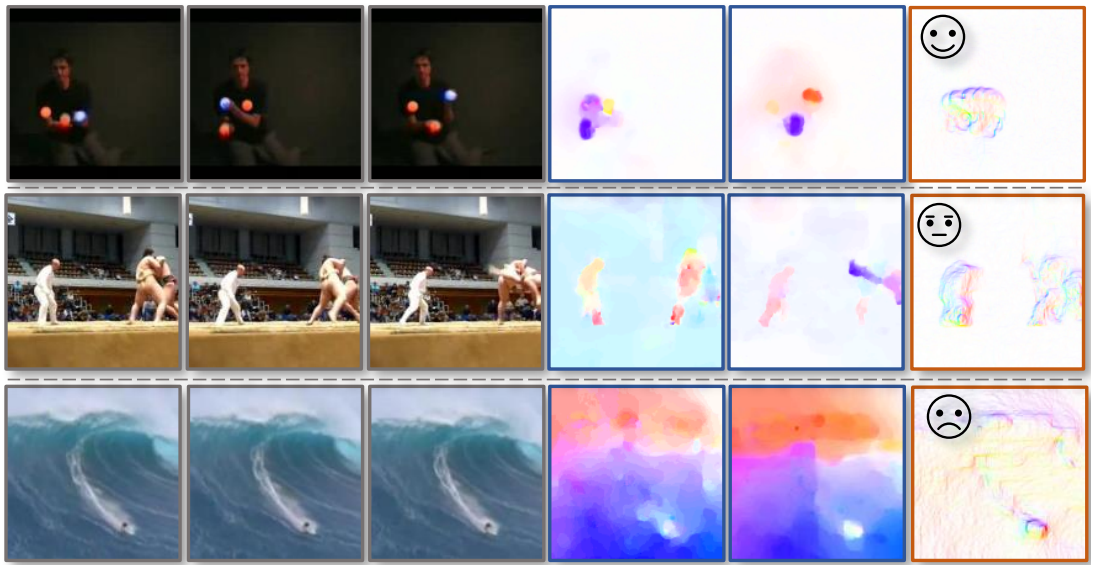

Figure 3.6: **Three video samples of the curriculum learning strategy.** From left to right, the difficulty to regress the motion statistical labels of each video clip is increasing. For each sample, the top three images are the first, middle, and last frames of a video clip. In the bottom row, the first two images are the corresponding optical flows and the last image is the summarized motion boundaries M_u/M_v with the maximum magnitude sum.

3.6 Comparison with State-of-the-art Approaches

In this section, we validate the proposed method both quantitatively and qualitatively, and compare with state-of-the-arts on four video understanding tasks: action recognition (Sec. 3.6.1), video retrieval (Sec. 3.6.2), dynamic scene recognition (Sec.3.6.3), and action similarity labeling (Sec. 3.6.4).

3.6.1 Action Recognition

Table 3.4 compares our method with other self-supervised learning methods on the task of action recognition. We have the following observations: (1) Compared with random initialization (training from scratch), networks fine-tuned on pre-trained models with the proposed self-supervised method achieve significant improvement on both UCF101 (77.8% vs. 56%) and HMDB51 (40.5% vs. 22.0%). Such results demonstrate the great potential of self-supervised video representation learning. (2) Our method achieves state-of-the-art performance on both datasets, improving UCF101 by 2.1% and HMDB51 by 4.8% compared with DPC [69]. Note that the input size of DPC is 224×224 and when considering the same input size 112×112 as ours, the proposed method improves DPC on UCF101 by 9.6%. (3) Similar to the observation in Sec. 3.5.1, besides pretext tasks, backbone networks also play an important role in self-supervised video representation learning. For example, pretext tasks using 3D neural networks significantly outperforms those using 2D neural networks.

Attention Visualization

Fig. 3.7 visualizes the attention maps on several video samples using [12]. For action classes with subtle differences, *e.g.*, *Apply lipstick* and *Apply eye makeup*, the pre-trained model is sensitive to the location that is exactly the largest motion

Table 3.4: Comparison with state-of-the-art self-supervised learning methods on the action recognition task. * indicates that the input spatial size is 224 × 224.

Method	Pre-training			Evaluation	
	Backbone	#Params.	Dataset	UCF101	HMDB51
Random	R(2+1)D	14.4M	-	56.0	22.0
Fully supervised	R(2+1)D	14.4M	K-400	93.1	63.6
Object Patch[96]	AlexNet	62.4M	UCF101	42.7	15.6
ClipOrder[4]	CaffeNet	58.3M	UCF101	50.9	19.8
Deep RL[73]	CaffeNet	58.3M	UCF101	58.6	25.0
OPN [72]	VGG	8.6M	UCF101	59.8	23.8
VCP [36]	C3D	34.4M	UCF101	68.5	32.5
VCOP [7]	R(2+1)D	14.4M	UCF101	72.4	30.9
RotNet3D [79]	R3D-18	33.6M	K-400	62.9	33.7
ST-puzzle [74]	R3D-18	33.6M	K-400	65.8	33.7
DPC [69]	R3D-18	14.2M	K-400	68.2	34.5
DPC* [69]	R3D-34	32.6M	K-400	75.7	35.7
Ours	R(2+1)D	14.4M	K-400	76.5	37.9
Ours (CL)	R(2+1)D	14.4M	K-400	**77.8**	**40.5**

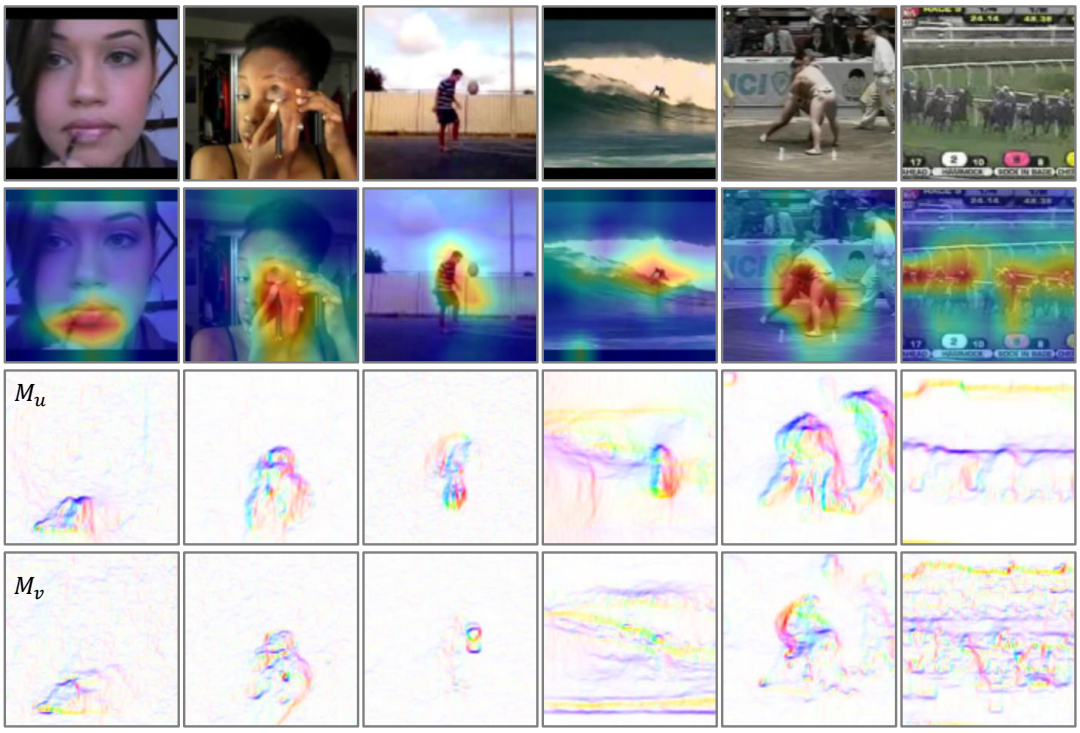

Figure 3.7: **Attention visualization.** For each sample from top to bottom: A frame from a video clip, activation based attention map of conv5 layer on the frame by using [12], summarized motion boundaries M_u, and summarized motion boundaries M_v computed from the video clip.

location as quantified by the summarized motion boundaries M_u and M_v. It is also interesting to note that for the *Sumo Wrestling* video sample (the fifth column), although three persons (two players and one judge) have large motion in direction u, only players demonstrate larger motion in direction v. As a result, the attention map is mostly activated around the players.

The performances on the action recognition downstream task strongly validate the great power of self-supervised learning methods. The proposed pretext task is demonstrated to be effective in driving backbone networks to learn spatio-temporal features for action recognition. While to the goal of learning generic

features, it is also important and interesting to evaluate the absolute effect of the learned features without fine-tuning on the downstream task. In the following, we directly evaluate the features on three different problems by using the networks as feature extractors.

3.6.2 Video Retrieval

We evaluate spatio-temporal representations learned from the self-supervised method on video retrieval task. Followed [36, 7], given a video, ten 16-frame clips are first sampled uniformly. Then the video clips are fed into the self-supervised pre-trained models to extract features from the last pooling layer (pool5). Based on the extracted video features, cosine distances between videos of testing split and training split are computed. Finally, the video retrieval performance is evaluated on the testing split by querying Top-k nearest neighbours from the training split based on cosine distances. Here, we consider k to be 1, 5, 10, 20, 50. If the test clip class label is within the Top-k retrieval results, it is considered to be successfully retrieved.

Table 4.8 and Table 4.9 compare our method with other self-supervised learning methods on UCF101 dataset and HMDB51 dataset, respectively. It can be seen that our method achieves the state-of-the-art results and outperforms VCOP [7] and VCP [36] on both datasets across three different backbone networks (shown in bold). We are interested in if the performances could be further improved, as the video features extracted from the pool5 layer tend to be more task-specific while lack generalizability for the retrieval downstream task. To validate this hypothesis, we extract video features from all the preceding pooling layers and evaluate them on the video retrieval task. Typically, we compare the self-supervised method (pre-trained on the proposed pretext task) and supervised method (pre-trained on the action labels) on HMDB51 dataset in Fig. 3.8

Table 3.5: Comparison with state-of-the-art self-supervised learning methods on the video retrieval task with the UCF101 dataset. The best results from pool5 w.r.t. each 3D backbone network are shown in **bold**. The results from pool4 on our method are in *italic* and highlighted.

	Method	Top1	Top5	Top10	Top20	Top50
AlexNet	Jigsaw[52]	19.7	28.5	33.5	40.0	49.4
	OPN[72]	19.9	28.7	34.0	40.6	51.6
	Deep RL[73]	25.7	36.2	42.2	49.2	59.5
C3D	Random	16.7	27.5	33.7	41.4	53.0
	VCOP[7]	12.5	29.0	39.0	50.6	66.9
	VCP[36]	17.3	31.5	42.0	52.6	67.7
	Ours	**20.5**	**39.6**	**50.8**	**62.2**	**76.7**
	Ours (p4)	*30.1*	*49.6*	*58.8*	*67.6*	*78.5*
R3D-18	Random	9.9	18.9	26.0	35.5	51.9
	VCOP[7]	14.1	30.3	40.4	51.1	66.5
	VCP[36]	18.6	33.6	42.5	53.5	68.1
	Ours	**23.9**	**43.9**	**54.3**	**64.9**	**78.2**
	Ours (p4)	*28.7*	*47.7*	*58.3*	*67.8*	*78.5*
R(2+1)D	Random	10.6	20.7	27.4	37.4	53.1
	VCOP[7]	10.7	25.9	35.4	47.3	63.9
	VCP[36]	19.9	33.7	42.0	50.5	64.4
	Ours	**21.2**	**40.1**	**51.5**	**62.5**	**77.1**
	Ours (p4)	*26.2*	*45.9*	*56.5*	*66.3*	*78.4*

(UCF101 dataset follows the similar trend).

We have the following key observations: (1) In our self-supervised method, with the evaluation layer going deeper, the retrieval performance would increase to a peak (usually at pool3 or pool4 layer) and then decrease. Similar observation is also reported in self-supervised image representation learning [104]. The corresponding performance of pool4 layer is reported in Table 4.8 and Table 4.9 (highlighted in blue). (2) R3D-18 is more robust to such performance decline as its turning point occurs at pool4 layer while others usually occur at pool3 layers, especially on the Top-20 and Top-50 experiments. (3) Our self-supervised method significantly outperforms the supervised method, especially at deeper layers. This suggests that features learned from our self-supervised method are more robust and generic when transferring to the video retrieval task. Some qualitative video retrieval results are shown in Fig. 3.9.

3.6.3 Dynamic Scene Recognition

We further study the transferability of the learned features on dynamic scene recognition problem with the YUPENN dataset [37], which contains 420 video samples of 14 dynamic scenes. Following prior work [10], each video sample is first split into 16-frame clips with 8 frames overlapped. Then the spatio-temporal feature of each clip is extracted based on the self-supervised pre-trained models from pooling layers. In practice, similar to Sec. 3.6.2, we investigate the best-performing pooing layer w.r.t. each backbone network in such a problem, where for C3D and R(2+1)D, the best-performing layer is *pool3*; for R3D-18, the best-performing layer is *pool4*. Next, video-level representations are obtained by averaging the corresponding video-clip features, followed by L_2 normalization. Finally, a linear SVM is used for classification and we follow the same leave-one-out evaluation protocol as described in [37].

Table 3.6: Comparison with state-of-the-art self-supervised learning methods on the video retrieval task with the HMDB51 dataset. The best results from pool5 w.r.t. each 3D backbone network are shown in **bold**. The results from pool4 on our method are in *italic* and highlighted.

	Method	Top1	Top5	Top10	Top20	Top50
C3D	Random	7.4	20.5	31.9	44.5	66.3
	VCOP[7]	7.4	22.6	34.4	48.5	70.1
	VCP[36]	7.8	23.8	35.5	49.3	71.6
	Ours	**10.6**	**26.1**	**39.7**	**55.0**	**77.2**
	Ours (p4)	*13.9*	*33.3*	*44.7*	*59.5*	*78.1*
R3D-18	Random	6.7	18.3	28.3	43.1	67.9
	VCOP[7]	7.6	22.9	34.4	48.8	68.9
	VCP[36]	7.6	24.4	36.6	53.6	76.4
	Ours	**8.4**	**23.1**	**35.6**	**50.4**	**72.1**
	Ours (p4)	*14.2*	*32.2*	*44.1*	*60.2*	*81.3*
R(2+1)D	Random	4.5	14.8	23.4	38.9	63.0
	VCOP[7]	5.7	19.5	30.7	45.8	67.0
	VCP[36]	6.7	21.3	32.7	49.2	73.3
	Ours	**9.3**	**23.8**	**36.2**	**50.5**	**74.1**
	Ours (p4)	*12.1*	*30.0*	*41.4*	*56.7*	*78.0*

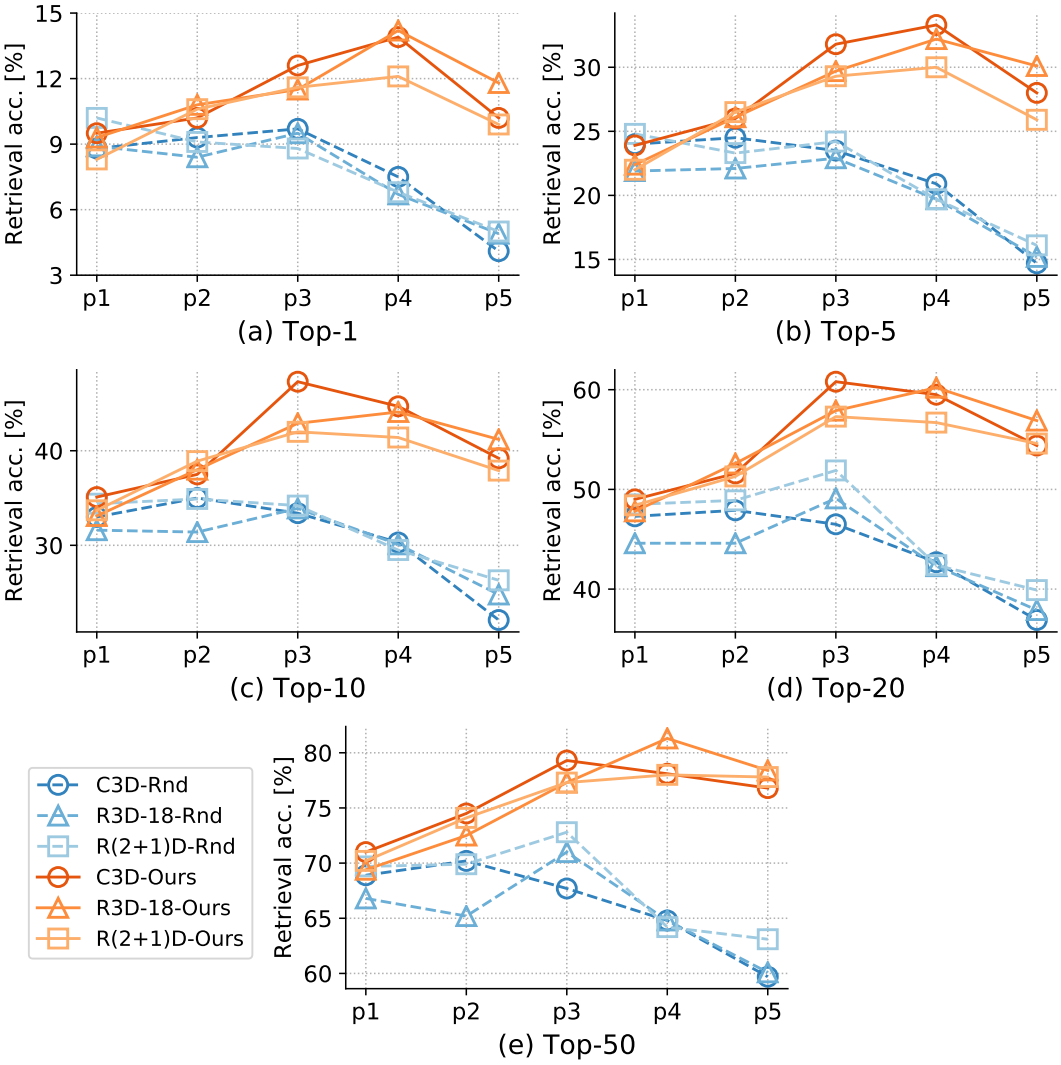

Figure 3.8: **Evaluation of features from different stages of the network, *i.e.*, pooling layers, on the video retrieval task with the HMDB51 dataset.** The dotted blue lines show the performances of the supervised pre-trained models on the action recognition problem, *i.e.*, random initialization (Rnd). The orange lines show the performances of the self-supervised pre-trained models with our method (Ours). Better visualization with color.

(a) Random (supervised learning)

(b) Ours (self-supervised learning)

Figure 3.9: **Qualitative results on video retrieval.** From top to bottom: three qualitative examples of video retrieval on the UCF101 dataset. From left to right: one query frame from the testing split, frames from the top-3 retrieval results based on the supervised pre-trained models, and frames from the top-3 retrieval results based on our self-supervised pre-trained models. The correctly retrieved results are marked in blue while the failure cases are in orange. Better visualization with color.

Table 3.7: Comparison with state-of-the-art hand-crafted methods and self-supervised representation learning methods on the dynamic scene recognition task.

Method	Hand-crafted	Self-supervised	YUPENN
SOE[37]	✓		80.7
SFA[106]	✓		85.5
BoSE[105]	✓		96.2
Object Patch[96]		✓	70.5
ClipOrder[4]		✓	76.7
Geometry[5]		✓	86.9
Ours, C3D		✓	**96.7**
Ours, R3D-18		✓	93.8
Ours, R(2+1)D		✓	93.1

We compare our approach with state-of-the-art hand-crafted features and other self-supervised learning methods in Table 3.7. It can be seen from the table that the proposed method significantly outperforms the second best self-supervised learning method Geometry [5] by 9.8%, 6.9%, and 6.2% w.r.t. C3D, R3D-18, and R(2+1)D backbone networks, respectively. Besides, our method also outperforms the best hand-crafted feature BoSE [105] by 0.5%. Note that BoSE combined different sophisticated feature encodings (FV, LLC and dynamic pooling) while we only use average pooling with a *linear* SVM. It is therefore demonstrated that the spatio-temporal features learned from the proposed self-supervised learning method have impressive transferability.

3.6.4 Action Similarity Labeling

In this section we introduce a challenging downstream task – action similarity labeling. The learned spatio-temporal representations are evaluated on the ASLAN dataset [102], which contains 3,631 video samples of 432 classes. Unlike action recognition task or dynamic scene recognition task that aims to predict the ac-

Table 3.8: Comparison with different hand-crafted features and fully-supervised models on the ASLAN dataset.

Features	Hand-crafted	Sup.	Self-sup.	Acc.
C3D[10]		✓		78.3
P3D[44]		✓		80.8
HOF[102]	✓			56.7
HNF[102]	✓			59.5
HOG[102]	✓			59.8
Ours, C3D			✓	60.9
Ours, R3D-18			✓	60.9
Ours, R(2+1)D			✓	**61.6**

tual class label, the action similarity labeling task focuses on the *similarity* of two actions instead of the actual class label. That is, given two video samples, the goal is to predict whether the two samples are of the same class or not. This task is quite challenging as the test set contains *never-before-seen* actions [102].

To evaluate on the action similarity labeling task, we use the self-supervised pre-trained models as feature extractors and use a *linear* SVM for the binary classification, following prior work [10]. Specifically, given a pair of videos, each video sample is first split into 16-frame clips with 8 frames overlapped and then fed into the network to extract features from the pool3, pool4 and pool5 layers. The video-level spatio-temporal feature is obtained by averaging the clip features, followed by L_2 normalization. After extracting three types of features for each video, we then compute 12 different distances for each feature as described in [102]. The computation methods of the 12 differences are shown in Table 3.9. Then the three 12 (dis-)similarities are concatenated together to obtain a 36-dimensional feature. Since the scales of each distance are different, we normalize the distances separately into zero-mean and unit-variance, following [10]. A linear SVM is used for classification and we use the 10-fold leave-one-out cross validation same as [102, 10].

Table 3.9: The 12 differences used to compute the dissimilarities between videos.

1	2	3	4
$\sum(x_1. * x_2)$	$\sqrt{\sum(x_1. * x_2)}$	$\sqrt{\sum(\sqrt{x_1}. * \sqrt{x_2})}$	$\sqrt{\sum \frac{x_1. * x_2}{x_1 + x_2}}$
5	6	7	8
$\sum(x_1. * x_2)/(\sqrt{\sum(x_1^2)} * \sqrt{\sum(x_2^2)})$	$\sqrt{\sum \frac{(x_1. - x_2)^2}{x_1 + x_2}}$	$\sum \lvert x_1 - x_2 \rvert$	$\sqrt{\sum(\sqrt{x}_1 - \sqrt{x}_2)^2}$
9	10	11	12
$(\sum x_1 \log \frac{x_1}{x_2} + \sum x_2 \log \frac{x_2}{x_1})/2$	$\sqrt{\sum(x_1 - x_2)^2}$	$\sum \frac{\sqrt{\max(x_1, x_2)}}{\sqrt{(x_1 + x_2)}}$	$\sum \min(x_1, x_2)/(\sum x_1 \sum x_2)$

Table 3.8 compares our method with full-supervised methods and hand-crafted features. We set a new baseline for the self-supervised method as no previous self-supervised learning methods have been validated on this task. We have the following observations: (1) Our method outperforms the hand-crafted features: HOF, HOG, and HNF(a composition of HOG and HOF). While there is still a big gap between the full supervised method. (2) Unlike the observations in previous experiments (*e.g.*, action recognition), the performances of the three backbone networks are comparable with each other. We suspect the reason lies on the fine-tuning scheme leveraged in previous evaluation protocols, where the backbone architecture plays an important role. As a result, we suggest that the proposed evaluation on the ASLAN dataset (Table 3.8) could serve as a complementary evaluation task for self-supervised video representation learning to alleviate the influence of backbone networks.

3.7 Discussion

In this chapter, we further conducted an in-depth investigation of the proposed spatio-temporal statistics regression pretext task. We uncovered three crucial insights on self-supervised video representation learning:(1) Architectures of backbone networks play an important role in self-supervised learning. However, no best model is guaranteed for different pretext tasks. In most cases, the combi-

nation of 2D spatial convolution and 1D temporal convolution achieves better results. (2) Downstream task performances are log-linearly correlated with the pre-training dataset scale. Attentive selection should be given on the training samples. (3) In addition to the main advantage of self-supervised video representation learning, *i.e.*, leveraging large number of unlabeled videos, we demonstrate that features learned in a self-supervised manner are more generalizable and transferable than features learned in a supervised manner. A curriculum learning strategy was incorporated to further improve the representation learning performance. To validate the effectiveness of the proposed method, we conducted extensive experiments on four downstream tasks of action recognition, video retrieval, dynamic scene recognition, and action similarity labeling, over three different backbone networks, C3D, R3D-18 and R(2+1)D. Our method was shown to achieve state-of-the-art performance on various datasets accordingly. When directly evaluating the learned features by using the pre-trained models as feature extractors, the proposed approach demonstrated great robustness and transferability to the downstream tasks and significantly outperformed the competing self-supervised methods.

While remarkable results have been achieved, the proposed statistics pretext task has a major drawback of using pre-computed optical flow, which is time and space consuming. In the next chapter, we aim to overcome this drawback and propo se a simple yet effective pretext task for self-supervised video representation learning.

□ End of chapter.

Chapter 4

Play Pace Variation and Prediction for Self-supervised Representation Learning

4.1 Motivation

In Chapter 2 and 3, we have shown that the proposed spatio-temporal statistics pretext task can achieve remarkable performance. However, the usage of pre-computed motion channel, *e.g.*, optical flow, could be an obstacle for this pretext task to reach the ultimate goal to relish the large amount of unlabeled data, as the computation of optical flow is both time and space consuming, especially when the pre-training dataset scales to trillions of data. To alleviate such a problem, in this chapter, we propose a simple and effective pretext task without leveraging motion properties but using the original RGB videos as inputs.

Inspired by the rhythmic montage in film making, we observe that human visual system is sensitive to motion pace and can easily distinguish different paces once understanding the covered content. Such a property has also been revealed

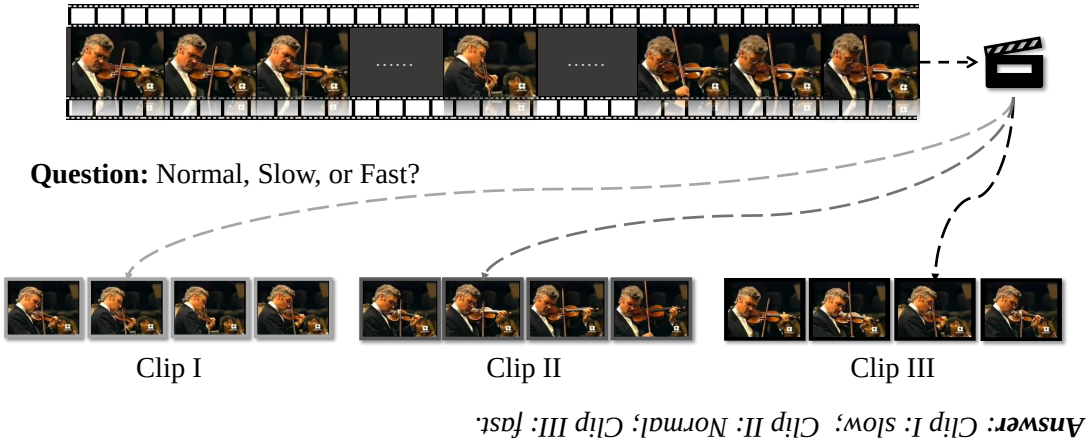

Figure 4.1: **Simple illustration of the pace prediction task.** Given a video sample, frames are randomly selected by different paces to formulate the final training inputs. Here, three different clips, clip I, II, III are sampled by normal, slow and fast pace randomly. Can you ascribe the corresponding pace label to each clip? The answer is shown in the below.

in neuroscience studies [107, 108]. To this end, we propose a simple yet effective task to perform self-supervised video representation learning: pace prediction. Specifically, given videos played in natural pace, videos clips are generated with different paces by different sampling rates. A learnable model then is trained to identify which pace the input video clip corresponds to. As aforementioned, the assumption here is that if the model is able to distinguish different paces, it has to understand the underlying content. Fig. 4.1 illustrates the basic idea of the proposed approach.

In the proposed pace prediction framework, we utilize 3D convolutional neural networks (CNNs) as our backbone network to learn video representations, following prior works [7, 36]. Specifically, we investigated several alternative architectures, including C3D [10], 3D-ResNet [26, 45], and R(2+1)D [26]. Furthermore, we incorporate contrastive learning to enhance the discriminative capability of the model for video understanding. Extensive experimental evaluations

with several video understanding tasks demonstrate the effectiveness of the proposed approach. We also present a study of different backbone architectures as well as alternative configurations of contrastive learning. The experimental result suggests that the proposed approach can be well integrated into different architectures and achieves state-of-the-art performance for self-supervised video representation learning.

The main contributions of this work are summarized as follows.

- We propose a simple yet effective approach for self-supervised video representation learning by pace prediction. This novel pretext task provides a solution to learn spatio-temporal features without explicitly leveraging the motion channel, *e.g.*, optical flow.
- We further introduce contrastive learning to regularize the pace prediction objective. Two configurations are investigated by maximizing the mutual information either between same video pace or same video context.
- Extensive experimental evaluations on three network architectures and two downstream tasks across three datasets show that the proposed approach achieves state-of-the-art performance and demonstrates great potential to learn from tremendous amount of video data available online, in a simple manner. Code and pre-trained models are made available.

4.2 Proposed Approach

4.2.1 Overview

We address the video representation learning problem in a self-supervised manner. To achieve this goal, rather than training with human-annotated labels, we train a model with labels generated *automatically* from the video inputs X. The essential

problem is how to design an appropriate transformation $g(\cdot)$, usually termed as pretext task, so as to yield transformed video inputs $\widetilde{X}$ with human-annotated free labels that encourage the network to learn powerful semantic spatio-temporal features for the downstream tasks, *e.g.*, action recognition.

In this work, we propose pace transformation $g_{pac}(\cdot)$ with a pace prediction task for self-supervised learning. Our idea is inspired by the concept *slow motion*, which is widely used in film making for capturing a key moment and producing dramatic effect. Humans can easily identify it due to their sensitivity of the pace variation and a sense of normal pace. We explore whether a network could also have such ability to distinguish video play pace. Our assumption is that a network is not capable to perform such pace prediction task effectively unless it understands the video content and learns powerful spatio-temporal features.

In the following, we first elaborate on the pace prediction task. Then we introduce two possible contrastive learning strategies. Finally, we present the complete learning framework with three different 3D network architectures.

4.2.2 Pace Prediction

We aim to train a model with pace-varying video clips as inputs and ask the model to predict the video play paces. We assume that such a pace prediction task will encourage the neural network to learn generic transferable video representations and benefit downstream tasks. Fig. 4.2 shows an example of generating the training samples and pace labels. Note that in this example, we only illustrate one training video with five distinct sampling paces. Whereas in our final implementation, the sampling pace is randomly selected from several pace candidates, instead of these five specific sampling paces.

As shown in Fig. 4.2, given a video in natural pace with 25 frames, training clips will be sampled in different paces p. Typically, we consider five pace candi-

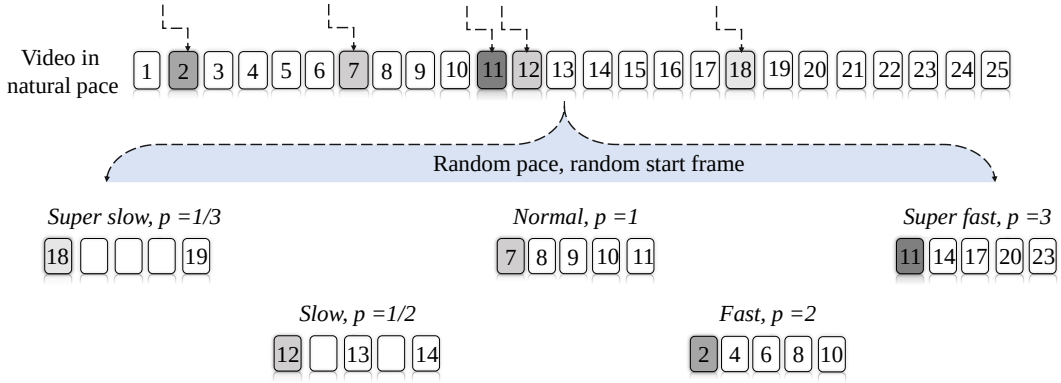

Figure 4.2: **Generating training samples and pace labels from the proposed pretext task.** Here, we show five different sampling paces, named as *super slow*, *slow*, *normal*, *fast*, and *super fast*. The darker the initial frame is, the faster the entire clip plays.

dates {super slow, slow, normal, fast, super fast}, where the corresponding paces p are 1/3, 1/2, 1, 2, and 3, respectively. Start frame of each video clip is then randomly generated to ensure the training clip will not exceed the total frame number. Methods to generate each training clip with a specific p are illustrated in the following:

- *Normal motion*, where $p = 1$, training clips are sampled consecutively from the original video. The video play speed is the same as the normal pace.

- *Fast motion*, where $p > 1$, we directly sample a video frame from the original video every p frames, *e.g.*, super fast clip with $p = 3$ contains frames 11, 14, 17, 20 and 23. As a result, when we play the clip in nature 25 fps, it looks like the video is speed up compared with the original pace.

- *Slow motion*, where $p < 1$, we put the sampled frames into the five-frames clip very $1/p$ frames instead, *e.g.*, slow clip with $p = 1/2$, only frames 1, 3, 5 are filled with sampled frames. Regarding the blank frames, one may consider to fill it with preceding frame, or apply interpolation algorithms

[109] to estimate the intermediate frames. In practice, for simplicity, we use the preceding frame for the blank frames.

Formally, we denote the pace sampling transformation as $g(x)$. Given a video x, we apply $g(x|p)$ to obtain the training clip $\widetilde{x}$ with a training pace p. The pace prediction pretext task is formulated as a classification problem and the neural network $f(\widetilde{x})$ is trained with cross entropy loss described as follow:

$$h = f(\widetilde{x}) = f(g_{pac}(x|p)), \tag{4.1}$$

$$\mathcal{L}_{cls} = -\sum_{i=1}^{M} y_i(\log \frac{\exp(h_i)}{\sum_{j=1}^{M} \exp(h_j)}), \tag{4.2}$$

where M is the number of all the pace rate candidates. .

Avoid shortcuts

As first pointed out in [1], when designing a pretext task, one must pay attention to the possibility that a network could be cheating or taking shortcuts to accomplish the pretext task by learning low-level features, *e.g.*, optical flows or frames differences, rather than the desired high-level semantic features. Such observations are also reported in [69, 74]. In this work, to avoid the model to learn trivial solutions to the pace prediction task, similar as [69], we use color jittering for a video clip as shown in Fig.4.3. Empirically, we find that color jittering applied to each frame achieves much better performance than to the entire video clip. We believe that this is because if we apply color jittering for the entire clip, it would be equivalent to apply nothing on the video clip.

Figure 4.3: **Illustration of color jittering used to avoid shortcuts.** Top: original input video frames. Bottom: video frames after color jittering. Typically, we randomly apply color jittering for each frame in a video clip instead of applying the same color jittering for the entire clip.

4.2.3 Contrastive Learning

To further enhance the pace prediction task and regularize the learning process, we propose to leverage contrastive learning as an additional objective. Contrastive learning in a self-supervised manner has shown great potential and achieved comparable results with supervised visual representation learning recently [32, 66, 67, 68, 69, 70]. It stems from Noise-Contrastive Estimation [110] and aims to distinguish the positive samples from a group of negative samples. The fundamental problem of contrastive learning lies in the definition of *positive* and *negative* samples. For example, Chen *et al.* [68] consider the pair with different data augmentations applied to the same sample as positive, while Bachman *et al.* [67] takes different views of a shared context as positive pair. In this work, we consider two possible strategies to define positive samples: same context and same pace. In the following, we elaborate on these two strategies.

Same Context

We first consider to use clips from the same video but with different sampling paces as positive pairs, while those clips sampled from different videos as negative pair, *i.e.*, content-aware contrastive learning.

Formally, given a mini-batch of N video clips $\{x_1, \ldots, x_N\}$, for each video input x_i, we randomly sample n training clips from it by different paces, resulting in an actual training batch size $n * N$. Here, for simplicity, we consider $n = 2$, and the corresponding positive pairs are $\{(\widetilde{x}_i, p_i), (\widetilde{x}_i', p_i')\}$, where $\widetilde{x}_i$ and $\widetilde{x}_i'$ are sampled from the same video. Video clips sampled from different video are considered as negative pairs, denoted as $\{(\widetilde{x}_i, p_i), (\widetilde{x}_\mathcal{J}, p_\mathcal{J})\}$. Each video clip is then encoded into a feature vector z_i in the latent space by the neural network $f(\cdot)$. Then the positive feature vector pair is (z_i, z_i') while the negative pairs are $\{(z_i, z_\mathcal{J})\}$. Denote $\text{sim}(z_i, z_i')$ as the similarity between feature vector z_i and z_i' and $\text{sim}(z_i, z'_\mathcal{J})$ as the similarity between feature vector z_i and $z'_\mathcal{J}$, the content-aware contrastive loss is defined as:

$$\mathcal{L}_{ctr\_sc} = -\frac{1}{2N} \sum_{i,\mathcal{J}} \log \frac{\exp(\text{sim}(z_i, z_i'))}{\sum_i \exp(\text{sim}(z_i, z_i')) + \sum_{i,\mathcal{J}} \exp(\text{sim}(z_i, z_\mathcal{J}))}, \tag{4.3}$$

where $\text{sim}(z_i, z_i')$ is achieved by the dot product ${z_i}^\top z_i'$ between the two feature vectors and so as $\text{sim}(z_i, z'_\mathcal{J})$.

Same Pace

Concerning the proposed pace prediction pretext task, another alternative contrastive learning strategy based on same pace is explored. Specifically, we consider video clips with the same pace as positive samples regardless of the underlying video content, *i.e.*, content-agnostic contrastive learning. In this way, the contrastive learning is investigated from a different perspective that is explicitly

Algorithm 3 Pace reasoning with contrastive learning on same video context.

Input: Video set X, pace transformation $g_{pac}(.)$, λ_{cls}, λ_{ctr}, backbone network f.
Output: Updated parameters of network f.

for sampled mini-batch video clips $\{x_1, \ldots, x_N\}$ **do**
  for $i = 1$ to N **do**
    Random generate video pace p_i, $p_i{}'$
    $\widetilde{x}_i = g_{pac}(x_i|p_i)$
    $\widetilde{x}'_i = g_{pac}(x_i|p_i{}')$
    $z_i = f(\widetilde{x}_i)$
    $z_i{}' = f(\widetilde{x}'_i)$
  end for
  for $i \in \{1, \ldots, 2N\}$ and $j \in \{1, \ldots, 2N\}$ **do**
    $\text{sim}(z_i, z_j) = z_i{}^{\top} z_j$
  end for
  Define $\mathcal{L}_{ctr\_sc} = -\frac{1}{2N} \sum_{i,\mathcal{J}} \log \frac{\exp(\text{sim}(z_i, z_i{}'))}{\sum_i \exp(\text{sim}(z_i, z_i{}')) + \sum_{i,\mathcal{J}} \exp(\text{sim}(z_i, z_{\mathcal{J}}))}$.

  $\mathcal{L}_{cls} = -\frac{1}{2N} \sum \sum_{i=1}^{M} y_i (\log \frac{\exp(h_i)}{\sum_{j=1}^{M} \exp(h_j)})$
  $\mathcal{L} = \lambda_{cls} \mathcal{L}_{cls} + \lambda_{ctr} \mathcal{L}_{ctr\_sc}$
  Update f to minimize $\mathcal{L}$
end for

related to pace.

Formally, given a mini-batch of N video clips $\{x_1, \ldots, x_N\}$, we first apply the pace sampling transformation $g_{pac}(\cdot)$ described above to each video input to obtain the training clips and their pace labels, denoted as $\{(\widetilde{x}_1, p_1)$,..., $(\widetilde{x}_N, p_N)\}$. Each video clip is then encoded into a feature vector z_i in the latent space by the neural network $f(\cdot)$. Consequently, (z_i, z_j) is considered as positive pair if $p_i = p_j$ while (z_i, z_k) is considered as negative pair if $p_i \neq p_k$, where $j, k \in \{1, 2, \ldots, N\}$. Denote $\text{sim}(z_i, z_j)$ as the similarity between feature vector z_i and z_j and $\text{sim}(z_i, z_k)$ as the similarity between feature vector z_i and z_k, the contrastive loss is defined

as:

$$\mathcal{L}_{ctr\_sp} = -\frac{1}{N}\sum_{i,j,k}\log\frac{\exp(\text{sim}(z_i, z_j))}{\sum_{i,j}\exp(\text{sim}(z_i, z_j)) + \sum_{i,k}\exp(\text{sim}(z_i, z_k))}, \tag{4.4}$$

where $\text{sim}(z_i, z_j)$ is achieved by the dot product ${z_i}^\top z_j$ between the two feature vectors and so as $\text{sim}(z_i, z_k)$.

Algorithm 4 Pace reasoning with contrastive learning on same video pace.

Input: Video set X, pace transformation $g_{pac}(.)$, λ_{cls}, λ_{ctr}, backbone network f.
Output: Updated parameters of network f.

for sampled mini-batch video clips $\{x_1, \ldots, x_N\}$ **do**
  for $i = 1$ to N **do**
    Random generate video pace p_i
    $\widetilde{x}_i = g_{pac}(x_i|p_i)$
    $z_i = f(\widetilde{x}_i)$
  end for
  for $i \in \{1, \ldots, N\}$ and $j \in \{1, \ldots, N\}$ **do**
    $\text{sim}(z_i, z_j) = {z_i}^\top z_j$
  end for
  Define $\mathcal{L}_{ctr\_sp} = -\frac{1}{N}\sum_{i,j,k}\log\frac{\exp(\text{sim}(z_i,z_j))}{\sum_{i,j}\exp(\text{sim}(z_i,z_j))+\sum_{i,k}\exp(\text{sim}(z_i,z_k))}$

  $\mathcal{L}_{cls} = -\frac{1}{N}\sum\sum_{i=1}^{M} y_i(\log\frac{\exp(h_i)}{\sum_{j=1}^{M}\exp(h_j)})$
  $\mathcal{L} = \lambda_{cls}\mathcal{L}_{cls} + \lambda_{ctr}\mathcal{L}_{ctr\_sp}$
  Update f to minimize $\mathcal{L}$
end for

Contrastive Learning Implementation Details

Fig. 4.4 demonstrates an illustration of implementation details of the two contrastive learning strategies, *i.e.*, how to compute the contrastive loss described in Eq. 4.3 and Eq. 4.4.

In terms of *same context*, suppose we have two video samples A_{ori} and B_{ori} in natural/original pace, by applying two different paces on each video, we can

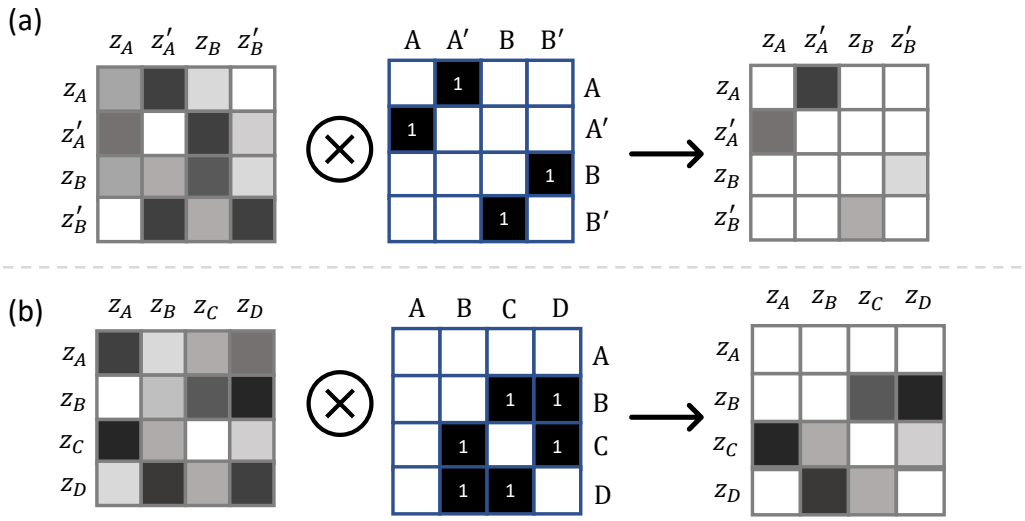

Figure 4.4: **Illustration of implementation details of the two contrastive learning strategies**.(a) Contrastive learning with same context. (b) Contrastive learning with same pace. More details are presented in Sec. 4.2.3.

then obtain four training clips, A, A', B, and B'. And the corresponding features vectors are z_A, $z_A^{'}$, z_B, and $z_B^{'}$. The similarity map of these four feature vectors is computed by $\text{sim}(z_i, z_j)$, where $i, j \in \{A, A', B, B'\}$ as shown in Fig. 4.4(a). The denominator of Eq. 4.3 can be computed by the sum of the similarity map. Based on the same context configuration, we then apply a mask on the similarity map to retain those similarities for the computation of the numerator in Eq. 4.3. As shown in Fig. 4.4(a), only (A, A'), (A', A), (B, B'), and (B', B) are considered to be positive in the same context strategy. Therefore, the the numerator of Eq. 4.3 is computed by the sum of $\text{sim}(z_A, z_A^{'})$, $\text{sim}(z_A^{'}, z_A)$, $\text{sim}(z_B, z_B^{'})$, and $\text{sim}(z_B^{'}, z_B)$.

Similarly, in terms of *same pace*, suppose we have four video samples A_{ori}, B_{ori}, C_{ori} , and D_{ori} play in natural/original pace, by applying pace transformation on each video, we can then obtain four training clips, A, B, C, D and we suppose $pace(B) = pace(C) = pace(D)$. The corresponding features vectors

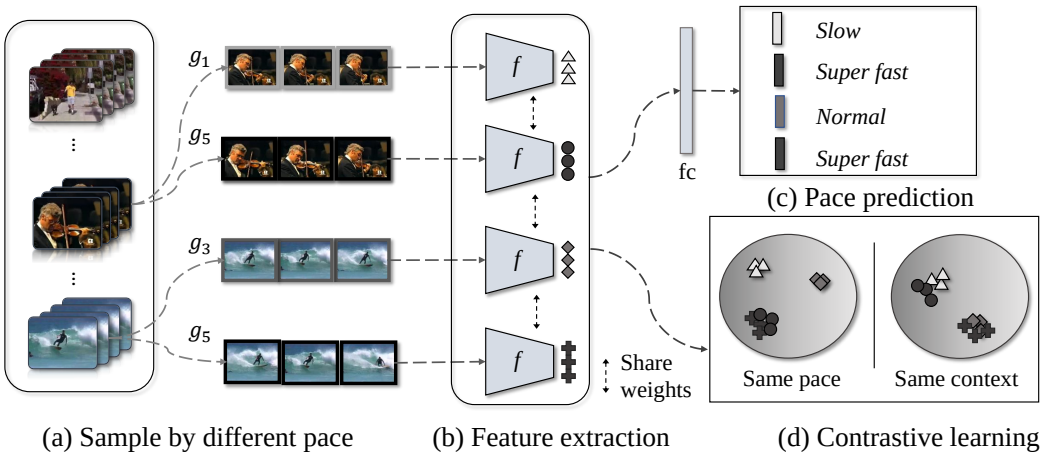

Figure 4.5: **Illustration of the proposed pace prediction framework.** (a) Training clips are sampled by different paces. Here, g_1, g_3, g_5 are illustrated as examples for slow, super fast and normal pace. (b) A 3D CNN f is leveraged to extract spatio-temporal features. (c) The model is trained to predict the specific pace applied to each video clip. (d) Two possible contrastive learning strategies are considered to regularize the learning process at the latent space. The symbols at the end of the CNNs represent feature vectors extracted from different clips, where the intensity represents different video pace.

are z_A,z_B, z_C, and z_D. The similarity map is computed by $\text{sim}(z_i, z_j)$, where $i, j \in \{A, B, C, D\}$ as shown in Fig. 4.4(b). Typically, the sum of the similarity map is the denominator of Eq. 4.4. Based on the same pace configuration, we then apply a mask on the similarity map to retain those similarities for the computation of the numerator in Eq. 4.4. As shown in Fig. 4.4(b), (B, C), (B, D), (C, B), (C, D), (D, B) and (D, C) are considered to be positive in the same pace strategy. Therefore, the the numerator of Eq. 4.4 is computed by the sum of $\text{sim}(z_B, z_C)$, $\text{sim}(z_B, z_D)$, $\text{sim}(z_C, z_B)$, $\text{sim}(z_C, z_D)$, $\text{sim}(z_D, z_B)$, and $\text{sim}(z_D, z_C)$.

4.2.4 Network Architecture and Training

The framework of the proposed pace prediction approach is illustrated in Fig. 4.5. Given a set of unlabeled videos, we firstly sample various video clips with

different paces. Then these training clips are fed into a deep model (3D CNN here) for spatio-temporal representation learning. The final objective is to optimize the model to predict the pace of each video clip and maximizing the agreement (mutual information) between positive pairs at the same time.

In terms of the network architecture, we mainly consider three backbone networks, *i.e.* C3D [10], 3D-ReseNet [45, 26] and R(2+1)D [26] to study the effectiveness of the proposed approach. C3D is a classic neural network which operates on 3D video volume by extending 2D convolutional kernel to 3D, with 5 convolutional blocks, 5 max-pooling layers, and 2 fully-connected layers. 3D-ResNet (R3D) [45, 26] is an extension of the ResNet [49] architecture on videos. A basic residual block in R3D contains two 3D convolutional layers with BatchNorm, ReLU, and shortcut connections. Following previous work [7, 36], we use 3D-ResNet18 (R3D-18) version for the R3D setting, which contains four basic residual block and one traditional convolutional block on the top. R(2+1)D is introduced by Tran *et al.* [26] that breaks the original spatio-temporal 3D convolution into a 2D spatial convolution and a 1D temporal convolution, which is shown to have fewer network parameters with promising performance on video understanding.

Apart from these three networks, we also use a state-of-the-art model S3D-G [46] to further exploit the potential of the proposed approach. Fig. 4.6 shows an illustration of the S3D-G. Similar as R(2+1)D, S3D-G also proposes to break the heavy 3D convolution to the sequential combination of 2D convolution and 1D convolution. In addition, it introduces a gating layer after the temporal convolutional layer, which can be viewed as self-attention on the outputs as shown in Fig. 4.6(c).

By jointly optimizing the classification objective (Eq. 4.2) and the contrastive

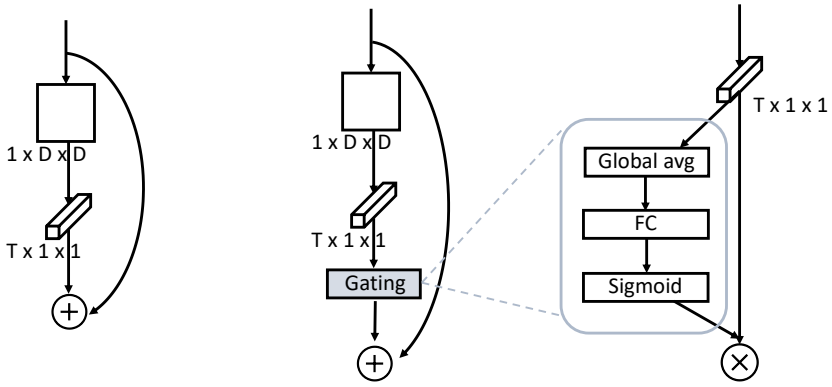

(a) R(2+1)D (b) S3D-G (c) Gating

Figure 4.6: **The illustration of backbone network S3D-G.** We show a typical convolutional block of S3D-G(ating). More details are presented in Sec. 4.2.4.

objective (Eq. 4.4 or 4.3), the final training loss is defined as:

$$\mathcal{L} = \lambda_{cls}\mathcal{L}_{cls} + \lambda_{ctr}\mathcal{L}_{ctr}, \tag{4.5}$$

where λ_{cls}, λ_{ctr} are weighting parameters to balance the optimization of classification and contrastive learning, respectively. The $\mathcal{L}_{ctr}$ refers to either contrastive with same pace $\mathcal{L}_{ctr\_sp}$ or with same context $\mathcal{L}_{ctr\_sc}$.

4.3 Implementation Detials

Datasets

Following prior work, we use three datasets as follows:

UCF101 dataset [34] is a widely used benchmark in action recognition, consisting of 13,320 video samples with 101 action classes. The covered actions are all naturally performed as they are collected from YouTube. The dataset is divided into three training/testing splits and in this work, following prior works [36, 69],

training split 1 is used as pre-training dataset and the average accuracy of the three testing splits are reported to have a fair comparison with others.

Kinetics-400 dataset [30] is a large action recognition benchmark proposed recently, which consists of 400 human action classes and around 306k videos. It is divided into three splits: training/validation/testing. In this work, we use the training split as our pre-training dataset, which contains around 240k samples, to validate our proposed method.

HMDB51 dataset [35] is a relatively small action recognition benchmark which contains around 7,000 videos and 51 action classes. This dataset is very challenging as it contains large variations in camera viewpoint, position, scale *etc.* In this work, we use it as a downstream evaluation benchmark to validate the proposed self-supervised pretext task. It is divided into three training/testing splits and we use the training/testing split 1 for ablation studies while when compared with other methods, we report the average accuracy (see Table 4.7).

Self-supervised pre-training stage

When pre-training on the Kinetics-400 dataset, for each video input, we first generate a frame index randomly and then start from the index, sample a consecutive 16-frame video clip. While when pre-training on UCF101 dataset, the video inputs are first split into non-overlapped 16 frame video clips and we randomly sample the prepared video clips during pre-training without index frame generation. Each video clip is reshaped to 128×171. As for data augmentation, we adopt spatial and temporal jittering by randomly cropping the video clip to 112×112 and flipping the whole video clip horizontally. We set the batch size to 30 and use the SGD optimizer with learning rate 1×10^{-3}. The leaning rate is divided by 10 for every 6 epochs and the training process is stopped after 20 epochs. When jointly optimizing $\mathcal{L}_{cls}$ and $\mathcal{L}_{ctr}$, λ_{cls} is set to 1 and λ_{ctr} is set to

0.1.

Supervised fine-tuning stage

Regarding the action recognition task, during the fine-tuning stage, weights of convolutional layers are retained from the self-supervised learning networks while weights of fully-connected layers are randomly initialized. The whole network is then trained with cross-entropy loss. Image pre-processing and training strategy are the same as the self-supervised pre-training stage, except that the initial learning rate is set to 3×10^{-3}.

Evaluation

During inference, follow previous evaluation protocol [7, 36], we sample 10 clips uniformly from each video in the testing set of UCF101 and HMDB51. For each clip, center crop is applied to obtain the input size 112×112. The predicted label of each video is generated by averaging the softmax probabilities of all clips in the video.

4.4 Ablation Studies

In this section, we firstly explore the best sampling pace design for the pace prediction task. We apply it to three different backbone networks to study the effectiveness of the pretext task and the network architectures. Experimental results show that using pace prediction task alone, good performances can be already achieved. When introducing the contrastive learning, same content configuration performs much better than same pace configuration. By jointly optimizing the pace prediction task and the same content contrastive learning, the performances can be further improved. More details are illustrated in the following.

4.4.1 Pace Prediction Task Design

Sampling pace

We investigate the best setting for pace prediction task with R(2+1)D backbone network [26] in Table 4.1. Typically, to study the relationship between the complexity of the pretext task and the effectiveness on the downstream task, we first consider a *relative* pace design, *i.e.*, only normal and fast motion. We use R(2+1)D [26] as the bakcbone network to investigate the best design for pace prediction, as shown in Table 4.1. Sampling pace $p = [a, b]$ is designed to have minimum pace a and maximum pace b with an interval 1. Sampling pace $p = [a, b]$ is designed to have minimum pace a and maximum pace b. It can be seen from the table that with the increase of the maximum pace, namely the number of training classes, the accuracy of the downstream action recognition task keeps increase, until $p = [1, 4]$. When the sampling pace increases to $p = [1, 6]$, the accuracy starts to drop. We believe that this is because such a pretext task is becoming too difficult for the network to learn useful semantic features. This provides an insight on the pretext task design that a pretext task should not be too simple or too ambiguous to solve, in consistent with the observations found in [52, 71].

We report the pretext task performance (*i.e.*, pace prediction accuracy) and the downstream task performance (*i.e.*, action recognition accuracy) on UCF101 dataset in Table 4.1. It can be seen from the table that with the increase of the maximum pace, the pretext task becomes harder for the network to solve, which leads to degradation of the downstream task. This further validate our claim in the paper that a pretext task should be neither too simple nor too ambiguous.

Table 4.1: Pace prediction accuracy w.r.t. different pace design.

Pre-training	Method	# Classes	Pace rea. acc.	UCF acc.
×	Random	-	-	56.0
✓	$p = [1, 3]$	3	77.6	71.4
✓	$p = [1, 4]$	4	69.5	**72.0**
✓	$p = [1, 5]$	5	61.4	72.0
✓	$p = [1, 6]$	6	55.9	71.1

Table 4.2: Evaluation of slow pace.

Config.	Pace	# Classes	UCF10 Acc.
Baseline	[1,2,3,4]	4	73.9
Slow	$[\frac{1}{4},\frac{1}{3},\frac{1}{2},1]$	4	72.6
Slow-fast	$[\frac{1}{3},\frac{1}{2},1,2,3]$	5	73.9

Slow pace

In our paper, we propose two different methods to generate video clips with slow pace: replication of previous frames or interpolation with existing algorithms [109]. We choose the replication in practice as most modern interpolation algorithms are based on supervised learning, while our work focuses on self-supervised learning, forbidding us to use any human annotations.

As shown in Table 4.2, compared with normal and *fast* paces, if we use normal and *slow* paces, the performance of the downstream task decreases (73.9→72.6). While when combining with both slow and fast pace (*absolute* pace as described in the paper), no performance change is observed, which again validates our choice of the pace configuration.

Pace step

Based on the better performance achieved by the fast pace as shown above, we take a closer look into the fast pace design, by considering different interval

Table 4.3: Evaluation of different pace steps.

Step	Pace	# Classes	UCF10 Acc.
1	[1,2,3,4]	4	73.9
2	[1,3,5,7]	4	74.9
3	[1,4,7,10]	4	74.7

steps, *i.e.*, frame skip. For simplicity, in the paper we showcase with the step that equals one (baseline) between each fast pace where the paces are {1,2,3,4}. Here we further explore the interval steps of two and three so as to introduce larger motion dynamics into the learning process. It can be observed from Table 4.3 that by increasing the interval steps, performance could be further improved, but tends to saturate when the step is too large.

Forwards *v.s.* backwards.

It has been a long standing problem that whether a forward played video can be considered as the same as its backward played version, in self-supervised video representation learning. Some works [4, 72] argue that these two versions should be attributed to the same semantic labels, while Wei *et al.* prone to distinguish the forwards and backwards video [111]. In the following, we investigate these two opinions based on our method as shown in Table 4.4.

As for the random backwards with four classes, we consider forwards and backwards videos as the same pace samples, while for backwards with eight classes, they are considered to be different samples. It can be seen from the table that, both configurations achieve lower performance than our baseline. We suspect the reason is that to distinguish the backwards from forwards, it is essentially a video order prediction task though in some order prediction work [72, 4] they are considered to be the same. When combing the proposed pace reasoning task with such an order prediction task, the network will be confused towards an ambiguous

Table 4.4: Evaluation of video forwards *v.s.* backwards.

Config.	Pace	# Classes	UCF10 Acc.
Baseline	[1,2,3,4]	4	73.9
Rnd backwards	[1,2,3,4]	4	73.0
Backwards	[±1, ±2, ±3, ±4]	8	73.7

Table 4.5: Explore the best setting for pace prediction task. Sampling pace $p = [a, b]$ represents that the lowest value of pace p is a and the highest is b with an interval of 1, except $p = [\frac{1}{3}, 3]$, where p is selected from $\{\frac{1}{3}, \frac{1}{2}, 1, 2, 3\}$.

Color jittering	Method	#Classes	UCF101
×	Random	-	56.0
×	$p = [1, 3]$	3	71.4
×	$p = [1, 4]$	4	**72.0**
×	$p = [1, 5]$	5	72.0
×	$p = [1, 6]$	6	71.1
✓	$p = [1, 4]$	4	**73.9**
✓	$p = [\frac{1}{3}, 3]$	5	73.9

target. As a result, the downstream task performance is deteriorated.

Color jittering

We further validate the effectiveness of color jittering based on the best sampling pace design $p = [1, 4]$. It can be seen from Table 4.1 that with color jittering, the performance is further improved by 1.9%. It is also interesting to note that the *relative* pace, *i.e.*, $p = [1, 4]$, achieves comparable result with the *absolute* pace, *i.e.*, $p = [\frac{1}{3}, 3]$, but with less number of classes. In the following experiments, we use sampling pace $p = [1, 4]$ along with color jittering by default.

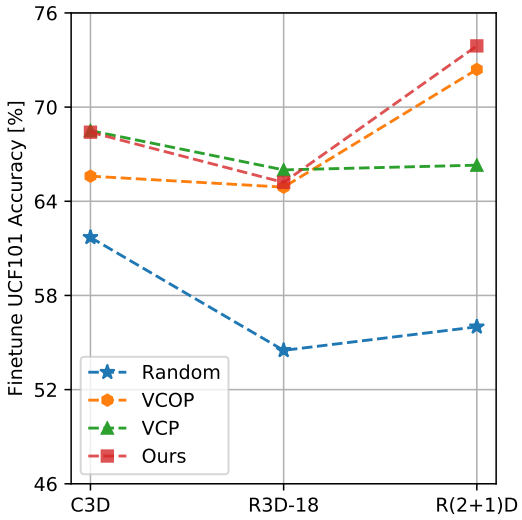

Figure 4.7: Action recognition accuracy on three backbone architectures (horizontal axis) using four initialization methods.

4.4.2 Backbone Network

We validate the proposed pace prediction task without contrastive learning using three alternative network architectures. Recently, some research works [7, 36] validated their proposed self-supervised learning approaches on modern spatio-temporal representation learning networks, such as R3D-18 [45, 26], R(2+1)D [26], *etc*. This practice could influence the direct evaluation of the pretext tasks, as the performance improvement can also come from the usage of more powerful networks. Therefore, the effectiveness of the pace prediction task are studied on three backbone networks and we also compare with some recent works on these three networks, as shown in Fig. 4.7. For a fair comparison, following [7, 36], we use the first training split of UCF101 as the pre-training dataset and evaluate on training/testing split 1.

Some key observations are listed in the following: (1) The proposed approach achieves significant improvement over the random initialization across

all three backbone networks. With C3D it improves UCF101 by 9.6%; with R3D-18 it improves UCF101 by 13.6%; and more remarkable, with R(2+1)D it improves UCF101 by 17.9%. (2) Although in the random initialization setting, C3D achieves the best results, R(2+1)D and R3D-18 benefit more from the self-supervised pre-training and R(2+1)D finally achieves the best performance. (3) Without contrastive learning, the proposed pace prediction task already demonstrates impressive effectiveness to learn video representations, achieving comparable performance with current state-of-the-art methods VCP [36] and VCOP[7] on C3D and R3D-18 and outperforms them when using R(2+1)D.

4.4.3 Contrastive learning

The performances of the two contrastive learning configurations are shown in Table 4.6. Some key observations are listed for a better understanding of the contrastive learning: (1) The same pace configuration achieves much worse results than the same context configuration. We suspect the reason is that in the same pace configuration, as there are only four pace candidates $p = [1, 4]$, video clips are tend to belong to the same pace. Therefore, compared with the same context configuration, much fewer negative samples are presented in the training batches, withholding the effectiveness of the contrastive learning. (2) Pace prediction task achieves much better performance compared to each of the two contrastive learning settings. This demonstrates the superiority of the proposed pace prediction task.

When combining the pace prediction task with contrastive learning, similar to the observation described above, regarding the same pace configuration, performance is slightly deteriorated and regarding the same context configuration, performance is further improved both on UCF101 and HMDB51 datasets. It shows that appropriate multi-task self-supervised learning can further boost the

Table 4.6: Evaluation of different contrastive learning configurations on both UCF101 and HMDB51 datasets. *Note that paramters when adding a fc layer only increase ∼4k, which is negligible compared to the original 14.4M parameters.

Experimental setup					Downstream tasks	
Pace Pred.	Ctr. Learn.	Network	Configuration	Params	UCF101	HMDB51
✓	×	R(2+1)D	-	14.4M	**73.9**	**33.8**
×	✓	R(2+1)D	Same pace	14.4M	59.4	20.3
×	✓	R(2+1)D	Same context	14.4M	67.3	28.6
✓	✓	R(2+1)D	Same pace	14.4M	73.6	32.3
✓	✓	R(2+1)D	Same context	14.4M	75.8	35.0
✓	✓	R(2+1)D + fc	Same context	14.4M*	**75.9**	**35.9**

performances, in consistent with the observation in [112]. Based on the same video content configuration, we further introduce a nonlinear layer between the embedding space and the final contrastive learning space to alleviate the direct influence on the pace prediction learning. It is shown that such a practice can further improve the performance (last row in Table 4.6).

4.5 Action Recognition

We compare our approach with other methods on the action recognition task in Table 4.7. We have the following key observations: (1) Our method achieve the state-of-the-art results on both UCF101 and HMDB51 dataset. When pre-trained on UCF101, we outperform the current best-performing method PRP [113]. When pre-trained on K-400, we outperform the current best-performing method DPC [69]. (2) Note that here the DPC method uses R3D-34 as their backbone network and the video input size is 224×224 while we only use 112×112. When the input size of DPC is at the same scale as ours, *i.e.*, 128×128, we outperform it by 8.9% on UCF101 dataset. We attribute such success to both our pace prediction task and the usage of R(2+1)D. It can be observed that with R(2+1)D and

Table 4.7: Comparison with the state-of-the-art self-supervised learning methods on UCF101 and HMDB51 dataset (Pre-trained on video modality only).*The input video clips contain 64 frames.

Method	Pre-training settings				Evaluation	
	Network	Input size	Params	Dataset	UCF101	HMDB51
Fully supervised	S3D-G	224 × 224*	9.6M	ImageNet	86.6	57.7
Fully supervised	S3D-G	224 × 224*	9.6M	K-400	96.8	74.5
Object Patch[96]	AlexNet	227 × 227	62.4M	UCF101	42.7	15.6
ClipOrder[4]	CaffeNet	227 × 227	58.3M	UCF101	50.9	19.8
Deep RL[73]	CaffeNet	227 × 227	-	UCF101	58.6	25.0
OPN [72]	VGG	80 × 80	8.6M	UCF101	59.8	23.8
VCP [36]	R(2+1)D	112 × 112	14.4M	UCF101	66.3	32.2
VCOP [7]	R(2+1)D	112 × 112	14.4M	UCF101	72.4	30.9
PRP [113]	R(2+1)D	112 × 112	14.4M	UCF101	72.1	35.0
Ours	R(2+1)D	112 × 112	14.4M	UCF101	**75.9**	**35.9**
MAS[80]	C3D	112 × 112	27.7M	K-400	61.2	33.4
RotNet3D [79]	R3D-18	224 × 224	33.6M	K-400	62.9	33.7
ST-puzzle [74]	R3D-18	224 × 224	33.6M	K-400	65.8	33.7
DPC [69]	R3D-18	128 × 128	14.2M	K-400	68.2	34.5
DPC [69]	R3D-34	224 × 224	32.6M	K-400	75.7	35.7
Ours	R(2+1)D	112 × 112	14.4M	K-400	**77.1**	**36.6**
SpeedNet [114]	S3D-G	224 × 224*	9.6M	K-400	81.1	48.8
Ours	S3D-G	224 × 224*	9.6M	UCF101	**87.1**	**52.6**

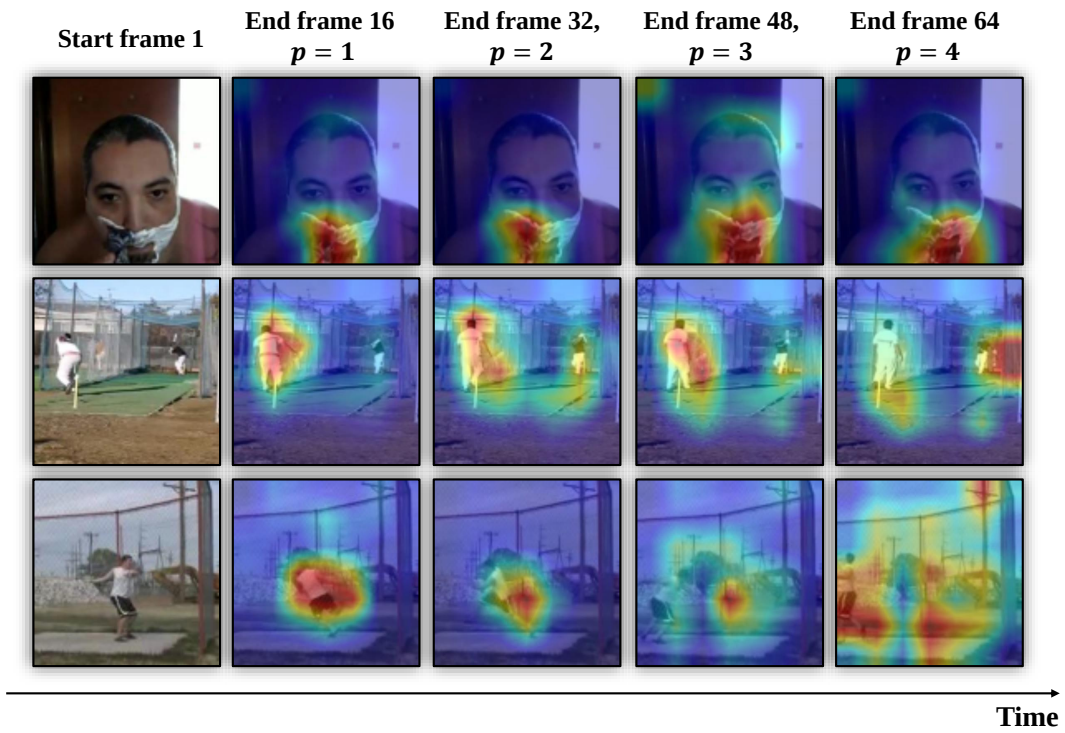

Figure 4.8: Attention visualization of the conv5 layer from self-supervised pre-trained model using [12]. Attention map is generated with 16-frames clip inputs and applied to the last frame in the video clips. Each row represents a video sample while each column illustrates the end frame *w.r.t.* different sampling pace p.

only UCF101 as pre-train dataset, VCOP [7] can achieve 72.4% on UCF101 and 30.9% on HMDB51. (3) Backbone networks, input size and clip length do play important roles in the self-supervised video representation learning. As shown in the last row, by using the S3D-G [46] architecture with 64-frame clips as inputs, pre-training only on UCF101 can already achieve remarkable performance, even superior to fully supervised pre-training on ImageNet (on UCF101).

To further validate the proposed approach, we visualize the attention maps based on the pre-trained R(2+1)D model, as shown in Fig. 4.8. It can be seen from the attention maps that the neural network will pay more attention to the

Table 4.8: Comparison with state-of-the-art nearest neighbour retrieval results on UCF101 benchmark.

	Method	Top1	Top5	Top10	Top20	Top50
AlexNet	Jigsaw[52]	19.7	28.5	33.5	40.0	49.4
	OPN[72]	19.9	28.7	34.0	40.6	51.6
	Deep RL[73]	25.7	36.2	42.2	49.2	59.5
C3D	Random	16.7	27.5	33.7	41.4	53.0
	VCOP[7]	12.5	29.0	39.0	50.6	66.9
	VCP[36]	17.3	31.5	42.0	52.6	67.7
	Ours (p5)	20.0	37.4	46.9	58.5	73.1
	Ours(p4)	**31.9**	**49.7**	**59.2**	**68.9**	**80.2**
R3D-18	Random	9.9	18.9	26.0	35.5	51.9
	VCOP[7]	14.1	30.3	40.4	51.1	66.5
	VCP[36]	18.6	33.6	42.5	53.5	68.1
	Ours (p5)	19.9	36.2	46.1	55.6	69.2
	Ours(p4)	**23.8**	**38.1**	**46.4**	**56.6**	**69.8**
R(2+1)D	Random	10.6	20.7	27.4	37.4	53.1
	VCOP[7]	10.7	25.9	35.4	47.3	63.9
	VCP[36]	19.9	33.7	42.0	50.5	64.4
	Ours (p5)	17.9	34.3	44.6	55.5	72.0
	Ours(p4)	**25.6**	**42.7**	**51.3**	**61.3**	**74.0**

motion areas when learning the pace prediction task. It is also interesting to note that in the last row, as attention map on $p = 4$ computes the layer information spanning 64 frames, it is activated at several motion locations.

4.6 Video Retrieval

We further validate the proposed approach on the video retrieval task. Basically, we follow the same evaluation protocol described in [36, 7]. Ten 16-frames clips are sampled from each video and then go through a feed-forward pass to generate features from the last pooling layer (p5). For each clip in the testing split, the

Table 4.9: Comparison with state-of-the-art nearest neighbor retrieval results on HMDB51 benchmark.

	Method	Top1	Top5	Top10	Top20	Top50
C3D	Random	7.4	20.5	31.9	44.5	66.3
	VCOP[7]	7.4	22.6	34.4	48.5	70.1
	VCP[36]	7.8	23.8	35.5	49.3	71.6
	Ours (p5)	8.0	25.2	37.8	54.4	77.5
	Ours(p4)	**12.5**	**32.2**	**45.4**	**61.0**	**80.7**
R3D-18	Random	6.7	18.3	28.3	43.1	67.9
	VCOP[7]	7.6	22.9	34.4	48.8	68.9
	VCP[36]	7.6	24.4	36.6	53.6	76.4
	Ours (p5)	8.2	24.2	37.3	53.3	74.5
	Ours(p4)	**9.6**	**26.9**	**41.1**	**56.1**	**76.5**
R(2+1)D	Random	4.5	14.8	23.4	38.9	63.0
	VCOP[7]	5.7	19.5	30.7	45.8	67.0
	VCP[36]	6.7	21.3	32.7	49.2	73.3
	Ours (p5)	10.1	24.6	37.6	54.4	77.1
	Ours(p4)	**12.9**	**31.6**	**43.2**	**58.0**	**77.1**

Table 4.10: Comparison of different pooling layers video retrieval results on UCF101 and HMDB51 dataset.

	Layer	UCF101					HMDB51				
		Top1	Top5	Top10	Top20	Top50	Top1	Top5	Top10	Top20	Top50
C3D	pool1	21.3	33.7	41.1	48.9	60.4	8.3	22.9	34.1	49.3	71.6
	pool2	23.2	37.3	46.0	55.1	67.5	8.8	24.8	37.8	52.8	75.9
	pool3	30.2	46.8	55.9	64.9	78.6	12.2	31.1	44.5	60.1	79.6
	pool4	**31.9**	**49.7**	**59.2**	**68.9**	**80.2**	**12.5**	**32.2**	**45.4**	**61.0**	**80.7**
	pool5	20.0	37.4	46.9	58.5	73.1	8.0	25.2	37.8	54.4	77.5
R3D-18	pool1	20.7	32.0	38.1	45.3	57.8	7.9	22.6	33.3	48.0	68.8
	pool2	21.1	33.5	39.7	46.7	58.4	8.5	24.4	36.2	50.6	71.5
	pool3	22.0	35.3	43.4	53.4	66.9	8.4	24.1	37.1	52.9	76.5
	pool4	**23.8**	**38.1**	**46.4**	**56.6**	**69.8**	**9.6**	**26.9**	**41.1**	**56.1**	**76.5**
	pool5	19.9	36.2	46.1	55.6	69.2	8.2	24.2	37.3	53.3	74.5
R(2+1)D	pool1	21.4	34.3	41.2	49.0	62.4	8.4	22.7	35.5	51.4	71.5
	pool2	**26.4**	40.7	49.1	58.1	70.5	13.1	29.8	41.0	55.0	74.1
	pool3	26.3	**44.2**	**53.9**	**63.3**	**75.7**	**13.1**	**33.2**	**46.0**	**59.9**	**77.9**
	pool4	25.6	42.7	51.3	61.3	74.0	12.9	31.6	43.2	58.0	76.9
	pool5	17.9	34.3	44.6	55.5	72.0	10.1	24.6	37.6	54.4	77.1

Top$k$ nearest neighbors are queried from the training split by computing the cosine distances between every two feature vectors. If the test clip class label is within the Top$k$ retrieval results, it is considered as correct. And the final accuracy is computed by averaging all the test results. We consider k to be 1, 5, 10, 20, 50. To align the experimental results with prior works [36, 7] for fair comparison, we use pre-trained models from the pace prediction task on UCF101 dataset. As shown in Table 4.8 and Table 4.9, our method outperforms the VCOP [7] and VCP [36] in most cases on the two datasets across the three backbone networks. In practice, we also find that significant improvement can be achieved by using the second last pooling layer (p4). The detailed performances of each pooling layer are shown in Table 4.10.

4.7 Discussion

In this chapter, we proposed a new perspective towards self-supervised video representation learning, by pace prediction. Contrastive learning was also incorporated to further encourage the networks to learn high-level semantic features. We conducted extensive experiments across four neural network architectures on two different downstream tasks to validate the proposed approach. The experimental results demonstrated the superiority of our method on learning powerful spatio-temporal features. Besides, the pace prediction task does not rely on any motion channel as input/information during training. As a result, such a pace prediction task can serve as a simple (yet effective) supervisory signal when applying the self-supervised video representation learning in real world, taking advantage of billions of video data on the Internet.

□ End of chapter.

Chapter 5

Conclusions and Future Work

5.1 Conclusions

In conclusion, we proposed *two novel pretext tasks*, spatio-temporal statistics regression and video play pace prediction, conducted *one systematical study* on self-supervised video representation learning in terms of backbone networks, pre-training dataset scale and feature transferability, and adopted *two learning strategies*, curriculum learning and contrastive learning to further improve the performance. With these works, we introduced new perspectives, broadened previous focuses on video order prediction and as a result, pioneered in self-supervised video representation learning, a newly-developed and promising field. Extensive experimental results demonstrated the feasibility of self-supervised learning to leverage large amount of unlabeled video data. The detailed summary of each chapter is illustrated in the following:

- Chapter 2 proposed a novel pretext task - spatio-temporal statistics regression, for self-supervised video representation learning. Specifically, given an unlabeled video clip, a series of spatio-temporal statistical summaries were computed, such as the spatial location and dominant direction of the

largest motion, the spatial location and dominant color of the largest color diversity along the temporal axis, *etc.* Then a neural network was built and trained to yield the statistical summaries given the video frames as inputs. In order to alleviate the learning difficulty, several spatial partitioning patterns were employed to encode rough spatial locations instead of exact spatial Cartesian coordinates. This approach was inspired by the observation that human visual system is sensitive to rapidly changing contents in the visual field, and only needs impressions about rough spatial locations to understand the visual contents. Unlike prior works that were concentrated on or to some extent stuck in the video order conception, this pretext task presented a completely new perspective for self-supervised video representation learning. It was also the first work that used 3D convolutional neural network to learn spatio-temporal features in a self-supervised manner. A preliminary evaluation was conducted on a classic and relatively shallow backbone network, C3D with five convolutional layers. The experimental results showed that the proposed method achieved competitive performances. While promising results have been achieved, the potential of the proposed method can be further explored by using a more powerful backbone network and a much larger pre-training dataset *etc.*

- To get a better understanding of the proposed statistics pretext task and further improve the performance, Chapter 3 presented an in-depth investigation on the spatio-temporal statistics regression pretext task by conducting extensive experiments. The potential of the spatio-temporal statistics was fully exploited by using a much larger dataset and some modern neural networks. A curriculum learning strategy was also introduced to further improve the representation learning. Besides, in Chapter 3, we also provided some fundamental insights on developing self-supervised video representa-

tion learning methods. Some key observations are listed as follows: (1) The backbone networks architectures play an important role in self-supervised learning. However, no best model is guaranteed for different pretext tasks. In most cases, the combination of 2D spatial convolution and 1D temporal convolution achieves better results. (2) Downstream task performances are log-linearly correlated with the pre-training dataset scale. Notably, using only 1/8 of the pre-training data can already achieve 1/2 of the improvement, which suggest that Attentive selection should be given on the training samples. (3) In addition to the main advantages of self-supervised video representation learning, *i.e.*, leveraging large amount of unlabeled videos, it was demonstrated that features learned in a self-supervised manner are more generalizable and transferable than features learned in a supervised manner. Experimental results showed that the proposed method achieved remarkable performances. However, this pretext task still has some limitations, where the major one is the usage of pre-computed optical flow. This is both time and space consuming, especially when the training dataset scales to millions/trillions of videos.

- In order to overcome the major limitation of the proposed statistics pretext task, Chapter 4 presented a simple and effective pretext task for self-supervised video representation learning by pace prediction. This pretext only based on the original input videos, without referring to the optical flow information. It stemmed from the observation that human visual system is sensitive to video pace, *e.g.*, slow motion, a widely used technique in film making. Specifically, given a video played in natural pace, we randomly sampled training clips in different paces and asked a neural network to identify the pace for each video clip. The assumption here was that the network can only succeed in such a pace reasoning task when it understands

the underlying video content and learns representative spatio-temporal features. In addition, we further introduced contrastive learning to push the model towards discriminating different paces by maximizing the agreement on similar video content. To validated the effectiveness of the proposed method, we conducted extensive experiments on action recognition and video retrieval tasks with several alternative network architectures. Experimental evaluations showed that our approach achieved state-of-the-art performance for self-supervised video representation learning across different network architectures and different benchmarks. It is also worth noting that due to the simplicity and effectiveness of the pace prediction task, it has various applications and could be an influential work in the future. For example, it can be used as an auxiliary loss, a data augmentation method, or an exemplary task for investigating the essence or principles of self-supervised video representation learning.

5.2 Future work

Based on the findings and results illustrated in this thesis, some future directions are listed in the following:

- The performance of self-supervised video representation learning can be further boosted by using multi-modal data, *e.g.*, the combination of audio and video. Specifically, the proposed pace prediction pretext task can be applied to any time-series signals. It would be interesting to apply this pretext task on audio modality, *i.e.*, ask the neural network to predict whether the audio is played in a slow, normal or fast pace. We believe the performance can be further improved by combing both video and audio modality for self-supervised video representation learning.

- It is interesting to investigate the influence of using non-curated video data for pre-training. Current self-supervised video representation learning approaches, including works described in this thesis, are mainly pre-trained on the large-scale dataset, kinetics-400 (K-400). The original action class labels of K-400 are discarded and training labels are generated automatically by various pretext tasks. However, essentially, K-400 is selected, cleaned, and annotated by human beings. While in the real world, video data is non-curated, which could be much more disorganized and chaotic. How would the self-supervised video representation learning methods be influenced by these data? Will the performance be deteriorated? If so, how can we alleviate or solve this problem? We believe it is an interesting direction to be explored.

- A more fundamental direction that needs to be investigated is that with only self-supervised video representation learning, can the video content be fully analyzed and understood? In this thesis, the motivation behind our works are mainly inspired by human visual system. In consistent with findings in neuroscience research, we observed that human beings understand video content from multiple perspectives, such as appearance and color, largest motion area and direction, video play pace, *etc.* Based on these observations, we proposed novel pretext tasks and demonstrated the superiority of the proposed approaches. However, analyzing video content and recognizing the exact action class is still one key element of video understanding while in the self-supervised learning paradigm, it deliberately discards every action class label and only uses pretext tasks to guide the feature learning. We hypothesize that the future of video representation learning lies in the combination of both supervised and self-supervised learning, as human beings understand the visual world from multiple aspects. It will

be interesting to take inspiration from self-supervised learning pretext tasks and further investigate them in semi-supervised learning paradigm.

□ **End of chapter.**

Appendix A

Publication List

The works presented in this thesis are published/submitted in the following papers:

- **Jiangliu Wang**, Jianbo Jiao, Linchao Bao, Shengfeng He, Yun-Hui Liu, and Wei Liu. "Self-supervised Spatio-temporal Representation Learning for Videos by Predicting Motion and Appearance Statistics". CVPR 2019.

  Code: https://github.com/laura-wang/video_repres_mas

- **Jiangliu Wang**, Jianbo Jiao, Linchao Bao, Shengfeng He, Wei Liu, and Yun-Hui Liu. "Self-supervised Video Reprepresentation Learning by Uncovering Spatio-temporal Statistics". TPAMI. Under review.

  Code: https://github.com/laura-wang/video_repres_sts

- **Jiangliu Wang**, Jianbo Jiao, and Yun-Hui Liu. " Self-supervised Video Representation Learning by Pace Prediction". ECCV 2020.

  Code: https://github.com/laura-wang/video-pace

Before delving into the marvelous self-supervised learning world, I also did some research on 3D human action recognition. The related publications are

listed in the following:

- **Jiangliu Wang** and Yun-Hui Liu. "Kinematics Features for 3D Action Recognition Using Two-Stream CNN". WCICA 2018.
- **Jiangliu Wang**, Kebin Yuan, and Yun-Hui Liu. "Image coding method, action recognition method, and computer device". Patent WO2019120108A1 .
- Qiang Nie, **Jiangliu Wang**, Xin Wang, and Yun-Hui Liu. " View-invariant human action recognition based on a 3d bio-constrained skeleton model". TIP 2019.

□ End of chapter.

Bibliography

[1] Carl Doersch, Abhinav Gupta, and Alexei A Efros. Unsupervised visual representation learning by context prediction. In *ICCV*, 2015.

[2] Spyros Gidaris, Praveer Singh, and Nikos Komodakis. Unsupervised representation learning by predicting image rotations. In *ICLR*, 2018.

[3] Richard Zhang, Phillip Isola, and Alexei A Efros. Colorful image colorization. In *ECCV*, 2016.

[4] Ishan Misra, C Lawrence Zitnick, and Martial Hebert. Shuffle and learn: unsupervised learning using temporal order verification. In *ECCV*, 2016.

[5] Chuang Gan, Boqing Gong, Kun Liu, Hao Su, and Leonidas J Guibas. Geometry guided convolutional neural networks for self-supervised video representation learning. In *CVPR*, 2018.

[6] Carl Vondrick, Hamed Pirsiavash, and Antonio Torralba. Generating videos with scene dynamics. In *NeurIPS*, 2016.

[7] Dejing Xu, Jun Xiao, Zhou Zhao, Jian Shao, Di Xie, and Yueting Zhuang. Self-supervised spatiotemporal learning via video clip order prediction. In *CVPR*, 2019.

[8] *http://people.duke.edu/~ng46/topics/color-spaces.htm*.

[9] Joe Yue-Hei Ng, Matthew Hausknecht, Sudheendra Vijayanarasimhan, Oriol Vinyals, Rajat Monga, and George Toderici. Beyond short snippets: Deep networks for video classification. In *CVPR*, 2015.

[10] Du Tran, Lubomir Bourdev, Rob Fergus, Lorenzo Torresani, and Manohar Paluri. Learning spatiotemporal features with 3d convolutional networks. In *ICCV*, 2015.

[11] Joao Carreira and Andrew Zisserman. Quo vadis, action recognition? a new model and the kinetics dataset. In *CVPR*, 2017.

[12] Sergey Zagoruyko and Nikos Komodakis. Paying more attention to attention: Improving the performance of convolutional neural networks via attention transfer. In *ICLR*, 2017.

[13] Suzana Herculano-Houzel. The human brain in numbers: a linearly scaled-up primate brain. *Frontiers in human neuroscience*, 3:31, 2009.

[14] Peter Dayan and Laurence F Abbott. *Theoretical neuroscience: computational and mathematical modeling of neural systems*. MIT press, 2001.

[15] Du Tran, Heng Wang, Lorenzo Torresani, Jamie Ray, Yann LeCun, and Manohar Paluri. A closer look at spatiotemporal convolutions for action recognition. In *CVPR*, 2018.

[16] Yang Liu, Samuel Albanie, Arsha Nagrani, and Andrew Zisserman. Use what you have: Video retrieval using representations from collaborative experts. *arXiv preprint arXiv:1907.13487*, 2019.

[17] Antoine Miech, Dimitri Zhukov, Jean-Baptiste Alayrac, Makarand Tapaswi, Ivan Laptev, and Josef Sivic. Howto100m: Learning a text-video

embedding by watching hundred million narrated video clips. In *ICCV*, 2019.

[18] Yu-Wei Chao, Sudheendra Vijayanarasimhan, Bryan Seybold, David A Ross, Jia Deng, and Rahul Sukthankar. Rethinking the faster r-cnn architecture for temporal action localization. In *CVPR*, 2018.

[19] Zheng Shou, Jonathan Chan, Alireza Zareian, Kazuyuki Miyazawa, and Shih-Fu Chang. Cdc: Convolutional-de-convolutional networks for precise temporal action localization in untrimmed videos. In *CVPR*, 2017.

[20] Zheng Shou, Dongang Wang, and Shih-Fu Chang. Temporal action localization in untrimmed videos via multi-stage cnns. In *CVPR*, 2016.

[21] Bairui Wang, Lin Ma, Wei Zhang, and Wei Liu. Reconstruction network for video captioning. In *CVPR*, 2018.

[22] Jingwen Wang, Wenhao Jiang, Lin Ma, Wei Liu, and Yong Xu. Bidirectional attentive fusion with context gating for dense video captioning. In *CVPR*, 2018.

[23] Ivan Laptev. On space-time interest points. *International Journal on Computer Vision*, 64(2-3):107–123, 2005.

[24] Alexander Klaser, Marcin Marszałek, and Cordelia Schmid. A spatio-temporal descriptor based on 3d-gradients. In *BMVC*, 2008.

[25] Heng Wang and Cordelia Schmid. Action recognition with improved trajectories. In *ICCV*, 2013.

[26] Du Tran, Heng Wang, Lorenzo Torresani, Jamie Ray, Yann LeCun, and Manohar Paluri. A closer look at spatiotemporal convolutions for action recognition. In *CVPR*, 2018.

[27] Christoph Feichtenhofer, Haoqi Fan, Jitendra Malik, and Kaiming He. Slowfast networks for video recognition. In *ICCV*, 2019.

[28] Karen Simonyan and Andrew Zisserman. Two-stream convolutional networks for action recognition in videos. In *NeurIPS*, 2014.

[29] Andrej Karpathy, George Toderici, Sanketh Shetty, Thomas Leung, Rahul Sukthankar, and Li Fei-Fei. Large-scale video classification with convolutional neural networks. In *CVPR*, 2014.

[30] Will Kay, Joao Carreira, Karen Simonyan, Brian Zhang, Chloe Hillier, Sudheendra Vijayanarasimhan, Fabio Viola, Tim Green, Trevor Back, Paul Natsev, et al. The kinetics human action video dataset. *arXiv preprint arXiv:1705.06950*, 2017.

[31] *https://www.tubefilter.com/2019/05/07/number-hours-video-uploaded-to-youtube-per-minute/.*

[32] Aaron van den Oord, Yazhe Li, and Oriol Vinyals. Representation learning with contrastive predictive coding. *arXiv preprint arXiv:1807.03748*, 2018.

[33] Humam Alwassel, Dhruv Mahajan, Lorenzo Torresani, Bernard Ghanem, and Du Tran. Self-supervised learning by cross-modal audio-video clustering. *arXiv preprint arXiv:1911.12667*, 2019.

[34] Khurram Soomro, Amir Roshan Zamir, and Mubarak Shah. Ucf101: A dataset of 101 human actions classes from videos in the wild. *arXiv preprint arXiv:1212.0402*, 2012.

[35] Hildegard Kuehne, Hueihan Jhuang, Estíbaliz Garrote, Tomaso Poggio, and Thomas Serre. Hmdb: a large video database for human motion recognition. In *ICCV*, 2011.

[36] Dezhao Luo, Chang Liu, Yu Zhou, Dongbao Yang, Can Ma, Qixiang Ye, and Weiping Wang. Video cloze procedure for self-supervised spatio-temporal learning. *arXiv preprint arXiv:2001.00294*, 2020.

[37] Konstantinos G Derpanis, Matthieu Lecce, Kostas Daniilidis, and Richard P Wildes. Dynamic scene understanding: The role of orientation features in space and time in scene classification. In *CVPR*, 2012.

[38] Noureldien Hussein, Efstratios Gavves, and Arnold WM Smeulders. Timeception for complex action recognition. In *CVPR*, 2019.

[39] Ivan Laptev, Marcin Marszalek, Cordelia Schmid, and Benjamin Rozenfeld. Learning realistic human actions from movies. In *CVPR*, 2008.

[40] Navneet Dalal, Bill Triggs, and Cordelia Schmid. Human detection using oriented histograms of flow and appearance. In *ECCV*, 2006.

[41] Fabian Caba Heilbron, Victor Escorcia, Bernard Ghanem, and Juan Carlos Niebles. Activitynet: A large-scale video benchmark for human activity understanding. In *CVPR*, 2015.

[42] Raghav Goyal, Samira Ebrahimi Kahou, Vincent Michalski, Joanna Materzynska, Susanne Westphal, Heuna Kim, Valentin Haenel, Ingo Fruend, Peter Yianilos, Moritz Mueller-Freitag, et al. The" something something" video database for learning and evaluating visual common sense. In *ICCV*, 2017.

[43] Gunnar A Sigurdsson, Gül Varol, Xiaolong Wang, Ali Farhadi, Ivan Laptev, and Abhinav Gupta. Hollywood in homes: Crowdsourcing data collection for activity understanding. In *ECCV*, 2016.

[44] Zhaofan Qiu, Ting Yao, and Tao Mei. Learning spatio-temporal representation with pseudo-3d residual networks. In *ICCV*, 2017.

[45] Kensho Hara, Hirokatsu Kataoka, and Yutaka Satoh. Can spatiotemporal 3d cnns retrace the history of 2d cnns and imagenet? In *CVPR*, 2018.

[46] Saining Xie, Chen Sun, Jonathan Huang, Zhuowen Tu, and Kevin Murphy. Rethinking spatiotemporal feature learning: Speed-accuracy trade-offs in video classification. In *ECCV*, 2018.

[47] Christian Szegedy, Wei Liu, Yangqing Jia, Pierre Sermanet, Scott Reed, Dragomir Anguelov, Dumitru Erhan, Vincent Vanhoucke, and Andrew Rabinovich. Going deeper with convolutions. In *CVPR*, 2015.

[48] Karen Simonyan and Andrew Zisserman. Very deep convolutional networks for large-scale image recognition. *arXiv preprint arXiv:1409.1556*, 2014.

[49] Kaiming He, Xiangyu Zhang, Shaoqing Ren, and Jian Sun. Deep residual learning for image recognition. In *CVPR*, 2016.

[50] Jie Hu, Li Shen, and Gang Sun. Squeeze-and-excitation networks. In *CVPR*, 2018.

[51] Alex Krizhevsky, Ilya Sutskever, and Geoffrey E Hinton. Imagenet classification with deep convolutional neural networks. In *NeurIPS*, 2012.

[52] Mehdi Noroozi and Paolo Favaro. Unsupervised learning of visual representations by solving jigsaw puzzles. In *ECCV*, 2016.

[53] Deepak Pathak, Philipp Krahenbuhl, Jeff Donahue, Trevor Darrell, and Alexei A Efros. Context encoders: Feature learning by inpainting. In *CVPR*, 2016.

[54] Mathilde Caron, Piotr Bojanowski, Armand Joulin, and Matthijs Douze. Deep clustering for unsupervised learning of visual features. In *ECCV*, 2018.

[55] Christian Ledig, Lucas Theis, Ferenc Huszár, Jose Caballero, Andrew Cunningham, Alejandro Acosta, Andrew Aitken, Alykhan Tejani, Johannes Totz, Zehan Wang, et al. Photo-realistic single image super-resolution using a generative adversarial network. In *CVPR*, 2017.

[56] Mehdi Noroozi, Hamed Pirsiavash, and Paolo Favaro. Representation learning by learning to count. In *ICCV*, 2017.

[57] Jonathan Long, Evan Shelhamer, and Trevor Darrell. Fully convolutional networks for semantic segmentation. In *CVPR*, 2015.

[58] Liang-Chieh Chen, George Papandreou, Iasonas Kokkinos, Kevin Murphy, and Alan L Yuille. Deeplab: Semantic image segmentation with deep convolutional nets, atrous convolution, and fully connected crfs. *IEEE transactions on pattern analysis and machine intelligence*, 40(4):834–848, 2017.

[59] Hengshuang Zhao, Jianping Shi, Xiaojuan Qi, Xiaogang Wang, and Jiaya Jia. Pyramid scene parsing network. In *CVPR*, 2017.

[60] Mark Everingham, Luc Van Gool, Christopher KI Williams, John Winn, and Andrew Zisserman. The pascal visual object classes (voc) challenge. *International journal of computer vision*, 88(2):303–338, 2010.

[61] Ross Girshick. Fast r-cnn. In *ICCV*, 2015.

[62] Shaoqing Ren, Kaiming He, Ross Girshick, and Jian Sun. Faster r-cnn: Towards real-time object detection with region proposal networks. In *NeurIPS*, 2015.

[63] Tsung-Yi Lin, Piotr Dollár, Ross Girshick, Kaiming He, Bharath Hariharan, and Serge Belongie. Feature pyramid networks for object detection. In *CVPR*, 2017.

[64] Tsung-Yi Lin, Michael Maire, Serge Belongie, James Hays, Pietro Perona, Deva Ramanan, Piotr Dollár, and C Lawrence Zitnick. Microsoft coco: Common objects in context. In *ECCV*, 2014.

[65] Gao Huang, Zhuang Liu, Laurens Van Der Maaten, and Kilian Q Weinberger. Densely connected convolutional networks. In *CVPR*, 2017.

[66] Ting Chen, Simon Kornblith, Mohammad Norouzi, and Geoffrey Hinton. A simple framework for contrastive learning of visual representations. *arXiv preprint arXiv:2002.05709*, 2020.

[67] Philip Bachman, R Devon Hjelm, and William Buchwalter. Learning representations by maximizing mutual information across views. In *NeurIPS*, 2019.

[68] Olivier J Hénaff, Ali Razavi, Carl Doersch, SM Eslami, and Aaron van den Oord. Data-efficient image recognition with contrastive predictive coding. *arXiv preprint arXiv:1905.09272*, 2019.

[69] Tengda Han, Weidi Xie, and Andrew Zisserman. Video representation learning by dense predictive coding. In *ICCV Workshops*, 2019.

[70] Zhirong Wu, Yuanjun Xiong, Stella X Yu, and Dahua Lin. Unsupervised feature learning via non-parametric instance discrimination. In *CVPR*, 2018.

[71] Basura Fernando, Hakan Bilen, Efstratios Gavves, and Stephen Gould.

Self-supervised video representation learning with odd-one-out networks. In *CVPR*, 2017.

[72] Hsin-Ying Lee, Jia-Bin Huang, Maneesh Singh, and Ming-Hsuan Yang. Unsupervised representation learning by sorting sequences. In *ICCV*, 2017.

[73] Uta Buchler, Biagio Brattoli, and Bjorn Ommer. Improving spatiotemporal self-supervision by deep reinforcement learning. In *ECCV*, 2018.

[74] Dahun Kim, Donghyeon Cho, and In So Kweon. Self-supervised video representation learning with space-time cubic puzzles. In *AAAI*, 2019.

[75] Andrew Owens and Alexei A Efros. Audio-visual scene analysis with self-supervised multisensory features. In *ECCV*, 2018.

[76] Bruno Korbar, Du Tran, and Lorenzo Torresani. Cooperative learning of audio and video models from self-supervised synchronization. In *NeurIPS*, 2018.

[77] Deepti Ghadiyaram, Du Tran, and Dhruv Mahajan. Large-scale weakly-supervised pre-training for video action recognition. In *CVPR*, 2019.

[78] Nitish Srivastava, Elman Mansimov, and Ruslan Salakhudinov. Unsupervised learning of video representations using lstms. In *ICML*, 2015.

[79] Longlong Jing, Xiaodong Yang, Jingen Liu, and Yingli Tian. Self-supervised spatiotemporal feature learning via video rotation prediction. *arXiv preprint arXiv:1811.11387*, 2018.

[80] Jiangliu Wang, Jianbo Jiao, Linchao Bao, Shengfeng He, Yunhui Liu, and Wei Liu. Self-supervised spatio-temporal representation learning for videos by predicting motion and appearance statistics. In *CVPR*, 2019.

[81] Jiangliu Wang, Jianbo Jiao, and Yun-Hui Liu. Self-supervised video representation learning by pace prediction. In *ECCV*, 2020.

[82] William Lotter, Gabriel Kreiman, and David Cox. Deep predictive coding networks for video prediction and unsupervised learning. *arXiv preprint arXiv:1605.08104*, 2016.

[83] Michael Mathieu, Camille Couprie, and Yann LeCun. Deep multi-scale video prediction beyond mean square error. In *ICLR*, 2016.

[84] Martin A Giese and Tomaso Poggio. Cognitive neuroscience: neural mechanisms for the recognition of biological movements. *Nature Reviews Neuroscience*, 4(3):179–192, 2003.

[85] Thomas Brox, Andrés Bruhn, Nils Papenberg, and Joachim Weickert. High accuracy optical flow estimation based on a theory for warping. In *ECCV*, 2004.

[86] Heng Wang, Alexander Kläser, Cordelia Schmid, and Cheng-Lin Liu. Action recognition by dense trajectories. In *CVPR*, 2011.

[87] *https://cs231n.github.io/convolutional-networks/*.

[88] Jeffrey Donahue, Lisa Anne Hendricks, Sergio Guadarrama, Marcus Rohrbach, Subhashini Venugopalan, Kate Saenko, and Trevor Darrell. Long-term recurrent convolutional networks for visual recognition and description. In *CVPR*, 2015.

[89] Sepp Hochreiter and Jürgen Schmidhuber. Long short-term memory. *Neural computation*, 9(8):1735–1780, 1997.

[90] Yangqing Jia, Evan Shelhamer, Jeff Donahue, Sergey Karayev, Jonathan Long, Ross Girshick, Sergio Guadarrama, and Trevor Darrell. Caffe: Convolutional architecture for fast feature embedding. In *ACM Multimedia*, 2014.

[91] *https://pytorch.org/.*

[92] *https://www.nvidia.com/en-us/deep-learning-ai/products/titan-rtx/.*

[93] *https://machinelearningmastery.com/learning-rate-for-deep-learning-neural-networks/.*

[94] R Hadsell, S Chopra, and Y LeCun. Dimensionality reduction by learning an invariant mapping. In *CVPR*, 2006.

[95] Hossein Mobahi, Ronan Collobert, and Jason Weston. Deep learning from temporal coherence in video. In *ICML*, 2009.

[96] Xiaolong Wang and Abhinav Gupta. Unsupervised learning of visual representations using videos. In *ICCV*, 2015.

[97] Christoph Feichtenhofer, Axel Pinz, and Richard P Wildes. Spacetime forests with complementary features for dynamic scene recognition. In *BMVC*, 2013.

[98] Sergey Ioffe and Christian Szegedy. Batch normalization: Accelerating deep network training by reducing internal covariate shift. In *ICML*, 2015.

[99] Yoshua Bengio, Jérôme Louradour, Ronan Collobert, and Jason Weston. Curriculum learning. In *ICML*, 2009.

[100] Omer Sumer, Tobias Dencker, and Bjorn Ommer. Self-supervised learning of pose embeddings from spatiotemporal relations in videos. In *ICCV*, 2017.

[101] Guy Hacohen and Daphna Weinshall. On the power of curriculum learning in training deep networks. In *ICML*, 2019.

[102] Orit Kliper-Gross, Tal Hassner, and Lior Wolf. The action similarity labeling challenge. *IEEE Transactions on Pattern Analysis and Machine Intelligence*, 34(3):615–621, 2011.

[103] Minyoung Huh, Pulkit Agrawal, and Alexei A Efros. What makes imagenet good for transfer learning? *arXiv preprint arXiv:1608.08614*, 2016.

[104] Alexander Kolesnikov, Xiaohua Zhai, and Lucas Beyer. Revisiting self-supervised visual representation learning. In *CVPR*, 2019.

[105] Christoph Feichtenhofer, Axel Pinz, and Richard P Wildes. Bags of space-time energies for dynamic scene recognition. In *CVPR*, 2014.

[106] Christian Theriault, Nicolas Thome, and Matthieu Cord. Dynamic scene classification: Learning motion descriptors with slow features analysis. In *CVPR*, 2013.

[107] Martin A Giese and Tomaso Poggio. Neural mechanisms for the recognition of biological movements. *Nature Reviews Neuroscience*, 4(3):179–192, 2003.

[108] Scott NJ Watamaniuk and Andrew Duchon. The human visual system averages speed information. *Vision research*, 32(5):931–941, 1992.

[109] Huaizu Jiang, Deqing Sun, Varun Jampani, Ming-Hsuan Yang, Erik Learned-Miller, and Jan Kautz. Super slomo: High quality estimation of multiple intermediate frames for video interpolation. In *CVPR*, 2018.

[110] Michael Gutmann and Aapo Hyvärinen. Noise-contrastive estimation: A new estimation principle for unnormalized statistical models. In *AISTATS*, 2010.

[111] Donglai Wei, Joseph J Lim, Andrew Zisserman, and William T Freeman. Learning and using the arrow of time. In *CVPR*, 2018.

[112] Carl Doersch and Andrew Zisserman. Multi-task self-supervised visual learning. In *ICCV*, 2017.

[113] Yuan Yao, Chang Liu, Dezhao Luo, Yu Zhou, and Qixiang Ye. Video playback rate perception for self-supervised spatio-temporal representation learning. In *CVPR*, 2020.

[114] Sagie Benaim, Ariel Ephrat, Oran Lang, Inbar Mosseri, William T Freeman, Michael Rubinstein, Michal Irani, and Tali Dekel. Speednet: Learning the speediness in videos. In *CVPR*, 2020.